

https://dspace.org/

# Analysis of specific absorption rate in humans for wearable wireless devices in underground mines

**Ashraf, Muhammad Ahsan**

**2020**

https://hdl.handle.net/10539/31117

Downloaded from a DSpace repository. https://dspace.org/

University of the Witwatersrand

Master Dissertation

# Analysis of Specific Absorption Rate in Humans for Wearable Wireless Devices in Underground Mines

*Author:*
Muhammad Ahsan Ashraf

*Supervisor*
Dr. Asad Mehmood
&
Professor Michiel Postema

*Co-supervisor*
Professor Frederick Cawood

School of Electrical and Information Engineering

June 30, 2020

# Declaration

I, **Muhammad Ahsan Ashraf**, declare that this Dissertation titled, "**Analysis of Specific Absorption Rate in Humans for Wearable Wireless Devices in Underground Mines**" and the work presented in it are my own. I confirm that:

- This work was done wholly or mainly while in candidature for a research degree at this University.
- Where any part of this thesis has previously been submitted for a degree or any other qualification at this University or any other institution, has been clearly stated.
- Where I have consulted the published work of others, this is always clearly attributed.
- Where I have quoted from the work of others, the source is always given. With the exception of such quotations, this dissertation is entirely my own work.
- I have acknowledged all main sources of help.

Signed: _____

Date: _____

# Abstract

In the last decades, the use of wireless communication has proliferated, which has mushroomed the amount of electromagnetic radiation (EMR) in the environment. Human body interacts directly or indirectly with these EMR, which may cause adverse health impact. The exposure of EMR is regulated by the guidelines anticipated by the standardisation bodies. Specific absorption rate (SAR) determines the amount of electromagnetic energy absorbed in human tissues and is used as an index to regulate EMR exposure to humans by standard regulatory authorities.
Underground mining is an important industry and especially vital for the South African economy. Underground mining processes can be made more productive and reliable by deploying different systems for monitoring, tracking and controlling different activities in the underground mines. Different tracking systems are deployed in the underground mines to track the exact location and vitals of the miner, particularly after a disaster. Most of these devices are wearable and mounted on the head or torso of the miners. Due to the proximity of these devices to human organs in a confined environment of underground mines and continuous operations for extended hours, the public concern for the use of these devices has arisen in recent years. This study evaluates the SAR variations for wearable wireless devices used in underground mines using frequencies of relevant ISM bands i.e. 433 MHz, 868 MHz and 2400 MHz. The SAR variations are evaluated by numerical simulations using two high resolution ($1\times\ 1\ \times\ 1\ mm^3$) human anatomical models and by modelling different underground mine scenarios. The SAR results of two human models on head without helmet, torso and head with helmet are compared for open space and underground mine scenarios for all frequencies. The results show that the SAR values are higher in all underground mine scenarios than the open space scenarios, and the SAR values are also higher for higher frequencies than the lower frequencies. It is observed that in terms of SAR, the torso is a suitable location to mount these devices on the body of the miner compared to the head. Recommendations based on the SAR guidelines are provided on head for maximum transmit power level of 1 W, 0.5 W and 0.12 W can be used at 433 MHz, 868 MHz and 2400 MHz, respectively, for short duration of time in case of a disaster to aid the rescue operation in underground mines. Finally, the SAR was investigated with variation of distance between human model and underground mine structure. It was concluded that the SAR values are higher than the open space scenario when

the distance between the boundaries of the underground mine and miner is less than 200 mm.

# Acknowledgements

My unfeigned acknowledgments are due to guidance, encouragement and contributions to make my research work triumphant:

- My supervisors, Dr Asad Mahmood and Professor Michiel Postema (School of Electrical & Information Engineering, University of Witwatersrand), and Professor Frederick Cawood (Wits Mining Institute, University of Witwatersrand) for their academic guidance throughout the research.
- I would like to thank and acknowledge the financial support provided by the Sibanye-Stillwater Digital Mining Laboratory (DigiMine), Wits Mining Institute (WMI).
- All the staff of Wits Mining Institute (WMI), School of Electrical & Information Engineering, University of Witwatersrand and colleagues of the DigiMine laboratory for their moral support throughout the research.

# Contents

**Declaration** i

**Abstract** ii

**Acknowledgements** iv

**Contents** v

**List of Figures** viii

**List of Tables** xii

**Abbreviations** xiii

**1 Introduction** 1
- 1.1 Introduction . . . 1
- 1.2 Classification of Radiations . . . 4
  - 1.2.1 Possible Health Effects of Non-Ionizing Radiations . . . 5
- 1.3 Research Questions . . . 6
- 1.4 Objectives of the Research . . . 7
- 1.5 Thesis Outline . . . 8

**2 Background Review** 10
- 2.1 Communication in Underground Mines . . . 10
  - 2.1.1 Wireless Communication Systems . . . 12
- 2.2 Overview of Electromagnetic Quantities . . . 14
- 2.3 Guidelines of Specific Absorption Rate . . . 17
- 2.4 Computation of Electromagnetism . . . 18
  - 2.4.1 Finite Element Method . . . 18
  - 2.4.2 Method of Moments . . . 19
  - 2.4.3 Finite-Difference Time-Domain Method . . . 19
  - 2.4.4 Finite Integration Technique . . . 20
  - 2.4.5 Commercial Software Packages for Computation of Electromagnetic . . . 22
  - 2.4.6 IEEE Standard for Numerical Simulations of SAR . . . 22

**3 Literature Review** 25
- 3.1 Classification of Literature . . . 25
- 3.2 Medical Approach . . . 26

3.3 Engineering Approach . . . . . 28
3.4 Conclusion . . . . . 32

**4 Methodology** **34**
4.1 Modelling of Electromagnetic Source . . . . . 34
4.2 Human Voxel Models . . . . . 36
4.2.1 Dielectric Properties of Biological Tissues . . . . . 38
4.3 Modelling of Underground Mine Scenarios . . . . . 40
4.3.1 Modelling of Mock Mine Scenarios for Head . . . . . 43
4.3.2 Modelling of Mock Mine Scenarios for Torso . . . . . 45
4.4 Modelling of Helmet . . . . . 48
4.5 Simulation Setup for Head without Helmet Scenario . . . . . 49
4.5.1 Setup for Open Space Scenario on Head without Helmet . . 50
4.5.2 Setup for Tunnel Scenario on Head without Helmet . . . . . 53
4.5.3 Setup for Tunnel Arch Scenario on Head without Helmet . . 55
4.5.4 Setup for Stope Scenario on Head without Helmet . . . . . 56
4.6 Simulation Setup for Torso Scenario . . . . . 57
4.6.1 Setup for Open Space Scenario on Torso . . . . . 58
4.6.2 Setup for Tunnel Scenario on Torso . . . . . 61
4.6.3 Setup for Tunnel Arch Scenario on Torso . . . . . 62
4.7 Simulation Setup for Head with Helmet Scenario . . . . . 62
4.7.1 Setup for Open Space Scenario on Head with Helmet . . . . 64
4.7.2 Setup for Tunnel Scenario on Head with Helmet . . . . . 64
4.7.3 Setup for Tunnel Arch Scenario on Head with Helmet . . . . 65
4.7.4 Setup for Stope Scenario on Head with Helmet . . . . . 66
4.8 Simulation Setup for Different Power Levels . . . . . 67
4.9 Simulation Setup for Variation of Distance . . . . . 68

**5 Simulation Results and Discussion** **69**
5.1 SAR Analysis for Head without Helmet Scenario . . . . . 69
5.2 SAR Analysis for Torso Scenario . . . . . 74
5.3 SAR Analysis for Head with Helmet Scenario . . . . . 78
5.4 SAR Analysis for Different Power Levels . . . . . 81
5.5 SAR Analysis for Variation of Distance . . . . . 85
5.6 Discussion . . . . . 88

**6 Conclusion and Future Work** **92**
6.1 Conclusion . . . . . 92
6.2 Future work . . . . . 94

**Bibliography** **95**

**Appendix A** **105**

**Appendix B** **107**

**Appendix C** **109**

**Appendix D** **111**

**Appendix E** **113**

# List of Figures


1.1 Classification of radiations in electromagnetic spectrum and associated health risks. . . . . 5

2.1 Classification of underground mine communication systems. . . . . 11
2.2 Discretisation of Faraday's law using finite integration technique. . . 21

3.1 Classification of the literature based on different methodologies used to study the impact of electromagnetic radiations. . . . . 26
3.2 Schematic for the position of the human model in a . . . . . 30
3.3 Simulated directivity of the implanted antenna at 4 GHz. . . . . 31
3.4 Simulated SAR variation in voxel head model . . . . . 31

4.1 Geometry and dimensions of the modelled dipole antenna. . . . . 35
4.2 $S_{11}$ of dipole antenna at 433 MHz, 868 MHz and 2400 MHz. . . . . 36
4.3 High resolution (1 mm) human voxel models used in this study (a) Hugo and (b) Tom. . . . . 38
4.4 Hierarchy of different scenarios used in this study for evaluation of SAR on head, torso and head with helmet. . . . . 42
4.5 Modelling of tunnel scenario for simulations on head (a) Mock mine tunnel with wall and roof (b) Surface roughness of the mock mine tunnel (c) Front and (d) Side view of modelled tunnel scenario for simulations on head. . . . . 44
4.6 Modelling of tunnel arch scenario for simulations on head (a) Presence of steel support arches in the mock mine tunnel (b) Close view of steel arch of the tunnel (c) Front and (d) Side view of modelled tunnel arch scenarios for simulations on head. . . . . 45
4.7 Modelling of stope scenario for simulations on head (a) Stope of the Wits mock mine (b) Support structure in the stope of the mock mine (c) Modelled stope scenario for simulations on head. . . . . 46
4.8 Modelling of tunnel scenario for simulations on torso (a) Front view of the modelled scenario (b) Side view of the modelled scenario with its surface roughness. . . . . 47
4.9 Modelling of tunnel arch scenario for simulations on torso (a) Front view of the modelled arch scenario (b) Side view of the modelled scenario with its dimensions. . . . . 48
4.10 Modelling of helmet for head (a) Modelled head helmet with polyimide material (b) Cross sectional view and placement of helmet on the head of Hugo model. . . . . 50

4.11 Complete simulation setup for the head without helmet in an open space scenario (a) Position of the dipole antenna on the head of Hugo model (b) Distance between the head of Hugo model and the dipole antenna (c) Complete setup for simulation with its boundary box. . . . . 52
4.12 Complete simulation setup for the head without helmet in tunnel scenario (a) Distance between the head of Tom model from the wall and roof of the modelled tunnel (b) Position of the head of Tom model for tunnel scenario (c) Complete setup for simulation with its boundary box. . . . . 54
4.13 Complete simulation setup for the head in tunnel arch scenario (a) Distance between the Hugo model and the modelled arch of the mock mine tunnel (b) Position of the head of Hugo model with modelled tunnel arch scenario (c) Complete setup for simulation with its boundary box. . . . . 56
4.14 Complete simulation setup for the head in stope scenario (a) Dimensions and Position of the head of Tom model from the face, roof and pillar of the stope (b) Complete setup for simulation with its boundary box. . . . . 58
4.15 Complete simulation setup for the torso in an open space scenario (a) Position of the dipole antenna on torso of the Hugo model (b) Distance between torso and the dipole antenna (c) Complete setup for open space scenario with a boundary box. . . . . 60
4.16 Complete simulation setup on the torso of Tom model for tunnel scenario. . . . . 61
4.17 Complete simulation setup for torso in tunnel arch scenario (a) Distance between the torso of Hugo model and the arch of the modelled mock mine tunnel (b) Position of the torso with modelled tunnel arch scenario (c) Complete setup of tunnel arch scenario with its boundary box. . . . . 63
4.18 Complete simulation setup for head with helmet in an open space scenario (a) Distance between the dipole antenna and modelled helmet (b) Mounting position of the dipole antenna on the head helmet. 64
4.19 Complete simulation setup for head with helmet of Tom model in tunnel scenario. . . . . 65
4.20 Complete simulation setup for head with helmet of Hugo model in tunnel arch scenario. . . . . 66
4.21 Complete simulation setup for head with helmet of Tom model in stope scenario with boundary box. . . . . 67

5.1 $SAR_{10g}$ distribution in the head of hugo model at (a) 2400 MHz, (b) 868 MHz and (c) 433 MHz, and in the head of Tom model at (d) 2400 MHz, (e) 868 MHz and (f) 433 MHz. . . . . 71
5.2 Comparison of $SAR_{10g}$ values in the head without helmet of both models for different scenarios at 2400 MHz. . . . . 71

5.3 Comparison of $SAR_{10g}$ values in the head without helmet of both models for different scenarios at 868 MHz. . . . . 72
5.4 Comparison of $SAR_{10g}$ values in the head without helmet of both models for different scenarios at 433 MHz. . . . . 73
5.5 $SAR_{10g}$ distribution in Cerebrospinal Fluid (CSF) for Hugo model at (a) 2400 MHz, (b) 868 MHz and (c) 433 MHz, and for Tom model at (d) 2400 MHz, (e) 868 MHz and (f) 433 MHz. . . . . 74
5.6 Power loss Density ($W/m^3$) in the torso of Hugo model at (a) 2400 MHz, (b) 868 MHz and (c) 433 MHz, and in the torso of Tom model at (d) 2400 MHz, (e) 868 MHz and (f) 433 MHz. . . . . 76
5.7 Comparison of $SAR_{10g}$ values in the torso of both models for different scenarios at 2400 MHz. . . . . 76
5.8 Comparison of $SAR_{10g}$ values in the torso of both models for different scenarios at 868 MHz. . . . . 77
5.9 Comparison of $SAR_{10g}$ values in the torso of both models for different scenarios at 433 MHz. . . . . 78
5.10 Comparison of $SAR_{10g}$ values in the head with helmet of both models for different scenarios at 2400 MHz. . . . . 79
5.11 Comparison of $SAR_{10g}$ values in the head with helmet of both models for different scenarios at 868 MHz. . . . . 80
5.12 Comparison of $SAR_{10g}$ values in the head with helmet of both models for different scenarios at 433 MHz. . . . . 81
5.13 Variation of $SAR_{10g}$ in the head for different power levels and scenarios at 2400 MHz. . . . . 83
5.14 Variation of $SAR_{10g}$ in the head for different power levels and scenarios at 868 MHz. . . . . 83
5.15 Variation of $SAR_{10g}$ in the head for different power levels and scenarios at 433 MHz. . . . . 84
5.16 Variation of $SAR_{10g}$ in the torso for different power levels and scenarios at 2400 MHz. . . . . 85
5.17 Variation of $SAR_{10g}$ in the torso for different power levels and scenarios at 868 MHz. . . . . 86
5.18 Variation of $SAR_{10g}$ in the torso for different power levels and scenarios at 433 MHz. . . . . 86

1 Comparison of $SAR_{1g}$ on head of both models without helmet for different scenarios at 2400 MHz. . . . . 109
2 Comparison of $SAR_{1g}$ on head of both models without helmet for different scenarios at 868 MHz. . . . . 110
3 Comparison of $SAR_{1g}$ on head of both models without helmet for different scenarios at 433 MHz. . . . . 110

4 Comparison of $SAR_{1g}$ on torso of both models for different scenarios at 2400 MHz. . . . . 111
5 Comparison of $SAR_{1g}$ on torso of both models for different scenarios at 868 MHz. . . . . 112

6 Comparison of $SAR_{1g}$ on torso of both models for different scenarios at 433 MHz. . . . . 112

7 Comparison of $SAR_{1g}$ on head of both models with helmet for different scenarios at 2400 MHz. . . . . 113

8 Comparison of $SAR_{1g}$ on head of both models with helmet for different scenarios at 868 MHz. . . . . 114

9 Comparison of $SAR_{1g}$ on head of both models with helmet for different scenarios at 433 MHz. . . . . 114

# List of Tables


2.1 Guidelines of SAR by different standard bodies with their averaging masses of tissues and time . . . . . 17
2.2 Commercially available electromagnetic-field simulators . . . . . 23

4.1 Optimized parameters of the dipole antenna at different frequencies 36
4.2 Overview of Hugo and Tom voxel models used in this study . . . . 37
4.3 Dielectric properties of different human tissues at 433 MHz, 868 MHz and 2400 MHz . . . . . 39
4.4 Summary of all simulation setups for head without helmet, torso and head with helmet. . . . . 68

5.1 Variation of $SAR_{10g}$ in different tissues of the head of Hugo model at different frequencies for open space scenario . . . . . 74
5.2 Variation of $SAR_{10g}$ in different tissues of the torso of Hugo model at different frequencies . . . . . 78
5.3 Variation of $SAR_{10g}$ in head without helmet, torso and head with helmet for different underground mine scenarios and distances at 2400 MHz . . . . . 87
5.4 Variation of $SAR_{10g}$ in head without hemet, torso and head with helmet for different underground mine scenarios and distances at 868 MHz . . . . . 88

1 Chronological record of studies using medical approach. . . . . 106

2 Chronological record of studies using engineering approach. . . . . 108

# Abbreviations

| | |
|---|---|
| **EMR** | **E**lectro-**M**agnetic **R**adiation |
| **SAR** | **S**pecific **A**bsorption **R**ate |
| **ISM** | **I**ndustrial **S**cientific **M**edical |
| **CST MWS** | **C**omputer **S**imulation **T**echnology **M**icro-**W**ave **S**tudio |
| **ICNIRP** | **I**nternational **C**ommission on **N**on-**I**onizing **R**adiation **P**rotection |
| **FCC** | **F**ederal **C**ommunications **C**ommission |
| **IEEE** | **I**nstitute of **E**lectrical and **E**lectronics **E**ngineers |
| **IEC** | **I**nternational **E**lectrotechnical **C**ommission |

# Chapter 1

# Introduction

## 1.1 Introduction

The use of wireless technology has increased drastically due to its diverse applications in daily life, particularly for communication, monitoring and control systems. With the development of wireless technology, more and more communication devices are becoming wireless. A commonly used wireless technology is cellular communication, which is growing enormously worldwide and has attracted the study concerning the exposure of electromagnetic radiation (EMR). A human body absorbs supplementary EMR radiated by a mobile phone throughout the communication. A human head is directly exposed to these radiations which can cause adverse health effects and has thus increased the public concern. Many studies have investigated adverse health effects of these radiations, such as cancer, genetic damage, tumours, DNA defects, memory loss, increased body temperature and immune system problems [1, 2].

The International Commission on Non-Ionising Radiation Protection (ICNIRP) and the Institute of Electrical and Electronic Engineering (IEEE) provide guidelines for the exposure of EMR to humans. The first report of ICNIRP was presented in 1998, which provided the guidelines for electromagnetic exposure for frequencies up to 300 GHz. It is frequently amended with the current literature on possible health risks associated with the exposure of EMR. The specific absorption rate (SAR) is the index parameter used by regulatory bodies to regulate the exposure of EMR for humans. At higher frequencies, the absorption rate of EMR becomes superficial, whereas for lower frequencies, the penetration of EMR

is more deeper.

Underground mining is one of the endeavours of humanity to excavate the minerals from the underground earth and it is important for economy of South Africa [3]. In the last few decades, many causalities of the miners working in underground mines have been reported. Most of the causalities are due to expanded duration of the rescue operation and no communication between the control room and miners, specifically after a disaster.

Communication systems play an essential role in optimizing mining processes and can ameliorate the health and safety conditions in the underground mines. Wired communication systems in underground mines are inconvenient and require expensive maintenance owing to dynamic environment of underground mines [4]. Wireless communication systems have low maintenance cost and are adaptive in nature. In recent years, different wireless communication systems are deployed in the confined environment of the underground mines. Different tracking and monitoring devices are used in underground mines to monitor the vital signs and for rigorous location tracking of the miners. The tracking devices are advantageous for the rescue team, especially to find the accurate location of the trapped miners after a disaster. These tracking devices are based on different architecture of wireless communication such as wireless sensor network, radio frequency identification and wireless local area networks. Recently, wireless sensor network based wearable devices have been proposed to determine the location of the miner in underground mines using different frequencies, i.e. 433 MHz, 868 MHz and 2400 MHz [5]. The impact of different frequencies electromagnetic signals on the health of miner can be distinct due to different characteristics. These tracking devices are suggested to be mounted on the head or torso of the miner for communication in the confined environment of underground mines. Therefore, there is a need to investigate the effect of wearable wireless devices on the body of the miner in underground mines. Moreover, these devices can increase the levels of transmit power when the connection between the two devices is lost. In this scenario, it is critically important to investigate how much power can be increased in underground mines without violating the SAR guidelines. Furthermore, the electromagnetic signals undergo

reflections from the surrounding rocks, walls and roof of the underground mines. The propagation of electromagnetic signal in the confined environment of underground mines mainly depends on the characteristics of the surrounding environment such as type of rocks, surface roughness, and geometry of the tunnel. Some studies have suggested less degradation of electromagnetic signals with respect to distance in tunnels of the underground mines than in the free space environment [6]. It is due to the confined spaces of the underground mines which reflect the electromagnetic signals and thus can travel for a longer distance. Therefore, the miners are exposed to the direct and reflected electromagnetic signals in the underground mines, which can potentially enhance the absorption of EMR by the body of the miners and can cause more adverse health effects than in the open space environment. Consequently, it is crucial to investigate the impact of EMR on the health of the miner before deploying these wearable tracking devices in the underground mines.

In this study, SAR is investigated by numerical modelling of different underground mine scenarios, and using two high-resolution anatomical models at 433 MHz, 868 MHz and 2400 MHz. Different underground mine scenarios similar to the wits mock mine are modelled for wearable devices at different frequencies. The SAR values are then compared for open space and underground mine scenarios for head without helmet, torso and head with helmet scenarios. The EMR exposure at different frequencies recommends the safer frequency in terms of SAR that can be used in underground mines. Recommendations based on minimum SAR values are also provided for the better place to mount these wearable devices on the body of the miner in underground mines. The variation of SAR values are also investigated for maximum power levels and different distances between the miner and boundaries of the underground mine. Finally, the recommendations based on SAR values are provided for maximum power levels that can be used in case of no communication with a miner after a disaster.

## 1.2 Classification of Radiations

All the wireless devices use different types of EMR to communicate with each other using air and vacuum medium. The propagation of the electromagnetic fields from the source results in EMR. When these fields interact with different materials, the impact of EMR on atoms and molecules of those materials depends on the properties of the material such as permittivity, conductivity and density. Similarly, when electromagnetic fields interact with the human body, the radiations are reflected and absorbed by the human body depending on the properties of the exposed human organs. The absorbed radiations cause the motion of the atoms and molecules present inside the human body which results in heating.
The classification of electromagnetic spectrum and their possible health hazards are shown in Fig. 1.1. Based on the energy levels and interaction with the human body, EMR has been divided into two categories of 1) Non-Ionizing Radiations and 2) Ionizing Radiations. Non-ionizing radiations are referred to as low frequencies and low power radiations. These radiations do not have adequate energy to affect at the atomic level and have insufficient energy to damage the human tissues. However, recently, increasing evidence suggests that non-ionizing EMR have the potential to cause biological effects in the human body [7]. In everyday life, the use of a mobile phone has increased exponentially, and has increased the public concerns about the exposure of EMR. Non-ionizing radiations include the extremely low frequencies (ELF), very low frequencies (VLF), radio frequencies (RF), Microwave and Infrared radiations [2]. Ionizing radiations usually have high frequencies and contain sufficient energy to exert a force on polarised molecules, and free moving electrons and ions present in the human body. The ionizing radiations causes the polarised molecules to rotate and free electrons to move as a current. Gamma and X-rays are ionizing radiations; these rays creates free-radicals in the body when the body is exposed to them even for a few seconds [8].

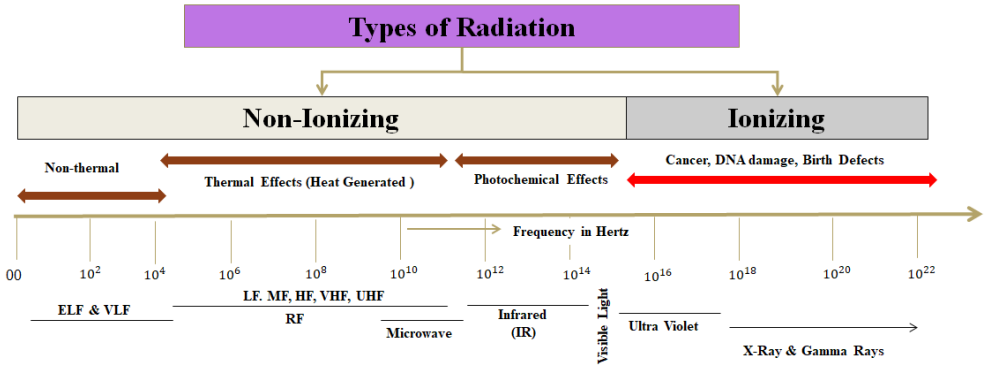



FIGURE 1.1: Classification of radiations in electromagnetic spectrum and associated health risks.

### 1.2.1 Possible Health Effects of Non-Ionizing Radiations

In recent literature, adverse health effects of Non-ionizing EMR has been reported [7, 9, 10]. Different medical journals have reported potential risks linked to the exposure of non-ionizing EMR in humans, such as the risks of cancer, reproductive dysfunction, central nervous system disorders. The health effects associated with EMR exposure are frequency-dependent. Therefore, at different frequencies, different health risks have been observed. Possible health effects linked to EMR exposures are described below:

1. **Brain Tumor and nervous system:** For long-term exposure, the current guidelines used for non-ionizing EMR exposure may still carry risks for brain tumours and nervous system defects. Alzheimer's disease, Parkinson's disease, and motor neuron diseases have studied during EMR exposure [7, 9]. Due to Alzheimer's disease, defect in the structure of a neuron and progressive loss in neuron function occur in the brain. In Parkinson's disease, a long-term degenerative disorder of the central nervous system occurs. The effects of both diseases are irreversible and have only temporary treatment.

2. **Breast Cancer:** It is suggested that if the human chest is exposed to EMR, the cancer cells grow faster [7]. Similarly, it has been investigated that animal breast cancer and tumours are sensitive to EMR exposure. Reduction in EMR exposure can thus reduce the effect of breast cancer in humans.

3. **DNA Damage:** Some studies reported DNA damage in rats exposed to low-intensity of magnetic fields [10]. It was concluded that the exposure to a 60 Hz magnetic field increases the free radial formation in brain and causes DNA strand breaks and cell death.

4. **Stress Response:** EMR causes damage to the tissues by heating, but at lower safety limits, it is sufficient to cause cell damage. The molecular damage activates the stress response in the body, which can lead to headache, dizziness, depressive symptoms, and difficulty in focusing [10].

## 1.3 Research Questions

In underground mines, miners are exposed to EMR within the confined environment, which may exceed the recommended guidelines of electromagnetic exposure and can cause harmful health effect for miners. In the concerned literature, to the best knowledge of the author, no study has been reported to observe the effect of electromagnetic signals on miners in underground mines, especially for wearable devices. The exposure to EMR in the confined space environment of underground mines has not been investigated. Therefore, it is vital to investigate the effect of EMR in the underground mine using a similar methodology used in recent studies for different wireless applications in the open environment.
The main research question addressed in this research is: ***What is the health impact of electromagnetic radiations in term of specific absorption rate when the wearable devices are mounted on the body of the miner in underground mines?***
Concerning this question, it is required to investigate the following sub-questions:

1. What is health impact in terms of SAR for a selected set of commonly used frequencies in wearable devices in an underground mine?

2. Between head and torso, which is a better location on the body of the miner to mount the concerned wearable device, with respect to the SAR impact?

3. What is the health impact in terms of SAR if the concerned wearable device is mounted inside or outside of the safety helmet of the miner in an underground mine?

4. In case of a disaster, how much increase is possible in the transmit power level of these wearable devices without causing serious health concerns in terms of SAR, when the connection is lost with the miner especially after a disaster?

After a disaster, it is required to evacuate the trapped miner quickly. In this case, it is crucial for a rescue team to rescue all the miners present in the underground mine without any fatalities. For this short duration of time, the communication between the trapped miner and the rescue team is critical than the long term effects of EMR exposure. During this time, the power levels of the devices can be increased for better communication which implies a higher electromagnetic exposure to the miner. Therefore, it is critical to investigate how much power level can be increased without violating the SAR limits in underground mines.

## 1.4 Objectives of the Research

The objectives and sub-objectives of this research are as follows:

1. To evaluate the health impact on human head at different frequencies commonly used in wearable devices.
    - To model electromagnetic source for all frequencies commonly used in wearable devices in underground mines, i.e. 433 MHz, 868 MHz, and 2400 MHz.
    - To model the underground mine scenario for head without helmet.
    - To perform SAR analysis for all frequencies.
2. To find a better location on the body, between head and torso, to mount these wearable devices.

- Analysis of SAR on torso for all frequencies in underground mines.
- To provide a recommendation of a better location amongst head and torso whether the SAR values will be minimal.

3. To evaluate SAR based impact of safety helmet in an underground mine.
   - To model the safety helmet in an appropriate electromagnetic analysis software.
   - To compare SAR impact on the miner for wearable devices, with and without a safety helmet in underground mines.
4. To evaluate maximum power level that should be allowed after a disaster in the underground mine.
   - Analysis of SAR at different power levels for head and torso.
   - To provide a recommendation, based on SAR impact, for a maximum power level that can be used after a disaster to communicate without causing health damage to the miner.

## 1.5 Thesis Outline

***Chapter 2*** provides an overview of the concepts required for the SAR studies, particularly in underground mines. In the first section, types of communication devices used in underground mine communication are explained briefly. Relevant electromagnetic quantities are briefly explained in the next section. The SAR guidelines provided by the standardisation bodies for the safe exposure of EMR are also discussed. Then, the overview of the numerical techniques used in evaluation of SAR is described in detail. In last, the standard procedure for the numerical computation of SAR is explained. It assists to validate the SAR analysis in humans for underground mines.

***Chapter 3*** elaborates the current literature and methodologies used for the SAR evaluation. This chapter also classifies the literature based on the research methodology used in numerous studies. The current literature of classified medical and

engineering approaches has been described. Lastly, a critical analysis of literature and factors affecting the variation of SAR is explained briefly.

***Chapter 4*** illustrates the proposed research methodology. This chapter explains the methodology to model the electromagnetic sources, underground mine scenarios and hard helmet used in the evaluation of SAR in this study. It also explains the voxel based high-resolution human models used in this research. In this chapter, the simulation setups for human head without helmet, torso and head with helmet, and variable power levels and distance for open and underground mine scenarios are described.

***Chapter 5*** provides the analysis of results for all the simulations scenarios. The results for open space and different underground mine scenarios are compared for both the human models in order to investigate the difference in the exposure level. Two different models were used to validate the investigation of SAR, and it also provides analogy for human body of different sizes and masses. Similarly, for head without helmet and torso, SAR analysis provides the recommendation in terms of SAR for the better location to mount wearable devices on body of the miner. An investigation is conducted for maximum power levels which can be used in case of a disaster for short duration of time in underground mine scenarios without contravening SAR guidelines. Finally, an analysis of SAR for varying distance with both voxel models is provided.

***Chapter 6*** highlights the conclusion of the study and includes future research directions that can be used for further investigation.

# Chapter 2

# Background Review

In this chapter, concepts related to this research are discussed in detail. In section 2.1, the feasible wireless communication systems used in underground mines will be discussed in brief. Section 2.2 briefly explains the electromagnetic quantities related to exposure of EMR. In section 2.3, the guidelines of SAR prescribed by standardised bodies are explained. Lastly, in section 2.4 different techniques for numerical computation of SAR and standard procedure for numerical simulations has been explained.

## 2.1 Communication in Underground Mines

Mining can be defined as *an excavation in the earth to extract different minerals* whereas mining engineering is an occupation and industry to extract minerals from the earth. According to the extraction methods used in mines to extract different minerals, mining can be divided into two groups: 1) Surface (strip) mining, and 2) Underground mining. In surface mining, both the machinery and people work on the ground surface, whereas in underground mining, the work is to be done under the surface of the ground. Underground mining can be further divided into sub-groups depending upon the access methods, such as shaft, slope and drift mining [11]. In underground mining, emergency operations are needed to be continued in an uncertain environment such as vehicle accidents, toxic gases, fire explosions, and in floods. These fatalities make difficulties for emergency response teams to respond more quickly in underground mines. In such scenario, communication in underground mines plays a vital role to locate and communicate with the trapped

miners. In underground mines, communication is also crucial for other day-to-day operations to increase the productivity of the mining process. Extraction and moving of mineral products, control and remote monitoring operations are carried out only with the aid of communication. Based on environmental characteristics and transmission methods, the communication in the underground mine can be divided into two main categories 1) wired, and 2) wireless communication as shown in Fig. 2.1. These communication systems are further divided into subgroups depending on the mode and application of communication. Due to the harsh environment of the mines, the devices used for communication in underground mines should be capable of operating in broad temperature ranges, immune to dust and high moisture, small and light in weight [11].

The dynamic structure of underground mining introduces a change in radio propagation characteristics of wireless communication as the propagation of radio signals are susceptible to its surrounding environment.

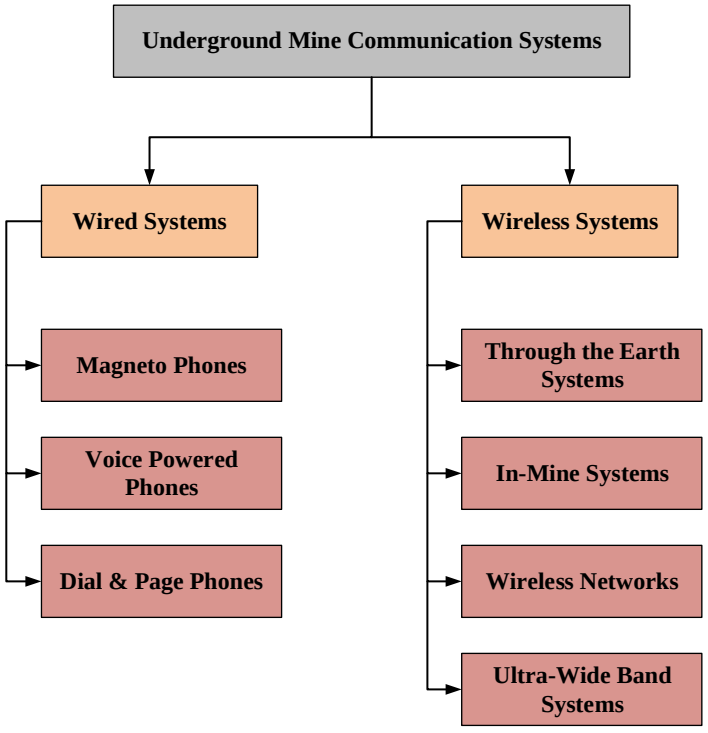



FIGURE 2.1: Classification of underground mine communication systems.

### 2.1.1 Wireless Communication Systems

In the underground environment, the behaviour of the radio signal is very unpredictable as compared to a typical above-ground environment. Therefore, it is essential to investigate the behaviour of the signal before deploying wireless communication system in underground mines. Generally, the structure of underground mines is not uniform due to the tunnel geometry. Similarly, the ceiling of the tunnel may be supported by pillars, and the ceiling generally consists of a rough surface of different materials. Thus, it is vital to deploy a communication system which has to cover the entire working space in order to communicate with workers especially in emergency conditions [11]. Wireless communication systems for underground mines are generally divided into the following types:

1. *Through-the-Earth communication:* Through-the-Earth systems can provide wireless communication in underground mines. Through-the-Earth systems are more suitable to underground explosives with less infrastructure than the typical communication systems. These systems operate at lower frequencies, usually less than 4 kHz (wavelength in thousandth of meters). The signal is transmitted vertically through the earth or horizontally in the tunnel. The half-duplex mode provides communication between the miner and surface of the earth. This communication provides voice, text or periodic beacon signal, which allows the rescue team to estimate the location of the miner. Through-the-Earth communication is affected by a number of factors such as transmitter power, frequency, the electrical properties of the overburden (rocks between the underground tunnel and ground surface) and its geological variations. The transmitted signal is also affected by the electrical noise, made by human-made and natural sources. Therefore, performance of system depends upon received power of signal, after attenuation of received power of signal through the earth. A large loop antenna can be used to transmit signal through the overburden, and a small loop antenna is used inside the mine. The signal reception depends upon the coupling between antennas, the surface and underground antenna [12]. In South Africa, the

first Through-the-Earth system was deployed successfully in 1946 [13]. This system was operating at 100 kHz and 350 kHz to transmit a signal to a distance of 6000 ft in the mine where the miner was wearing a helmet with a built-in loop antenna.

2. *In-mine Communications:*, A complete underground mine communication systems should also be able to communicate within the galleries of the mine. The propagation of the radio signal in mine tunnels can be investigated using two approaches 1) Theoretical Channel Modelling, and 2) Empirical Channel Modelling. The surface of the mine tunnels is rough and non-uniform, which requires a modelling for a better understanding about the propagation of the signal. Different methods are investigated to measure the wave propagation in the mine at 200 MHz, 415 MHz and 1000 MHz [14].

3. *Wireless Networks used in mines:* Wireless networks are divided into two subgroups 1) based on infrastructure, and 2) without infrastructure. Wireless local area network is example of a network with infrastructure, whereas, ad-hoc networks can be deployed without any infrastructure. Wireless local area network has been used for underground mine communication using different frequencies such as 900 MHz and reported in [15].

4. *Ultrawideband Systems:* Ultrawideband systems are defined as systems occupying a fractional bandwidth of more than 20% or 500 MHz absolute bandwidth. These systems are based on the low power very narrow pulses which result in high data rates. In underground mine communication, the Ultrawideband systems are used for location and tracking applications. These systems have a large bandwidth which provides precise distance measurement between the transmitter and receiver [16].

5. *Wireless Sensor Networks:* In an underground mine, different wireless sensor networks are deployed to track the accurate location of the miner. These systems are comprised of one central node, and other nodes are carried by the miners. The devices are mounted on the body of the miner. Different

systems were proposed for wireless sensor network at different frequencies [5].

## 2.2 Overview of Electromagnetic Quantities

It is essential to understand the concept of fundamental quantities used in the evaluation of SAR. The quantities relevant to the evaluation of SAR are explained briefly below:

1. *Conductivity* is the ratio of the magnitude of the conduction current density to the strength of the electric field in a particular medium. It is represented as $\sigma$, and its unit is siemens per meter (S/m).

2. *Relative permittivity* is the ratio of the complex permittivity to the free space permittivity. The expression of relative permittivity ($\epsilon_r^*$) [17] is given as

$$\begin{aligned} \epsilon_r^* = \epsilon_r^{'} - j\epsilon_r^{''} = & \quad \epsilon_r^{'} - j\frac{\sigma_t}{\omega\epsilon_o}, \qquad \text{in general} \\ = & \quad \epsilon_r^{'} - j\frac{\sigma_c}{\omega\epsilon_o}, \qquad \text{for low frequencies} \end{aligned}$$

$$\sigma_t = \sigma_c + \sigma_d$$

$$where, \quad \sigma_d = \omega\epsilon_{0\epsilon_{rd}^{''}}$$

   where, $\epsilon_o$ is the free space permittivity ($8.854 \times 10^{-12} F/m$), $\epsilon_r^{'}$ is the real part of relative permittivity, $\epsilon_r^{''}$ is the imaginary part of relative permittivity, $\sigma_t$ is the total conductivity in siemens per meter (S/m), $\sigma_c$ is the ionic conductivity, $\sigma_d$ is the dipole conductivity, $\sigma_{rd}^{''}$ is the dielectric loss and $\omega$ is angular frequency.

3. *Permeability* at any point is the ratio of the magnetic flux density to the magnetic field strength. The unit of permeability is Henry per meter (H/m).

4. *Penetration depth* is defined as the depth at which the electric field strength of an incident plane wave penetrates into a lossy medium for a given frequency. The penetration depth $\delta$ [18, 19] can be written as

$$\delta = \frac{1}{\omega}\left[\frac{\mu_0 \epsilon_r^{'} \epsilon_0}{2}\left(\sqrt{1+(\frac{\sigma}{\omega \epsilon_r^{'} \epsilon_0})^2}-1\right)\right]^{-\frac{1}{2}} \tag{2.1}$$

where, $\omega$ is the angular frequency, $\mu_0$ is the permeability of free space, $\epsilon_r^{'}$ is the relative permittivity, $\epsilon_0$ is the free space permittivity and $\sigma$ is the conductivity of the medium.

5. *Electromagnetic Field* is a time-varying field associated with electric and magnetic forces described by Maxwell's equations. It can be expressed as scalar or vector as a function of space and time.

6. *Antenna* is a part of transceiver system used to radiate and receive electromagnetic waves. It is designed to radiate and receive electromagnetic waves at particular frequencies or band of frequencies.

7. *Near-field region* is the region located near in the field of the antenna, in which angular field distribution is dependent upon the distance from the antenna. This region may not exist for the antenna which has a maximum dimension not larger compared to the wavelength. The outer boundary for the near-field of the antenna is taken to be distance $R < \frac{2D^2}{\lambda}$ [20].

8. *Far-field region* is a region of the antenna where the electric and magnetic field has substantial plane-wave characteristics. The region with a distance $R > \frac{2D^2}{\lambda}$ is referred to as a far-field region of the antenna. In this region, angular field distribution is independent of the distance from the antenna.

9. *Antenna Reflection Coefficient* provides the relation between output of transmitter and input of antenna usually knows as S-parameters. When the voltage or current signal is applied to the port, the reflection coefficient explains the power transmitted to the structure of the antenna and the mismatch between the port and the antenna structure, which reflects the power to the

signal source. The $S_{11}$ parameter provides information about the forward power to the antenna structure and bandwidth of the antenna. The lower and upper frequencies at which the $S_{11} < -10\ dB$ is regarded as a bandwidth of the antenna. If $S_{11} = 0\ dB$, all the power is reflected from the antenna structure, and subsequently no power is radiated. If $S_{11} = -10\ dB$, it implies that if 3 dB of power is transmitted to the antenna structure then -7 dB of power is the reflected [21].

10. *Specific Absorption Rate (SAR)* is the measure of the energy absorbed by the human body when it is exposed to the EMR. The expression that describes SAR in term of an electric field can be expressed as [22]:

$$SAR = \frac{\sigma \cdot E^2}{2\rho} \tag{2.2}$$

where, $\sigma(S/m)$ represents conductivity of the material exposed to exposure, $\rho$ $(kg/m^3)$ represents the density of the material and $E(V/m)$ represents the electric field strength. From Eq 2.2, it can be observed that the absorbed electromagnetic energy is proportional to the square of the electric field strength and the conductivity of the material and inversely proportional to the density of the material.

**Note:** The evaluation of SAR for tissues can be for a mass of 10g, 1g or any custom value. The SAR value averaged with 10g of tissue (with cubical shape of volume) is referred as $SAR_{10g}$ whereas SAR value averaged with 1g of tissue (with cubical shape of volume) is referred as $SAR_{1g}$.

11. *Peak spatial-average specific absorption rate* is the maximum average SAR value within a local region (any human organ under observation) based on a specific average volume. It is written as $SAR_{10g\ peak}$ and $SAR_{1g\ peak}$ for 10g and 1g averaged volume, respectively.

12. *Whole body average specific absorption rate* is calculated as power absorbed in the entire body divided by its total mass. It can be written as $SAR_{WB}$.

## 2.3 Guidelines of Specific Absorption Rate

Different guidelines for non-ionizing radiations were prescribed by different regulation bodies such as Federal Communication Commission (FCC), Institute of Electrical and Electronics Engineers (IEEE) and International Commission on Non-Ionizing Radiation Protection (ICNIRP). These guidelines are based on the current literature available to observe the effect of electromagnetic signals on human health. The IEEE [23] and ICNIRP [8] guidelines incorporate the SAR averaging with 10g cubic volume of tissues, whereas the FCC [24] standard averaging the SAR with 1g cubic volume of tissue. Therefore, the FCC and ICNIRP standards cannot be compared for SAR limits as both standards have a different averaging mass of the tissue. It is remarkable to specify that the volume of tissues used to average the SAR value has a significant influence on the SAR values. The prescribed limit of peak spatial $SAR_{1g}$ by FCC is 1.6 W/Kg, whereas the prescribed limit of peak spatial $SAR_{10g}$ by IEEE and ICNIRP is 2.0 W/Kg. Most of the countries are using the ICNIRP and IEEE C95.1 [25] guidelines to protect humans from electromagnetic exposure. There are no guidelines provided by any standardisation body for the exposure of EMR in any confined environment, such as underground mines. Therefore, in this dissertation, the SAR limits provided by IEEE C95.1 and ICNIRP will be followed for the evaluation of SAR on humans in underground mines. Table 2.1 summarises the SAR limits prescribed by standardized regulatory bodies.

Table 2.1: Guidelines of SAR by different standard bodies with their averaging masses of tissues and time [26]

| Standard bodies | SAR (W/Kg) | Averaging Mass (g) | Averaging Time (min) |
|---|---|---|---|
| IEEE C95.1 [25] | 2 | 10 | 6 |
| ICNIRP [8] | 2 | 10 | 6 |
| FCC [24] | 1.6 | 1 | 30 |

## 2.4 Computation of Electromagnetism

In recent years, a wide range of applications in the propagation of the electromagnetic wave has led to the development of a large number of numerical techniques for modelling of electromagnetic wave and propagation [27]. All the numerical techniques have advantages and drawbacks depending on the applications. The existing and emerging numerical techniques are summarised in [28] with their drawbacks and advantages. Most of the software packages used for numerical simulation of electromagnetism is based on the following numerical techniques:

1. Finite Element Method (FEM);
2. Method of Moments (MoM);
3. Finite-Difference Time-Domain Method (FDTD);
4. Finite Integration Technique (FIT).

The following sections explain the FEM, MoM and FDTD briefly, whereas FIT is explained in detail since it is used in this thesis for evaluation of SAR on humans in underground mines.

### 2.4.1 Finite Element Method

Finite Element Method is used to find the approximate solution of a partial differential equation and integral equation, and was initially proposed by Courant in 1943 [29]. This method has been used in waveguide problems, microstrips and absorption of EMR by biological bodies. The partial differential equations are eliminated by rendering the partial differential equation into an ordinary differential equation in order to provide the solution. Finally, the standard techniques are used to solve the equation. Finite element method is preferred for solving the partial differential equations for complex domains, specifically when the precision varies over the entire computation domain. It comprises four steps to solve any problem [30]:

1. Discretisation of the region into a finite number of sub-regions or elements;
2. Deriving governing equations for a typical element;
3. Assembling of all the elements in the solution region; and
4. Solving the system of the equation obtained.

### 2.4.2 Method of Moments

The method of moments is the first full-wave numerical method used for antenna applications and electromagnetic compatibility. In the last few years, the drastic increase in the computation power has reduced the importance of method of moments, but it still provides advantages for certain structures such as metal objects and wires. This method is used to solve linear partial differential equations by formulating as integral equations. The procedure to apply the method of moments comprises of the following four steps:

1. Derivation of the appropriate integral equations;
2. Conversion of the integral equations into a matrix equation using basic weighting functions;
3. Evaluation of the matrix elements;
4. Solving the matrix equation and obtaining the parameter of interest.

### 2.4.3 Finite-Difference Time-Domain Method

The finite difference time domain method is a popular technique for computational electromagnetic modelling such as evaluation of SAR. It is easy to understand and implement in different software packages used for the computation of electromagnetism. A wide range of frequency problems can be solved in a single run due to the time-domain characteristics of the method. This method provides a direct

solution of Maxwell's curl equations. The following steps are applied in the finite difference time domain method to solve the electromagnetic problem:

1. Maxwell's equations are modified to central difference equations and discretise in the software;
2. The leapfrog manner [31] is followed to solve the equation for the electric and then the magnetic field at a given instant in time;
3. This process is repeated over and over for the whole simulation domain.

The finite difference time domain technique has some limitations for its suitability to handle complex problems.

### 2.4.4 Finite Integration Technique

Finite integration technique was developed by Weiland in 1977 [32], it discretises the integral form of Maxwell's equations rather than the differential form. The resulting matrix equations can be used for efficient numerical simulations on the computer. The finite discretisation of the volume for Maxwell's equation depends on the usage of integral balances which proves the stability and conservation of the discrete fields before starting the numerical simulations. The discrete formulation enables the development of long term stable numerical time and accurate eigenvalue solvers. By starting with a general cell-based approach to spatial discretisation, it is obvious that the finite-integration theory is not restricted to the three-dimensional cartesian meshes. It provides consideration of all type of coordinate meshes [33].

In Faraday's law, in the integral form (Fig. 2.2, Equation A), the unknowns are electric voltages and the magnetic fluxes denoted by **e** on the edge of discretisation mesh and **b** on the mesh faces, respectively. To discretise (Equation A) on a mesh face, it is clear that the left-hand side of (Equation A) encompasses a line integral of the electric field whereas the right-hand side is a time derivative of the magnetic flux through the face. These integrals can be represented as an algebraic sum of

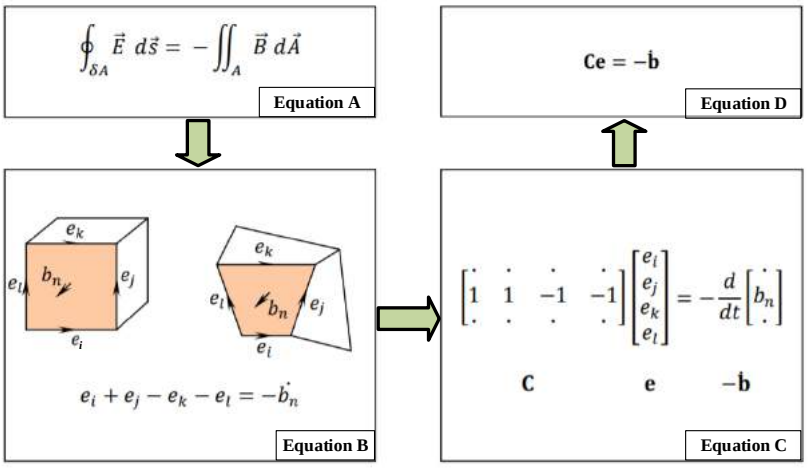



FIGURE 2.2: Discretisation of Faraday's law using finite integration technique.

the edge unknowns.

No supplementary equation discretisation error is involved when passing from the continuous to its discrete form for any fixed mesh with a space discretisation error. Alternatively, the passage from (Equation A) to (Equation B) depends on the mathematical properties of the integral. Contrarily, an equation discretisation error will exist when discretising the material property relations. By organizing the +1 and -1 coefficients of the algebraic sum into a matrix $\mathbf{C}$, and the electric and magnetic unknowns in vector $\mathbf{e}$ and $\mathbf{b}$, respectively, a matrix form results, similar to the differential form of Faraday's law i.e. $\nabla \times \overrightarrow{E} = -\dot{\overrightarrow{b}}$.

In the same manner, all Maxwell's equations can be discretised with the FIT to return the discrete counterparts with a matrix form [32]. The discrete curl operator ($\mathbf{C}$) and the discrete divergence operator ($\mathbf{S}$) are topological matrices, containing 1, -1 and 0 entries. The finite element method uses the same form to discretise Maxwell's equations [34]. The discretisation of Maxwell's integral

equations are given as:

$$\oint_{\partial A} \overrightarrow{E} \cdot d\overrightarrow{S} = -\frac{\partial}{\partial t} \iint_{A} \overrightarrow{B} \cdot d\overrightarrow{A} \qquad \mathbf{Ce} = -\mathbf{b} \qquad (2.3)$$

$$\oint_{\partial A} \overrightarrow{H} \cdot d\overrightarrow{s} = \iint_{A} \left( \frac{\partial \overrightarrow{D}}{\partial t} + \overrightarrow{J} \right) \cdot d\overrightarrow{A} \qquad \tilde{\mathbf{C}}\mathbf{h} = \dot{\mathbf{d}} + \mathbf{j} \qquad (2.4)$$

$$\oiint_{\partial V} \overrightarrow{B} \cdot d\overrightarrow{A} = 0 \qquad \mathbf{SB} = \mathbf{0} \qquad (2.5)$$

$$\oiint_{\partial V} \overrightarrow{D} \cdot d\overrightarrow{A} = Q \qquad \tilde{\mathbf{S}}\mathbf{d} = \mathbf{q} \qquad (2.6)$$

It is also the mathematical base for simulation software CST MICROWAVE STUDIO® (CST MWS) [35].

### 2.4.5 Commercial Software Packages for Computation of Electromagnetic

With the development in the computation power of computers and software, a variety of electromagnetic simulation software is commercially available. All the software have not the same capabilities and performance, and suitable for a particular type of problem. The critical factors for the selection of proper simulator for a particular type of problems are accuracy, setup time and speed of execution. Table 2.2 shows the different well-known commercial simulators for electromagnetic field analysis with their numerical methods, applications and providers. In this study, CST MWS has been used for the numerical computation of SAR on humans in underground mines.

### 2.4.6 IEEE Standard for Numerical Simulations of SAR

The numerical evaluation and measurements of SAR comprise different standard procedures to be followed for accurate investigation of SAR on human bodies. For this, IEEE presents different standards according to the methodology used for the investigation of SAR. The IEEE and International Electrochemical Commission

Table 2.2: Commercially available electromagnetic-field simulators

| Simulator | Method | Type | Provider |
|---|---|---|---|
| CST MWS | FIT | Time domain | CST Computer Simulation technology AG. |
| HFSS | FEM | Frequency domain | ANSYS Inc., USA. |
| HyperLynx | FDTD | Time domain | Zeland Software Inc. |
| FEKO | MoM/ FEM/ FDTD | Frequency domain | EM Software & Systems -S.A. (Pty) Ltd. |
| SEMCAD | FDTD | Time domain | Schmid & Partner Engg. AG (SPEAG), Switzerland. |
| XFdtd | FDTD | Time domain | Remcom (USA) State College,PA. |

(IEC) contributes to preparing standards for the numerical simulation of SAR on the human body. The IEC/IEEE 62704-1 standard prescribes the methodology for the application of finite difference time domain (FDTD) technique to evaluate the spatial average SAR in the human body for the exposure of EMR from wireless communication devices [23]. It describes the methods to validate the numerical model and estimate its uncertainty for evaluation of SAR with numerical simulations. It also explains the SAR averaging procedure in the voxel for SAR simulations. Most of the electromagnetic simulators follow these standard procedures during the numerical simulation of SAR. In this dissertation, CST WMS software is used for the numerical simulation of SAR on humans in underground mines. It implements finite integration technique to evaluate the SAR. On the cartesian grid, the finite integration technique is equivalent to the finite difference time domain technique [36].

CST WMS simulator has different SAR averaging standards such as IEC/IEEE 62704-1 [23] and IEEE C95.3 [25] etc. Different studies used IEC/IEEE 62704-1 averaging method to investigate SAR with CST WMS EM simulator. Therefore, in CST WMS, IEC/IEEE 62704-1 standard is used for averaging of SAR in this thesis. The IEC/IEEE 62704-1 standard describes the minimum distance between the antenna and biological tissues should be 10mm, and maximum distance should

be less than 200 mm. It also describes the maximum mesh resolution for simulation should be 1/10 of the wavelength of the higher frequency under observation and other standard parameters for the numerical simulations of SAR. In this dissertation, all standard recommendations provided by IEC/IEEE 62704-1 standard have been followed in numerical simulation of SAR using CST WMS simulator for different underground mine scenarios.

# Chapter 3

# Literature Review

In this chapter, the current literature related to the effects of non-ionizing radiations on human health is discussed. Section 3.1 explains the classification of literature based on the methodology used in past research studies. The literature using medical and engineering approach is explained in section 3.2 and 3.3, respectively. In section 3.4, the current literature and impact of different parameters on exposure to EMR is concluded.

## 3.1 Classification of Literature

Many studies have been published to investigate health risks associated with the effects of EMR. Several studies have been conducted to observe the effects of EMR on specific body parts/ organs such as head, torso, fingers, eyes and ears or the whole human body with different poses. Due to the ethical issue of the exposure of EMR on the human body, different models of humans and animals have been used in many studies. All these human models are identical to the anatomy of the human body. Based on the methodology used in the research for the assessment of associated health risks, the literature can be divided into two groups as 1) medical approach, and 2) engineering approach. In the medical approach, most of the researchers are from medical and other science fields, and such studies use different surveys, questionnaire, epidemiological studies and experimentation on tissues or animals. In the engineering approach, most of the researchers have an engineering background. Such approaches uses the numerical modelling to evaluate the exposure of EMR using different human models and parts of the human body,

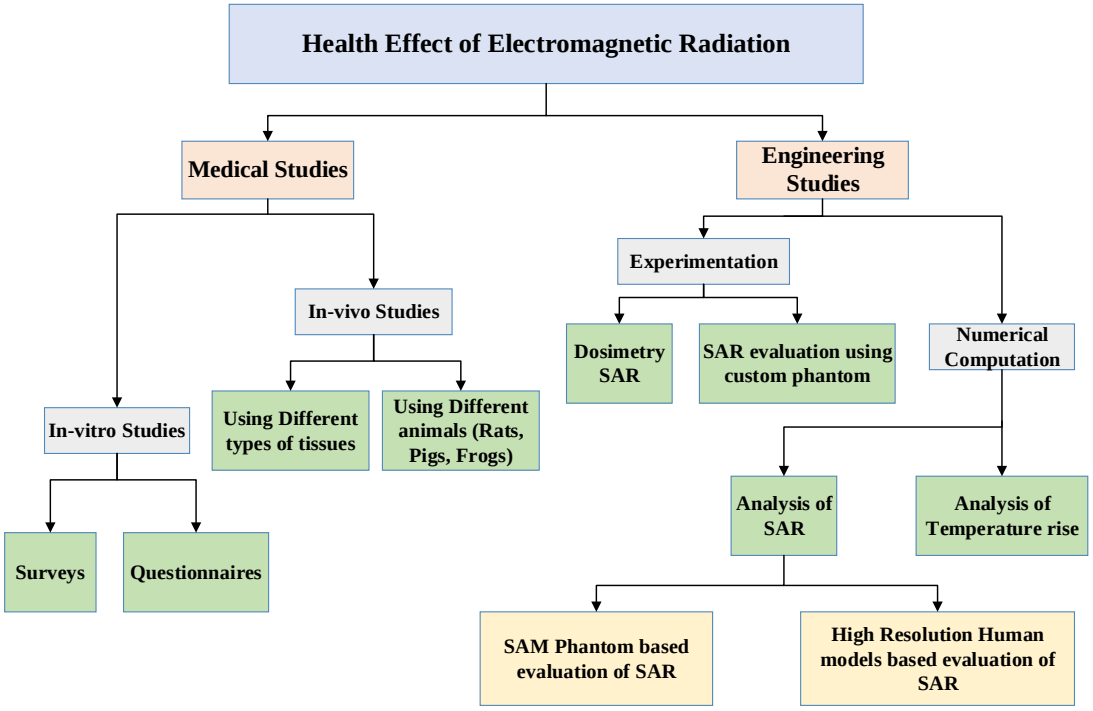



FIGURE 3.1: Classification of the literature based on different methodologies used to study the impact of electromagnetic radiations.

and standard experimentation of SAR using conservative human models. The classification of literature based on different approaches is shown in Fig. 3.1. In this study, the engineering approach has been used to evaluate the exposure of EMR by numerical computation of SAR with high resolution human models.

## 3.2 Medical Approach

The medical approach imitates the methodology of in-vitro and in-vivo studies to summarise possible potential health risks of EMR on humans, as shown in Fig. 3.1. In in-vitro studies, different types of surveys, clinical examination and questionnaires are used to predict associated health risk of EMR, which in general, provide insufficient evidence for certain serious health risks. In in-vivo studies, experiments are conducted on different types of human tissues and animals. All the animals with an anatomy similar to human anatomy can provide relative health risks associated with EMR. In epidemiological studies, the individuals are divided into two groups, and both groups have the same analogy with each other except

one particular condition such as one group is exposed to EMR. However, the other group is a control group which is not exposed to EMR. Many studies have been conducted using different types of live tissues in the test tube and exposed to the EMR. After the exposure, different clinical tests were performed to evaluate possible health risks.

Similarly, in many in-vivo studies, experimentation has been performed on different animals or human organs after the exposure to EMR with different frequencies and time duration [37, 38]. These type of studies concluded clear evidence of adverse health effects associated with EMR exposure [39, 40]. Several studies concluded the effect of EMR on pigs, rats and tadpoles as these animals have the same anatomy with the human body. The possible health risks identified in these studies are cancer, leukaemia, miscarriage, genotoxic effects, neurological and neurodegenerative diseases, immune system, allergic problems, cardiovascular effects and inflammatory responses [7]. In Appendix A, Table 1 shows some studies using the medical approach to assess the health risks associated with EMR.

In [37], the mice were exposed to the electromagnetic signals of 5 GHz with different radiated power for 60 days. In-vivo approach was used to determine the effects of EMR to the mice. It was concluded that the EMR have harmful effects on the physiological and reproductive system of the mice. In [1], the research methodology was based on a survey by taking interviews of different doctors and radiologists. The results show that wireless devices such as mobile phone, bluetooth devices, laptops and wireless router affect human health by a factor which was quantified as 96%, 32%, 54% and 20%, respectively. In [41], long term exposure was evaluated on rats to observe the effects of GSM-900 on cognition function. Two groups of rats were used in which one group was exposed to electromagnetic signals, and the second group was a control group which was not exposed to the electromagnetic signals. A memory test was performed on rats of both groups to evaluate the effect of EMR. The result suggested a significant reduction in memory functions of rats exposed to EMR. In [42], the effect of EMR on Blood-Brain Barrier (BBB) in Fisher 344 rats of both sexes was evaluated by sectioning the group of rats exposed to electromagnetic signals. The rats were exposed to two types of

electromagnetic signals, i.e. a continuous wave of 915 MHz and a pulsed wave with different power levels from 0.001 W to 10 W, and with various time intervals from 2 min to 960 min. The results showed that there was less effect on the groups of rats which were exposed to the pulsed wave than those exposed to the continuous wave signal. In [43], an experiment was performed on eggs and tadpoles of the common frog for an exposure duration of two months. One group of tadpoles was exposed to EM signals, and the other group was enclosed in a Faraday cage as a control group. It was observed that the growth rate in the exposed group of rats was not similar than the control group of rats.

In [39, 44], it was reported that the breakage of DNA double-strand structure is frequency dependant when exposed to GSM and UMTS signals. In [40], the breakage of DNA double-strand in brain cells was reported when 2450 MHz signal with 50 Hz modulation was exposed to male rats for 2 hours/day, for 35 days. The rate of breakage of DNA double-strand structure was significant in the exposed groups of rats than the control group of rats.

## 3.3 Engineering Approach

In the engineering approach, different human models have been used to observe the distribution of SAR in different layers of the human body at different frequencies and for different scenarios. Various computational techniques has been used to simulate these human models in different scenarios such as indoor and open environment, e.g. for a passenger sitting in a bus. In some studies [45–47], new measurements methods were presented to measure the SAR and comparison with the different numerical techniques was performed using different human voxel models. The human body is composed of different types and layers of tissues, bones and cells, which makes it very complicated and thus mostly it is resorted to perform a numerical simulation (also prone to error) for electromagnetic analysis than the standard experimentation which only provide conservative analysis. It is quite challenging to build an exact human model to get the best results for EMR exposure which should be equal to the actual electromagnetic exposure. Even if

an approximate model of the human body is obtained, it is troublesome to measure SAR within thicker parts of the human model where skin layers are a few millimetres thick. In Appendix B, Table 2 summarises some of the research papers which use the engineering approach to observe the SAR distribution for different applications.

In [48], the influence of the metallic structure of a car body frame on the SAR produced by the cell phone was analysed. The variation of SAR was analysed by placing a human body model at different locations inside the vehicle. Finite difference time domain technique was used in the simulation for modelling of the whole system. The $\lambda/2$ dipole excitation source was modelled at 835 MHz located as a handheld device and hands-free device. The CAD file of the car model was obtained from the manufacturer (SEAT SA, Barcelona, Spain). The DXF format of the car model was converted in finite difference time domain format using the procedure explained in [49]. An accurate human model can be obtained based on CT or MRI imaging. A commercially available human model was used for analysis of SA and SAR values. The schematic for the simulation is shown in Fig. 3.2. Uniform meshing with 36 mm of cell sides was used for an overall size of $4644 \times 2160 \times 1764\ mm^3$, which includes vehicle, the human body and the surrounding air. The SAR computation was performed in Matlab by using finite difference time domain code using geometry and conductivity information. The results for SAR variation were calculated for three planes for the driver's and front passenger's location. In the first case, the emitter was used as a hand-free device placed at a distance of 5.1 cm. For this case, a significant increase in the SAR values was noticed than in free space. In the second case, the device was used as a handheld device by driver and passenger; the SAR results were obtained for all three planes. In this case, no significant change in the SAR distribution was observed, even when the devices were close to the human model [48].

In [50], the effect of impulse radio ultra-wideband (IR-UWB) signal used in the implantable devices at 4 GHz was analysed. In this study, the simulation was performed to observe the SAR, Specific Absorption (SA) and temperature variation in the human head caused by UWB antenna with 10 dB bandwidth. The

numerical simulations were performed in CST studio using CST voxel head model, which consists of a mixture of tissue material such as brain, bone, fat and skin. The dependency of SAR on permittivity and conductivity of the exposed tissues was also discussed. The relation between human age and permittivity was also described for the accurate evaluation of the exposure. SAR parameter also depends on the antenna parameters such as directivity and gain. Therefore, an antenna was designed with the minimum absorption characteristics in the CST studio by matching the impedance with surrounding tissues. The gain of the antenna was plotted for different scenarios of the antenna as shown in Fig. 3.3. An IR-UWB signal centred at 4 GHz with a bandwidth of 1 GHz was applied to the antenna with a power of 0.0024 mW. The variation of SAR was plotted for following scenarios; (1) SAR variation with a different input power of the signals, (2) SAR variation depending upon the antenna orientation, and (3) SAR variation in different tissue material in the human head, as shown in Fig. 3.4. The results show that there is higher variation of SAR with impulse signal than with the continuous input signal. The temperature variation was also plotted using bio-heat equation in CST studio. It was observed that SAR also depends on the bandwidth of the IR-UWB signal. It was found that a pulse with a peak power higher than the

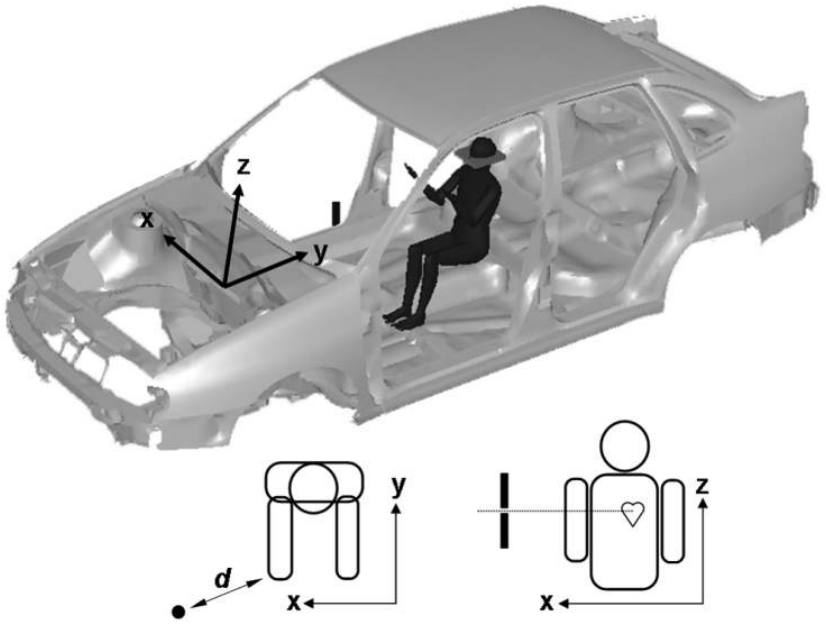



FIGURE 3.2: Schematic for the position of the human model in a car, adopted from [48].

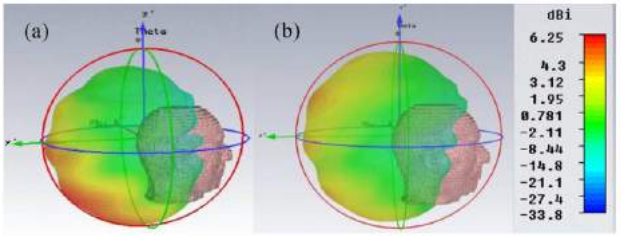



FIGURE 3.3: Simulated directivity of the implanted antenna at 4 GHz. (a) Antenna radiating outwards of the adult brain. (b) Antenna radiating towards the adult brain [50].

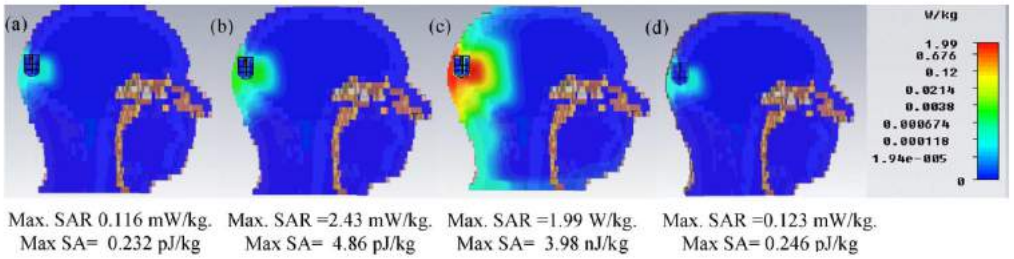



FIGURE 3.4: Simulated SAR variation in voxel head model when the antenna main lobe is situated outwards of the brain for the peak spectral power limits of: (a) -41.3 dBm/MHz, (b) -27.4 dBm/MHz and (c) 0.9 dBm/MHz, and (d) when the antenna main lobe is situated towards the brain for the peak spectral power limit of -41.3 dBm/MHz [50].

FCC regulated peak power can be utilized without violating the SAR guidelines.

In [51], the effect of EMR in the presence of a metallic wall was observed numerically and experimentally. The main goal of this study was to observe the effect of the reflected signals on SAR. The mobile phone was modelled with a dipole antenna at 900 MHz which radiates continuously. Two metal wall arrangements were modelled for reflection of the signals and the change in the SAR for different distances was observed. The results show that SAR values are higher near the metallic wall than in a free space environment. This study helps to explore the effect of SAR when the reflection in the environment are higher than the free space environment. Similarly, in metal ore mines, exposure of EMR can be higher due to the reflections of electromagnetic signals from the walls, roof and ground of underground mine. Therefore, exposure to EMR in underground mines should be investigated when the miners are exposed to the electromagnetic signals in presence of different metal structures present in underground mines.

In [52], the effects of electromagnetic signals for a human head has been investigated in the frequency range of 900 MHz and 1800 MHz. The simulated results show that shielding of a human head using a nano-ferrite textile and carbon fibre textile material can be used to reduce the SAR and exposure to electromagnetic signals. This study is useful in a scenario when SAR values are slightly higher than the recommended guidelines of ICNIRP. Similarly, in underground mines, if the SAR levels exceed the safety guidelines of ICNIRP for that frequency, shielding can be designed to reduce the exposure of EMR on miners. However, the shielding may also degrade communication in underground mines. Therefore, a tradeoff exists between electromagnetic exposure and power of electromagnetic signals present in underground mines.

In [53], the effect of EMR on the human body in the presence of a metallic zip and a coin has been investigated. The numerical simulation was performed at mobile phone frequencies using dipole and PIFA antenna with high-resolution Gustav human voxel model. The results show that the zip increases the SAR values whereas the presence of coin in the pocket reduces the exposure of EMR on the human body.

## 3.4 Conclusion

In literature, most of the studies have focused on the frequencies used in mobile communication for evaluation of SAR using numerical simulations with different human voxel models. The variation of SAR with different parameters has been investigated in past studies. The studies have investigated different parameters which influence the variation of SAR such as presence of any metal object close to the human body during exposure, size of the human head, the orientation of the antenna and the frequency of EMR. The numerical simulations provide SAR analysis in different type of human tissues than the in-vitro studies and experimentation of SAR with SAM phantom. Currently, all the measurement methods of SAR provide conservative exposure of EMR and provides no information about

the exposure of EMR on sensitive organs of the human body. The use of multi-layered voxel models provides SAR evaluation in different sensitive human organs and parts of body. Therefore, it is crucial to use high-resolution voxel models for the evaluation of SAR in humans for wearable devices in underground mines. After, extensive literature review, the following factors have been identified, which impact the variation of SAR and exposure of EMR:

1. Types of tissues exposed to EMR exposure.
2. Dielectric properties of the biological tissues and age.
3. Size of the human head.
4. Frequency of electromagnetic signals.
5. Distance between the antenna and biological body.
6. Bandwidth of the antenna.
7. Transmit power of the antenna.
8. Orientation and polarization of the antenna.
9. Vicinity environment of the antenna and biological model.

Within current literature, to the best knowledge of the author, no study has investigated the EMR exposure in underground mines when a miner has wearable tracking devices on the body. The electromagnetic signal can be reflected, scattered and absorbed by the surrounding rocks and support structure in underground mines where the miner is exposed to EMR for a shift of 6 to 8 hours/day. Therefore, it is vital to investigate the impact of EMR on the health of the miner in underground mine scenarios.

# Chapter 4

# Methodology

In this chapter, the research methodology followed in this study will be discussed. In section 4.1, the modelling of electromagnetic source at 433 MHz, 868 MHz and 2400 MHz frequency is explained in detail. Section 4.2 explains the human voxel models and the dielectric properties of the biological tissues used in this study. The modelling of underground mine scenarios is explained in section 4.3. The modelling of helmet used in this study to evaluate the impact of helmet on EMR is explained in section 4.4. Section 4.5, 4.6 and 4.7 explain the simulation setup of different scenarios for head without helmet, torso and head with helmet, respectively. Lastly, the simulation setup for variation of SAR with different power levels and distances are discussed in section 4.8 and 4.9, respectively.

## 4.1 Modelling of Electromagnetic Source

In literature, a dipole antenna is used in many studies to investigate the SAR on humans for different scenarios [46–48, 54–56]. The presented study focuses on the investigation of SAR levels in a confined space of underground mines in a scenario where communication devices are used as wearables. This study does not focus on the impact of different types of antennas have been used in underground mine environments. Hence, a dipole antenna is used as an electromagnetic source to investigate the SAR on humans in underground mines.

A dipole antenna is a reference antenna with simple structure and omnidirectional radiation pattern. The half-wavelength dipole antenna is a particular case of a dipole antenna where the length of the dipole is equal to the half-wavelength at

the frequency of operation. A half-wavelength dipole antenna was modelled at 433 MHz, 868 MHz and 2400 MHz in CST WMS software. The dipole of the antenna is modelled using lossy metal copper (annealed) material with a conductivity of $5.8 \times 10^7$ $S/m$. The impedance of the dipole antenna is 73 Ω, and the gain is 2.19 dBi. The geometry of the dipole antenna modelled in CST WMS is shown in Fig. 4.1. The dimensions of the dipole antenna for all three frequencies i.e. 433 MHz, 868 MHz and 2400 MHz was calculated using expression [57]:

$$\lambda = \frac{c}{f} \tag{4.1}$$

$$L = \frac{143}{f(MHz)} \tag{4.2}$$

$$g = \frac{L}{200} \tag{4.3}$$

$$D = 2 \times \frac{\lambda}{1000} \tag{4.4}$$

where, $\lambda$ is the wavelength, $c$ is the speed of light, $f$ is the frequency, $L$ is the length of one dipole, $D$ is the diameter of the dipole and $g$ is the gap between two dipoles.

The reflection coefficient ($S_{11}$ < -10dB) provides the bandwidth of the antenna. The bandwidth of the antenna is 45.16 MHz, 95.4 MHz and 250 MHz at 433 MHz, 868 MHz and 2400 MHz, respectively, as shown in Fig. 4.2. The parametric sweep on the length and gap between two dipoles was performed to optimize the bandwidth of the antenna. Table 4.1 shows the optimized dimensions of the half-wavelength dipole antenna at 433 MHz, 868 MHz and 2400 MHz.

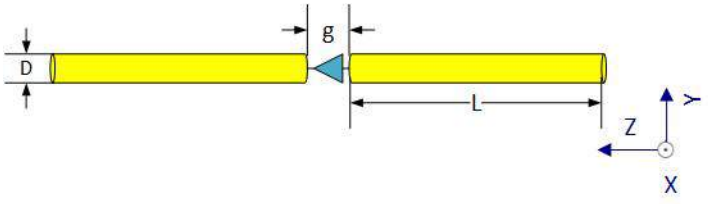



FIGURE 4.1: Geometry and dimensions of the modelled dipole antenna.

TABLE 4.1: Optimized parameters of the dipole antenna at different frequencies

| Frequency (MHz) | L (mm) | D (mm) | g (mm) |
|---|---|---|---|
| 433 | 166.28 | 1.384 | 0.83 |
| 868 | 82.949 | 0.692 | 0.414 |
| 2400 | 30 | 0.25 | 0.15 |

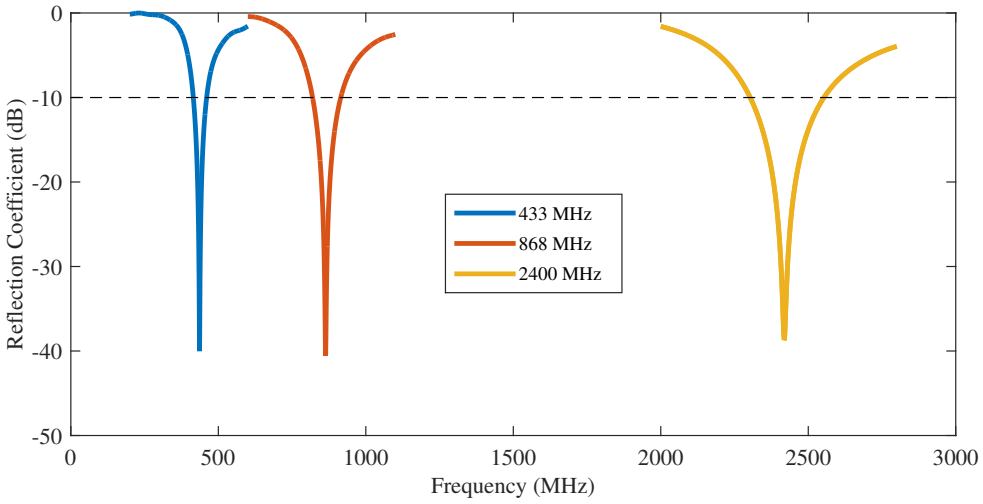



FIGURE 4.2: $S_{11}$ of dipole antenna at 433 MHz, 868 MHz and 2400 MHz.

## 4.2 Human Voxel Models

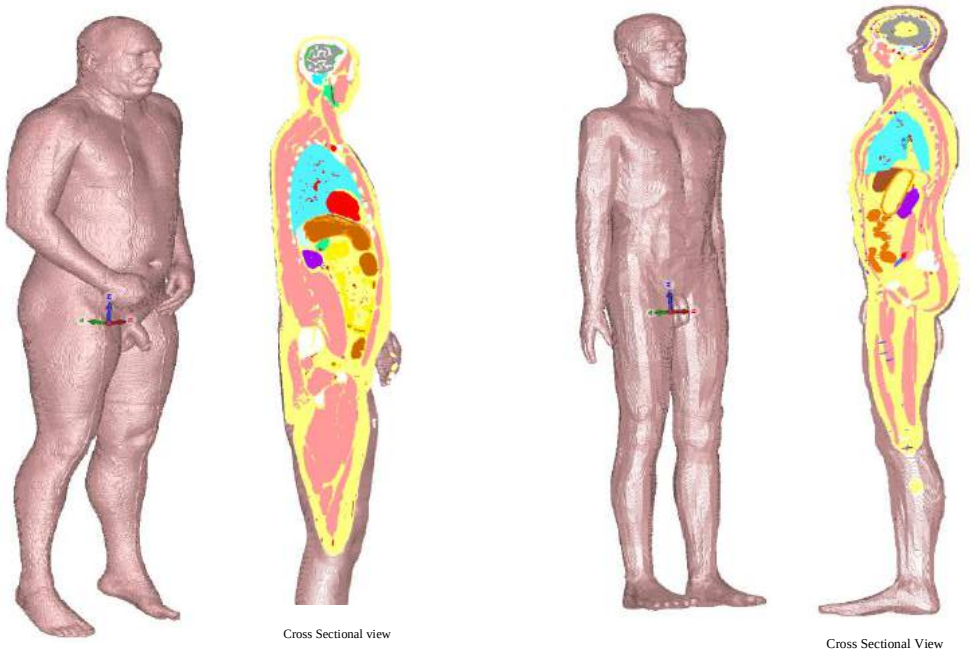
In recent years, the rapid advancement of magnetic resonance imaging (MRI) has implemented high-resolution anatomical models of the human body [58]. When two-dimensional digital images are extended into three dimensions and forms, the cuboid volume is known as voxel (volume pixels). These voxel models have been used in many studies to determine SAR with finite difference time domain simulations for exposure of non-ionizing radiations [48, 53, 54]. Multi-Layer voxel models anticipate the accurate exposure of EMR on different organs of the human body and provide vulnerable health risks associated with different human organs. In the past, many studies determined the exposure of non-ionizing radiations using SAM phantom, which consists of shell and filled with saline solution. A SAM phantom provides a conservative value of SAR which does not provide an exact analysis of the EMR impact on different human organs. Therefore, it is advantageous to use high-resolution voxel models for the investigation of EMR exposure specifically for

wearable devices.

The voxel family of the CST MWS software consists of eight high-resolution human voxel models of different age, gender and stature, under the license of CST Studio®. Due to limit of the time, this study was only focused on the male models. In underground mines, the working areas have more number of male miners than the female miners. Therefore, this study involved two male models for the investigation of SAR. A male Hugo model has been used in many studies for analyzing the impact of exposure to non-ionizing radiations [50, 59]. It has different resolutions of 1 mm, 2 mm and 5 mm, and includes 31 types of tissues with a total mass of 103 Kg and a height of 180 cm [60]. The CST surface bio model is also used in this study in order to make a comparison with the CST voxel family. The surface bio model family consists of one male Tom, one female Ana and four children voxel models. The Tom male model was chosen for a fair comparison with the male Hugo model in this study. The Tom model has different resolutions of 0.5 mm, 1 mm, 2 mm and 4 mm, and includes 33 types of tissues with a total mass of 77 Kg, and a height of 183 cm [60]. The overview of Hugo and Tom models is described in Table 4.2. Following are the reasons to use Hugo and Tom models for the investigation of SAR in underground mines: (1) both models have same resolution ($1 \times 1 \times 1\ mm^3$), (2) both have approximately same number of tissues, (3) both models are posable, (4) both have different head sizes which allows analysis of exposure on different head sizes of the miners, and (5) both have different mass which allows analysis of exposure on the miners with different masses. The high-resolution Hugo and Tom human voxel models are shown in Fig. 4.3.

Table 4.2: Overview of Hugo and Tom voxel models used in this study

| Model | Sex | Size (cm) | Mass (kg) | No. of Tissues | Resolution ($mm^3$) | Remarks |
|---|---|---|---|---|---|---|
| Hugo | Male | 180 | 103 | 31 | $1 \times 1 \times 1$ | posable |
| Tom | Male | 183 | 77 | 33 | $1 \times 1 \times 1$ | posable, generic |




(a) (b)

FIGURE 4.3: High resolution (1 mm) human voxel models used in this study (a) Hugo and (b) Tom.

### 4.2.1 Dielectric Properties of Biological Tissues

The dielectric properties, such as permittivity and conductivity of the human tissues and organs, are frequency dependant. The dielectric properties of human tissues can be obtained using the Cole-Cole equation [61]:

$$\underline{\varepsilon} = \varepsilon_\infty + \frac{\Delta\varepsilon}{1 + (j\omega\tau)^{1-\alpha}} \tag{4.5}$$

$$\Delta\varepsilon = \varepsilon_s - \varepsilon_\infty \tag{4.6}$$

where, $\underline{\varepsilon}$ is the complex dielectric constant, $\varepsilon_s$ and $\varepsilon_\infty$ are the static and infinite frequency dielectric constants, $\Delta\varepsilon$ is the difference in static and infinite permittivity of the tissues, $\omega$ is the angular frequency, $\tau$ is a relaxation time constant, and $\alpha$ is an empirical distribution parameter.

The Cole-Cole equation is the contemporary material model used to forecast dielectric properties of the human tissues. Several online applications are available to review dielectric properties of the human tissues at particular frequency [62, 63].

In CST MWS, the biological properties of the human tissues can be evaluated using the *macros* tool which uses Cole-Cole method to find the dielectric properties of the tissues at a particular frequency. The dielectric properties of the tissues at 433 MHz, 868 MHz and 2400 MHz are determined using the *macros* tool of CST MWS software, and are shown in Table 4.3.

TABLE 4.3: Dielectric properties of different human tissues at 433 MHz, 868 MHz and 2400 MHz

| Tissues | 433 MHz | | 868 MHz | | 2400 MHz | |
|---|---|---|---|---|---|---|
| | $\varepsilon_r$ | $\sigma(S/m)$ | $\varepsilon_r$ | $\sigma(S/m)$ | $\varepsilon_r$ | $\sigma(S/m)$ |
| Air inside body | 1 | 0 | 1 | 0 | 1 | 0 |
| Blood | 63.83 | 1.36 | 61.46 | 1.52 | 58.34 | 2.50 |
| Bone cortical | 13.07 | 0.09 | 12.48 | 0.14 | 11.41 | 0.38 |
| Bone medullary cavity | 22.26 | 0.24 | 20.86 | 0.33 | 18.61 | 0.79 |
| Brain grey matter | 56.83 | 0.75 | 52.88 | 0.93 | 48.99 | 1.77 |
| Brain white matter | 41.67 | 0.45 | 38.99 | 0.58 | 36.23 | 1.19 |
| Cartilage | 45.15 | 0.59 | 42.77 | 0.77 | 38.87 | 1.72 |
| Cerebellum | 55.14 | 1.05 | 49.66 | 1.25 | 44.89 | 2.07 |
| Cerebrospinal fluid | 70.64 | 2.26 | 68.71 | 2.40 | 66.32 | 3.41 |
| Eye bulb | 68.99 | 1.53 | 68.91 | 1.63 | 68.24 | 2.44 |
| Eye lens | 47.96 | 0.68 | 46.63 | 0.78 | 44.68 | 1.47 |
| Fat | 5.57 | 0.042 | 5.47 | 0.05 | 5.29 | 0.10 |
| Mucosa | 49.42 | 0.68 | 46.21 | 0.83 | 42.92 | 1.56 |
| Muscle | 56.87 | 0.80 | 55.11 | 0.93 | 52.79 | 1.71 |
| Nerve | 35.05 | 0.46 | 32.63 | 0.57 | 30.20 | 1.07 |
| Salivary glands | 61.33 | 0.89 | 59.76 | 1.03 | 57.27 | 1.93 |
| Skin | 47.75 | 0.69 | 43.89 | 0.84 | 40.49 | 1.50 |
| Teeth | 13.07 | 0.09 | 12.48 | 0.14 | 11.41 | 0.38 |
| Thyroid | 61.33 | 0.89 | 59.76 | 1.03 | 57.27 | 1.93 |
| Tongue | 57.38 | 0.78 | 55.36 | 0.92 | 52.69 | 1.76 |
| Tonsils | 61.33 | 0.88 | 59.75 | 1.03 | 57.27 | 1.92 |
| Liver | 50.69 | 0.67 | 46.98 | 0.84 | 43.12 | 1.65 |
| Lung | 38.89 | 0.54 | 36.80 | 0.65 | 34.48 | 1.22 |
| Kidney cortex | 65.45 | 1.12 | 58.94 | 1.37 | 52.86 | 2.39 |
| Pancreas | 61.33 | 0.88 | 59.75 | 1.03 | 57.27 | 1.93 |
| Spleen | 62.45 | 1.04 | 57.38 | 1.26 | 52.54 | 2.20 |
| Ureter | 19.62 | 0.33 | 18.97 | 0.38 | 18.02 | 0.67 |

## 4.3 Modelling of Underground Mine Scenarios

The major factors which differentiate a mine environment from an open space environment are the presence of surrounding rocks, increased humidity, high temperature and the confined space available for mining. An important consideration in the analysis of the effect of EMR on the health of miner is the reflection of the electromagnetic signals from the surrounding environment of the underground mine. The structure of underground tunnels, type of rocks and ores present in underground mines are diverse. The dielectric properties of rock and ore present in a particular underground mine are not available for all frequencies under observation in this study, and these properties can vary due to different composition of minerals in different underground mines. It is challenging to procure the dielectric properties of the concerned ore for the investigation of EMR. The interaction of EMR with the rough surface of tunnels and stopes in the underground mines result in the reflection of the radiations, which gives enhanced EMR exposure to the miner than that in the open space environment. Furthermore, it is crucial to get access to the working area of the underground mines to replicate the exact scenarios for modelling. Therefore, it is demanding to use the appropriate methodology for the numerical investigation of EMR exposure on miners in underground mines which can replicate the exact underground mine environment.

The Wits Mock-mine is an actual physical replica model of a true mine which is beneath the School of the Mining Engineering at the University of Witwatersrand. It allows to replicate the confined and reflective environment of the underground mines [64]. It comprises of a tunnel, a stope panel and a control room with the aim to perform realistic testing. Concrete material has been used to build 67 m long tunnel and a stope with different type of support structure [65]. Various studies have used the Wits mock mine to analyse the effect of tunnel structure on channel modelling and different parameters of antenna [66], and to test wireless sensor network based tracking devices for the rescue of miners in the collapsed mine scenario [5]. Hence, the Wits mock mine based model has been modelled in this study to model a confined space similar to the underground mines for the

investigation of the SAR.

In CST MWS software, plenty of underground mine scenarios can be modelled for the numerical investigation of EMR. In this study, three different critical underground mine scenarios were determined and modelled for numerical simulations of SAR in the human head. All these scenarios are explained as follows: (1) Firstly, the tunnel scenario was considered to provide a comparison of the interaction of EMR in an open environment with that in a reflective environment of the underground mines. The tunnels in underground mines have different shapes, lengths and geometries, which was comprised in the modelling of mock mine scenarios. (2) Secondly, the presence of metal arches in the tunnel was considered and modelled for numerical simulations. Many studies have investigated the impact of different metal objects on the exposure of EMR to the humans. In [51], it was concluded that the presence of a metal object near the electromagnetic source increases the reflections, and hence the SAR values. Therefore, it is vital to investigate the impact of the metal support structures present in underground mines on the effect of EMR to the miner. (3) In the third scenario, a stope similar to one side of the Wits mock mine was considered. The stope is the most confined and vulnerable environment of the mining which is supported with different support structures in the underground mines. Hence, because of more reflections from nearby distances in the stope, it is important to investigate the level of EMR exposure on the miner for stope. The detailed modelling of all the mock mine scenarios is explained later in this section.

The implementation of high-resolution voxel models and the modelling of 67 m long tunnel define the limitation of available computation resources. The use of high resolution models is crucial for the investigations of electromagnetic sources operating at lower frequencies. It has to cater for the impact of EMR on different human organs which are deep inside the human body. Therefore, it is not feasible to use single layer voxel models for the investigation of EMR, particularly for low frequencies. An alternative way to reduce computational processing is to model a fraction of tunnel. It is well known that the free space path loss is directly proportional to the distance between the transmitter and the receiver. The free space

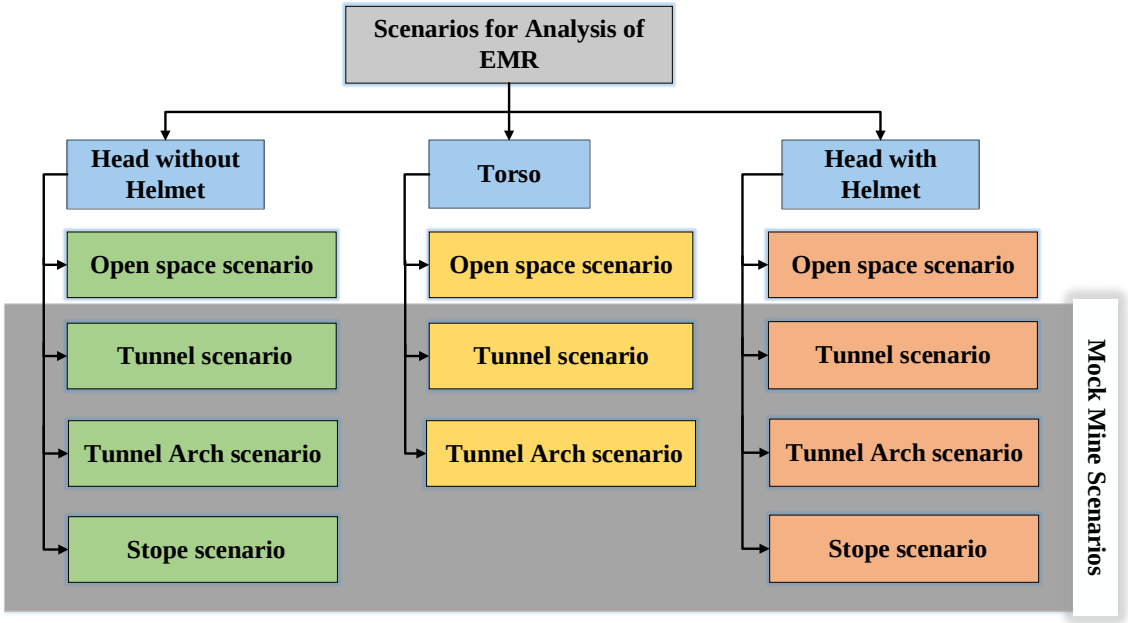



FIGURE 4.4: Hierarchy of different scenarios used in this study for evaluation of SAR on head, torso and head with helmet.

path loss is more significant for the signals travelling far away from the source. In the same manner, the signal travelling far from the tunnel has negligible health impact on the miner than the signal reflected from the nearby boundary of the tunnel. Thus, a small fraction of tunnel equivalent to ten times the size of antenna has been modelled for numerical simulations. The size of the antenna usually used in different devices at 433 MHz varied between 48 mm to 80 mm, thus ten times of 80 mm ($10 \times 80\ mm = 800\ mm$) was modelled in this study. In CST MWS, a forty year old concrete material, available in material library was used to model the tunnel of all the mock mine scenarios.

The hierarchy used in this study to investigate the impact of EMR on the head without helmet, torso and head with a helmet for different scenarios is shown in Fig. 4.4. All the mock mine scenarios are compared with open space scenario to provide the difference in the exposure level of EMR on the body of the miner.

### 4.3.1 Modelling of Mock Mine Scenarios for Head

To investigate the EMR effects on the human head, the wall and roof of tunnel near to the head of the miner were modelled. The detail of three different mock mine scenarios, used to analyse the exposure of EMR on human head is explained as:

1. **Tunnel Scenario:** A model replicating the tunnel of the mock mine as shown in Fig. 4.5a was modelled in CST MWS along with the surface roughness of the tunnel. A brick of concrete material was defined as the building block to model the tunnel. All the bricks with dimensions of 800 mm in length and variable width and height were defined which were arithmetically added to model a tunnel as one block. The face of every brick was modified using the *bend* and *shape* tool of CST MWS in order to model the roughness of the tunnel surface. All the bricks were bent cylindrically with different angles and *extruded* to avoid the overlapping of the materials. The front and side view of the modelled tunnel scenario for the head is shown in Fig. 4.5c and Fig. 4.5d, respectively.

2. **Tunnel Arch Scenario:** A model replicating the arch as shown in Fig. 4.6a and Fig. 4.6b was modelled along with the support arch present in the tunnel. In order to model the tunnel arch scenario for the head, the model of tunnel scenarios was imported and modified to model the metal arch similar to tunnel. A steel (Steel-1008) metal with a conductivity of $7.69 \times 10^6 S/m$ was used to model the arch support of the tunnel. The same length and width of the arch present in the tunnel were used to model steel arch. The metal arch was bent along the boundary of the tunnel, and both faces were *extruded* to avoid overlapping of the material. The front and side view of modelled metal arch along with its dimensions is shown in Fig. 4.6c and Fig. 4.6d, respectively.

3. **Stope Scenario:** A model replicating the stope of mock mine as shown in Fig. 4.7b was modelled in CST MWS to investigate the impact of EMR in

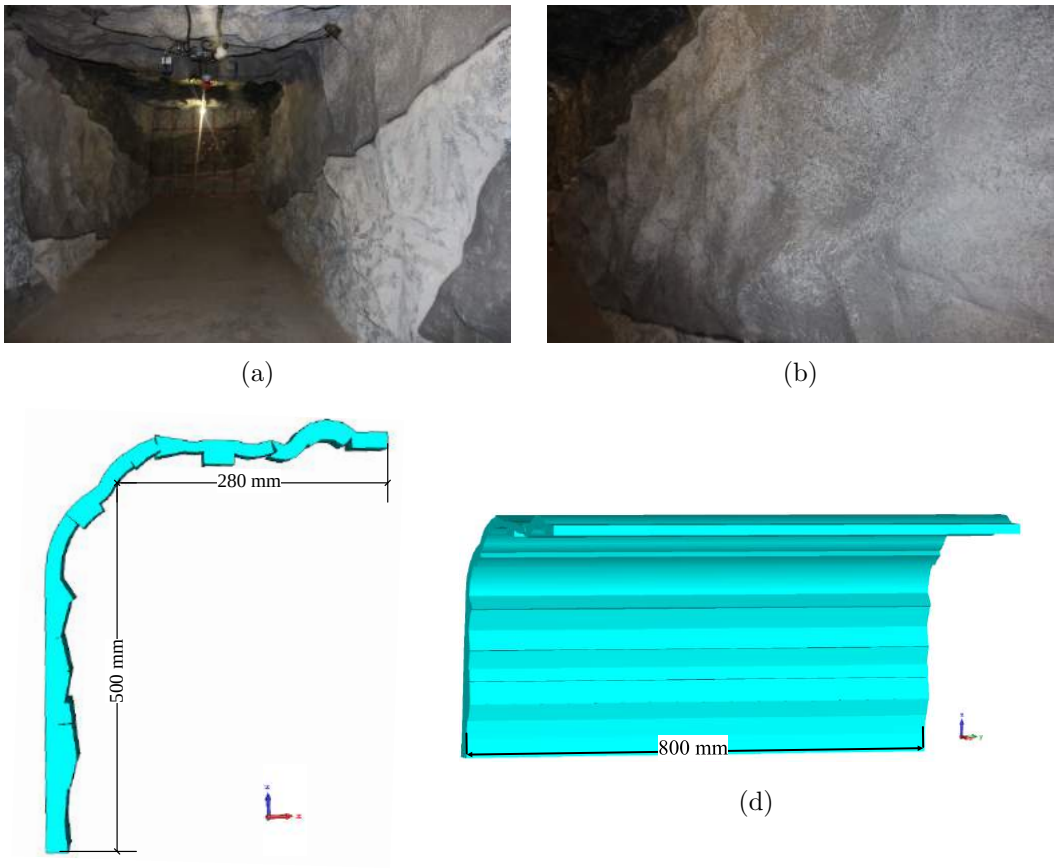
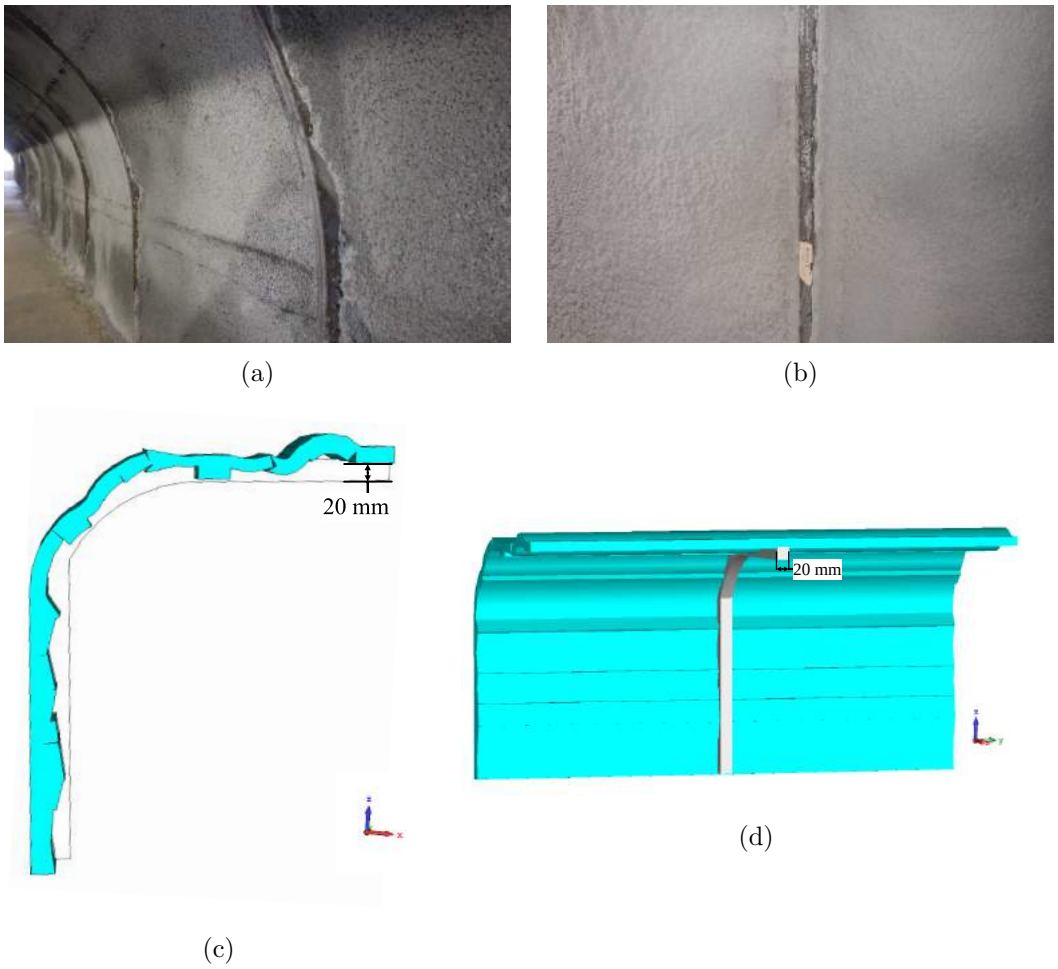



FIGURE 4.5: Modelling of tunnel scenario for simulations on head (a) Mock mine tunnel with wall and roof (b) Surface roughness of the mock mine tunnel (c) Front and (d) Side view of modelled tunnel scenario for simulations on head.

the confined space of a stope in the underground mines. The stope inside the Wits mock mine consists of different type of support structures. Same dimensions as that of the stope inside the Wits mock mine were used to model the stope. The same concrete material as used for the tunnel, and available in material library of the CST MWS was used to model the unit brick of the stope. A cylindrical support similar to the Wits stope was modelled with steel (Steel-1008) material to investigate the impact of steel pillar on the effect of EMR to the miner. The modelled stope scenario for numerical simulations for the head is shown in Fig. 4.7c.




(a) (b) (c) (d)

FIGURE 4.6: Modelling of tunnel arch scenario for simulations on head (a) Presence of steel support arches in the mock mine tunnel (b) Close view of steel arch of the tunnel (c) Front and (d) Side view of modelled tunnel arch scenarios for simulations on head.

### 4.3.2 Modelling of Mock Mine Scenarios for Torso

Two different mock-mine scenarios i.e. tunnel and tunnel arch scenarios were modelled for the simulations on torso. The stope scenario for torso was not included in this study due to limitation of computational resources. A simulation methodology similar to the one mentioned in the previous section 4.3.1 for head was followed for the modelling of the underground scenarios for the torso. The reflections from the nearby boundary of the tunnel and arch were incorporated in the exposure to EMR. A part of the tunnel was modelled, which is equivalent to ten times the size of the antenna for lowest frequency used in this study. The left part of the torso for both voxel models was considered in this study. To evaluate

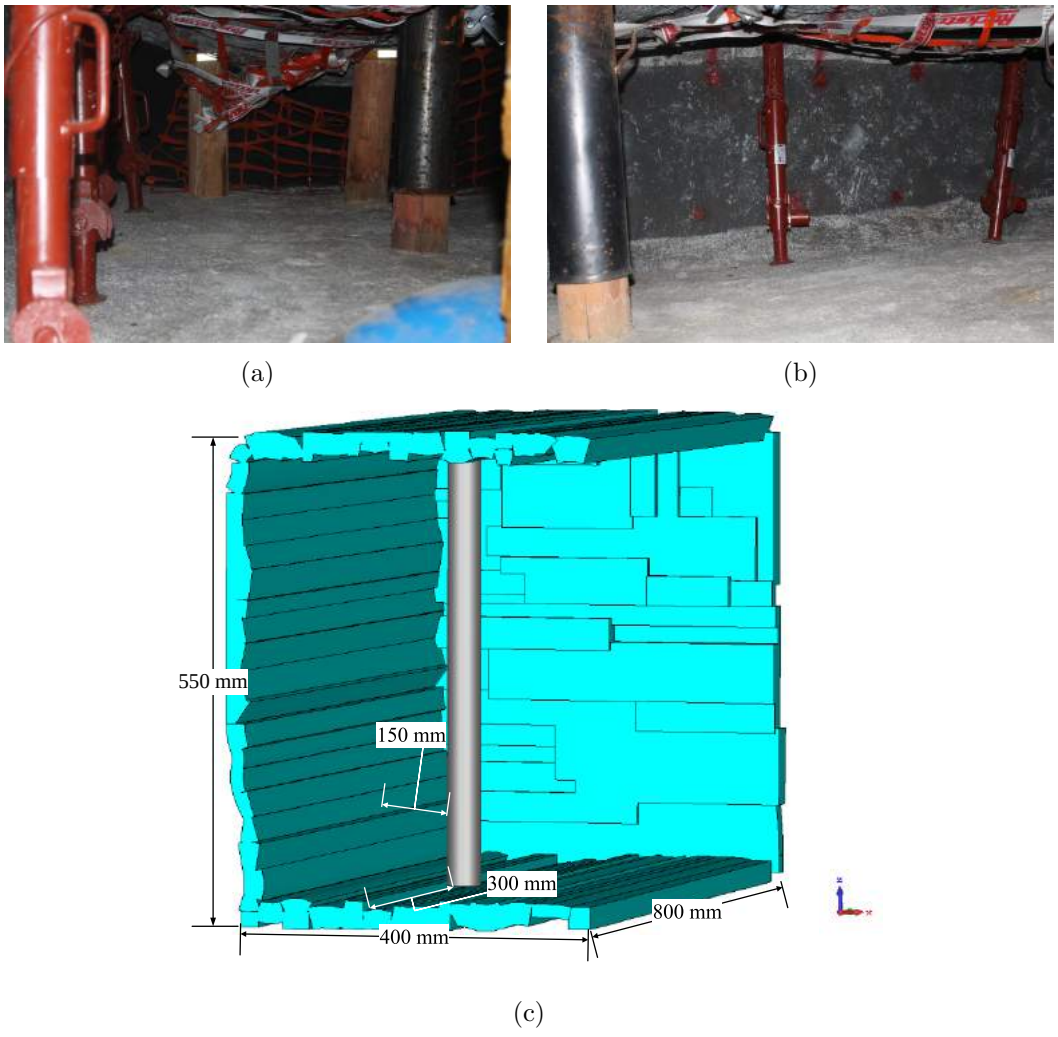


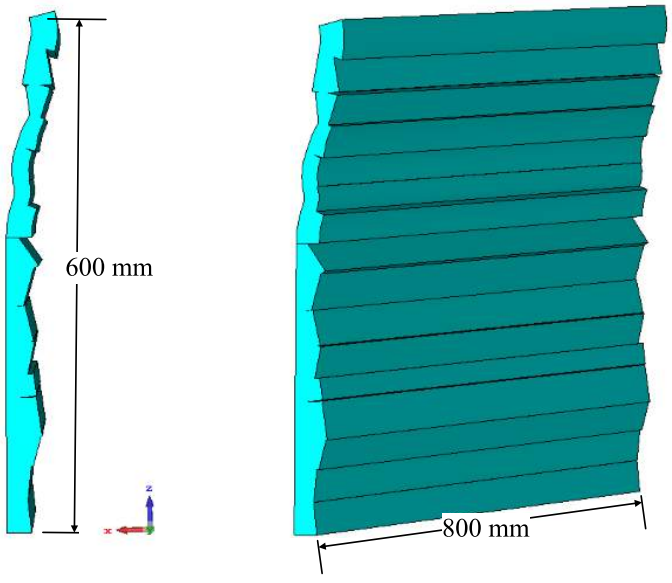

FIGURE 4.7: Modelling of stope scenario for simulations on head (a) Stope of the Wits mock mine (b) Support structure in the stope of the mock mine (c) Modelled stope scenario for simulations on head.

the complete torso of the voxel models, more computation resources were required. The SAR limit of ICNIRP for hand and arm is 4 W/Kg [67], which is two times the SAR limit for torso and head. Thus, the torso and head of the human body are more sensitive to EMR exposure than the limbs of the human body. Therefore, only human torso was considered in this study to investigate the exposure of EMR on the torso of the miner, and the arms and hands were excluded.

A simulation methodology similar to the one used for head was followed to model the mock mine scenarios for numerical simulations of SAR for the human torso. These simulations help to recommend the better location in terms of SAR to mount these wearable devices on the body of the miner. The recommendations

were based on the minimum value of SAR for human head and torso. The detailed modelling of both mock mine scenarios for the torso is described as follows:

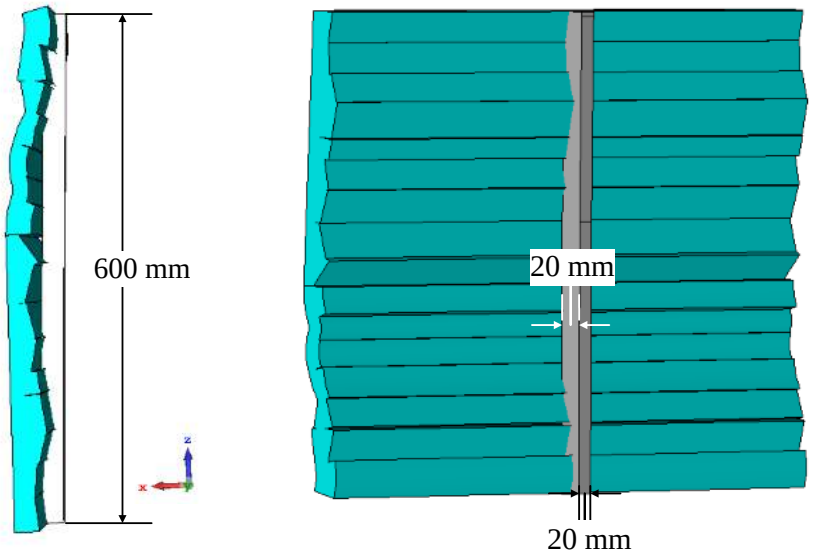
1. **Tunnel Scenario:** In order to model mock mine scenarios for the torso, the same concrete material, which was used for simulations on head, was used to model a brick of length 800 mm with variable height and width of the tunnel. The faces of all the bricks were modified using same tools of CST MWS. The total height of the modelled mock mine tunnel for torso was 600 mm, which is ten times the size of the antenna for lowest frequency observed in this study. The rough surface of the wall impacts the exposure of EMR in the environment, particularly because of reflection from the boundaries. The surface roughness of the mock mine tunnel is less in front of the torso than the head scenario because the bent of the tunnel near head makes the surface less plane. The front and side view of the modelled mock mine tunnel scenario for the torso is shown in Fig. 4.8a and Fig. 4.8b, respectively.




(a) (b)

FIGURE 4.8: Modelling of tunnel scenario for simulations on torso (a) Front view of the modelled scenario (b) Side view of the modelled scenario with its surface roughness.

2. **Tunnel Arch Scenario:** In this scenario, the impact of the metal arch on the exposure of EMR on the torso was modelled. The same steel (Steel-1008) material was used to model the arch with same dimensions as used for modelling of head scenarios. The front and side view of the modelled tunnel arch scenario for the torso is shown in Fig. 4.9a and Fig. 4.9b, respectively.




(a) (b)

FIGURE 4.9: Modelling of tunnel arch scenario for simulations on torso (a) Front view of the modelled arch scenario (b) Side view of the modelled scenario with its dimensions.

## 4.4 Modelling of Helmet

A helmet is used in underground mines for the health and safety of the miner and it is mandatory for every miner working in underground mine. It was recommended to mount these wearable devices on the helmet of the miner either on the outside or inside the helmet. Therefore, it is vital to investigate the impact of EMR when it is mounted on the helmet of the miner.

The safety helmet in underground mines has usually one standard size and holds a strip at the back to adjust the size according to the head size of every miner. Therefore, only one size of the helmet was modelled and used in this study for

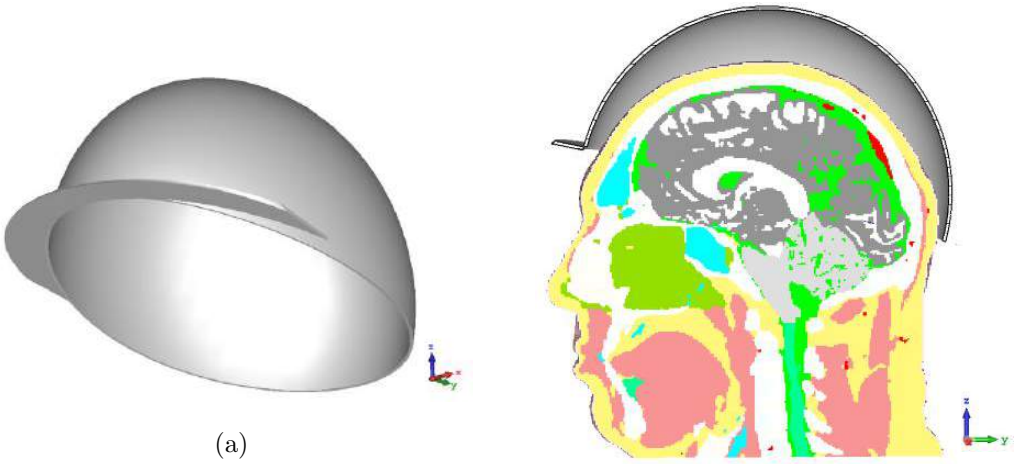
investigation of EMR on different size of the head of two voxel models. The head with a bigger size is more closer to the boundaries of the helmet and consequently closer to the wearable wireless device than the head with smaller size. Thus, the head with small size has more distance between the wearable device and the head, and hence, relatively reduces the exposure to the human body.

A hard head safety helmet was modelled in CST MWS using dimensions of the Hugo's head in this study. The head size of the Hugo model is bigger than the head size of the Tom model. Therefore, the helmet is modelled according to the head size of the Hugo model. The same helmet was also used for the simulations with the Tom model. This would provide the difference in SAR for two different size of the heads with the same helmet.

A helmet was modelled using the Polyimide (loss-free) material used in the manufacturing of hard helmets for the underground mines. Polyimide material is available in CST MWS material library with a relative permittivity of 3.5 and a density of 1400 Kg/m$^3$. The helmet was modelled using two semi-circles with diameters of 217 mm and 219 mm. The inner semi-circle was subtracted from the outer semi-circle using boolean subtract function in order to model a shell of the helmet. The shape of the helmet was modified using *bend* tool. The modelled helmet for the evaluation of SAR is shown in Fig. 4.10a. The helmet was placed and adjusted on head of both voxel models to avoid overlapping of the material with the skin of the models. Cross-sectional view of the modelled helmet placed on Hugo's head is shown in Fig. 4.10b.

## 4.5 Simulation Setup for Head without Helmet Scenario

The simulation setup for the head without helmet for open space and all modelled mock mine scenarios is discussed in this section. The standard procedure was followed for all simulation setups, as explained in IEEE/IEC 62704 standard [23]. The simulation setup procedure for some of the scenarios on head without helmet scenario are explained below and the same procedure was repeated for all rest



(a) (b)

FIGURE 4.10: Modelling of helmet for head (a) Modelled head helmet with polyimide material (b) Cross sectional view and placement of helmet on the head of Hugo model.

of the simulation scenarios. The error of numerical simulations was checked by running all simulations twice. If error was found, all the steps were repeated.

### 4.5.1 Setup for Open Space Scenario on Head without Helmet

An open space scenario was used for comparisons with all underground mine scenarios. The comparison aims to quantify the difference in EMR effect to the miner in the open space to that in the underground environment by considering all the other factors as the same. In the open space scenario, both Hugo and Tom head models were exposed to the electromagnetic signal of frequency 433 MHz, 868 MHz and 2400 MHz, in a one by one manner. The IEEE standard was followed for numerical evaluation of EMR exposure on the miner in underground mines. The distance between the antenna and the head was 10 mm, and the size of human head is selected according to the IEEE standard [23]. The procedure for simulation setup of Hugo model for open space scenario at 2400 MHz frequency is given as follows:

1. The Hugo model was imported from the CST voxel family with a resolution of $1 \times 1 \times 1mm^3$ and the head was selected. The CST file with the head of Hugo was saved for provision of the same size of the head model used in other scenarios.

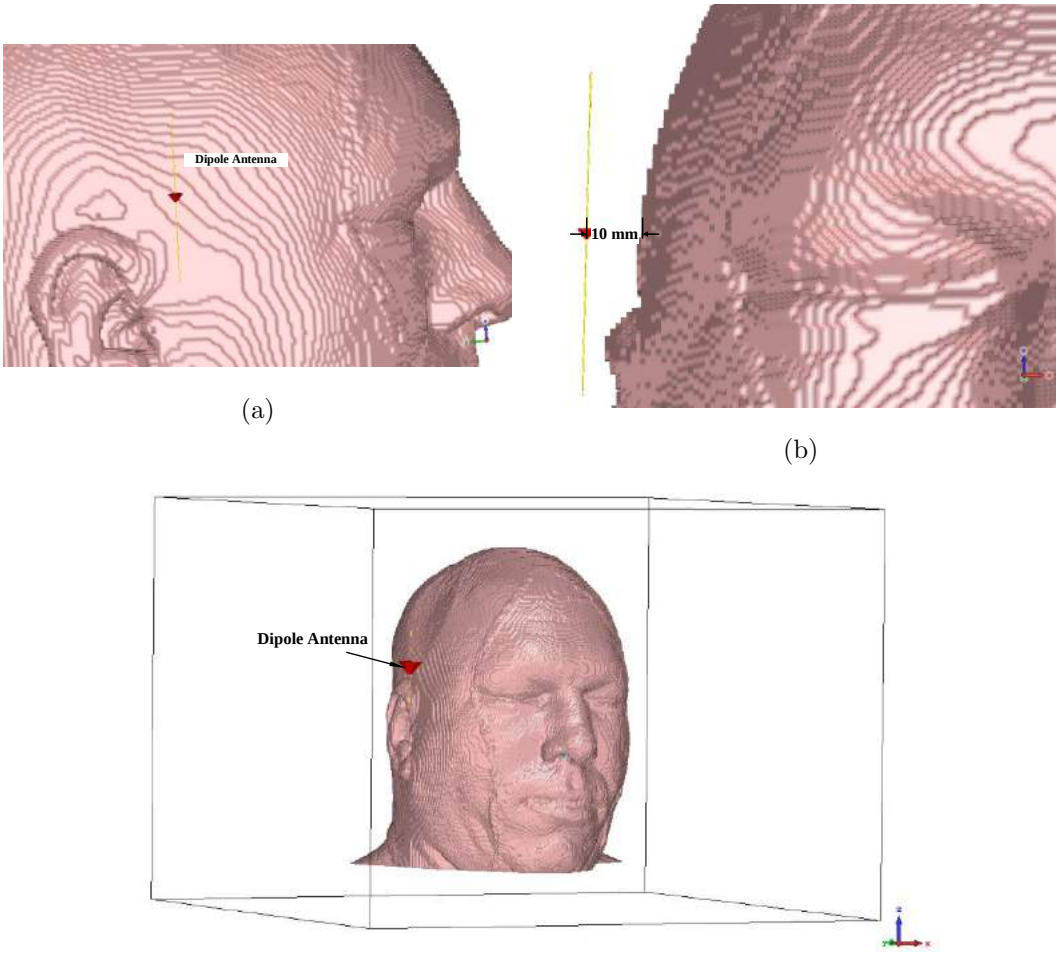
2. The modelled dipole antenna at 2400 MHz was imported as a sub-project, and adjusted on the human head. The position on the human head was chosen with respect to the helmet on the head of the miner, which is above the head extremity organs such as ear, nose etc. The position of the dipole antenna on the Hugo head model is shown in Fig. 4.11a.

3. The Hugo head and the dipole antenna was separated by a distance of 10 mm using the *transform* tool of CST MWS as shown in Fig. 4.11b.

4. The biological properties of the Hugo head model was updated for 2400 MHz using the *macros* tool.

5. A *far-field* and the *power loss density/ SAR* monitors were defined at 2400 MHz. The post-processing was performed to evaluate the SAR with an average mass of 10g. The user-defined transmit power of 0.1 W was used in the evaluation of SAR, and the SAR averaging method as per IEEE/IEC 62704 was used to evaluate the SAR in this study [23]. The transmit power is referred as the power transmitted to the antenna structure without ohmic losses of the antenna which is similar to the *accepted power* used in post processing of SAR in CST MWS.

6. The hexahedral meshing technique [68] was used with ten times the maximum number of cells per wavelength as described in IEEE standard [23] for the numerical evaluation of SAR. The Hugo head model was simulated with 15 million mesh cells at 2400 MHz. The global and local mesh properties were modified to accurately evaluate the SAR for open space scenario. The complete setup of open space scenario with boundary box is shown in Fig. 4.11c.




(a)

(b)

(c)

FIGURE 4.11: Complete simulation setup for the head without helmet in an open space scenario (a) Position of the dipole antenna on the head of Hugo model (b) Distance between the head of Hugo model and the dipole antenna (c) Complete setup for simulation with its boundary box.

The time domain solver of CST MWS took 2 hours to complete the simulation for open space scenario. The computational resources used in all simulations were the Intel i7-8750H @2.2 GHz processor, 32GB of RAM and NVIDIA® Ge-Force 4GB graphic card memory. All the steps were repeated with Tom head model at 2400 MHz for evaluation of open space scenario. Similarly, the complete procedure was repeated for the evaluation of SAR at 433 MHz and 868 MHz with Hugo and Tom head models.

### 4.5.2 Setup for Tunnel Scenario on Head without Helmet

In the tunnel scenario, the interaction of electromagnetic signals with the concrete material and rough surface of the tunnel was analysed. The human head was exposed to the confined environment of the underground mine. The distance between the human head and tunnel was confined to 100 mm in order to evaluate worst-case scenario with respect to EMR reflections for underground tunnel scenario, as shown in Fig. 4.12a. Further steps for simulation setup using Tom head model with tunnel scenario at 2400 MHz were as follows:

1. The 3D CST MWS file of open space scenario with Tom head model was modified for simulation setup of the tunnel scenario.

2. The modelled tunnel scenario 3D CST MWS file was imported as a subproject in the main simulation file.

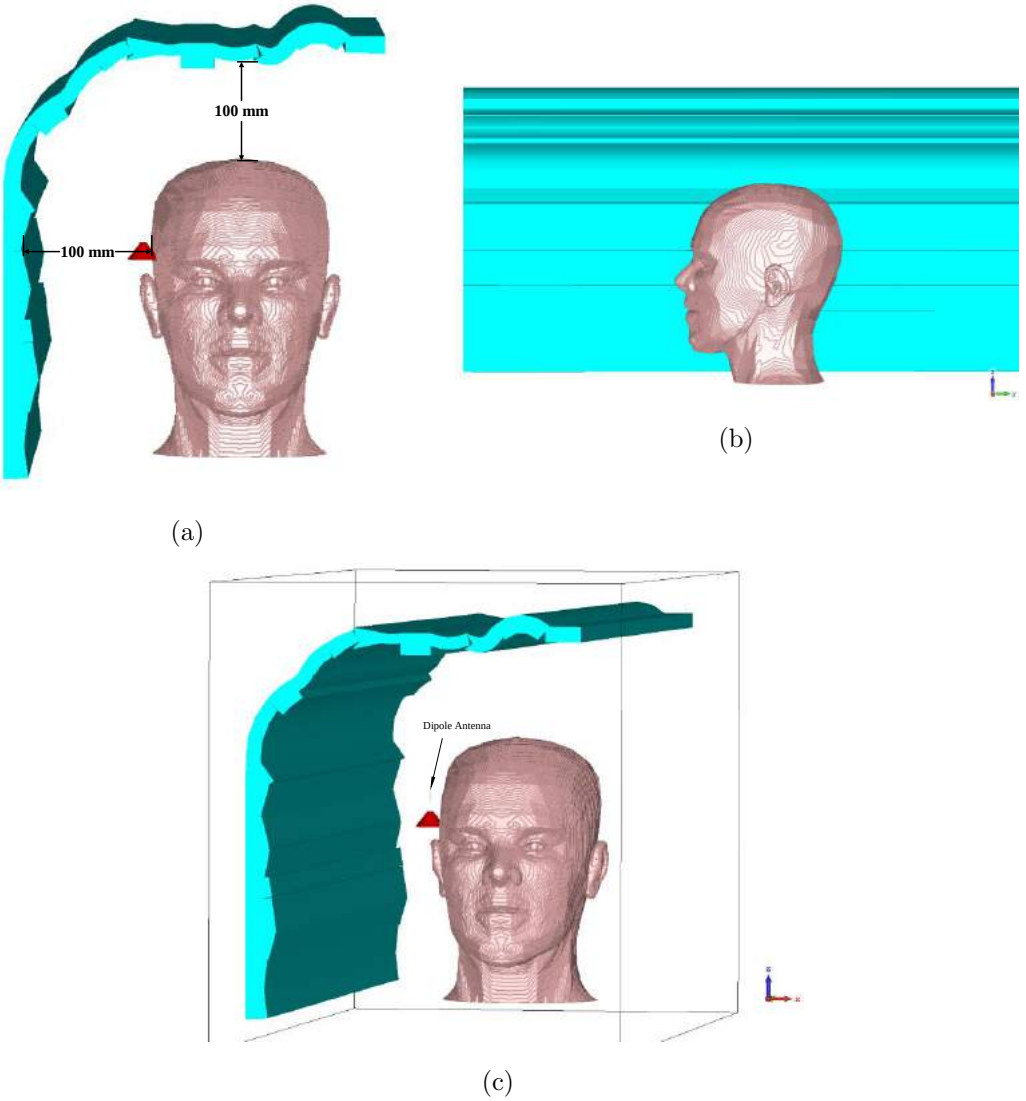
3. The head model was transformed into the middle of the modelled tunnel scenarios, as shown in Fig. 4.12b. The distance between the head model and tunnel was kept at 100 mm, whereas the distance between the dipole antenna and head model was kept as 10 mm.

4. The *far-field* and *power loss density/ SAR* monitors were defined to observe the effect on the far-field pattern of the dipole antenna and to evaluate the SAR value. The transmit power of 0.1 W was defined in post processing to evaluate the SAR.

5. The biological properties of the human tissues were updated at 2400 MHz using *macros* tool of CST MWS.

6. The maximum number of mesh cells used in the calculation domain was $10/\lambda$ as described in IEEE/IEC 62704 [23]. The highest frequency of the calculation range defines the maximum number of mesh cells. The mesh cell was refined using *volume* and *edge* refinement options available in *special mesh* properties under *global mesh* properties tab of the CST MWS. After

refinement of the mesh cells, the tunnel scenario was simulated with a total number of approximately 40 million mesh cells. The complete setup for simulation of tunnel scenario on the head without helmet is shown in Fig. 4.12c.




(a)

(b)

(c)

FIGURE 4.12: Complete simulation setup for the head without helmet in tunnel scenario (a) Distance between the head of Tom model from the wall and roof of the modelled tunnel (b) Position of the head of Tom model for tunnel scenario (c) Complete setup for simulation with its boundary box.

All the steps were repeated with Hugo head model at 2400 MHz for evaluation of SAR on the human head with tunnel scenario. Similarly, the complete procedure was repeated for the evaluation of SAR at 433 MHz and 868 MHz with both Hugo and Tom head models.

### 4.5.3 Setup for Tunnel Arch Scenario on Head without Helmet

In this scenario, the interaction of electromagnetic signals with metal (steel) arch, present in the tunnel of the mock mine to provide support, was simulated. The human head was placed close to the metal arch present in the confined environment of underground mines to support the tunnel structure. The distance between Hugo head model and the tunnel arch was kept as 100 mm, and the distance between the head model and the antenna was kept as 10 mm, as shown in Fig. 4.13a. The following steps explain the procedure followed to simulate the tunnel arch scenario using Hugo's head at a frequency of 2400 MHz:

1. The 3D CST MWS file of open space scenario with Hugo's head was modified for simulation setup of the tunnel arch scenario.
2. The tunnel arch scenario modelled in CST MWS was imported as a sub-project.
3. Hugo model was transformed in the middle of the tunnel arch scenario, as shown in Fig. 4.13b.
4. The *far-field* and *power loss/SAR* monitors were defined, and post-processing was performed for SAR with power of 0.1 W using same SAR averaging method.
5. The dielectric properties of the biological tissues were updated at 2400 MHz using the *macros* tool.
6. The tunnel arch scenario with Hugo head model was simulated with 52 million mesh cells, and it took 4-5 hours to complete one simulation and associated post processing calculations. The complete setup of the tunnel arch scenario is shown in Fig. 4.13c.

All the steps were repeated with Tom's head at 2400 MHz for evaluation of SAR on the human head with the tunnel arch scenario. Similarly, the complete procedure

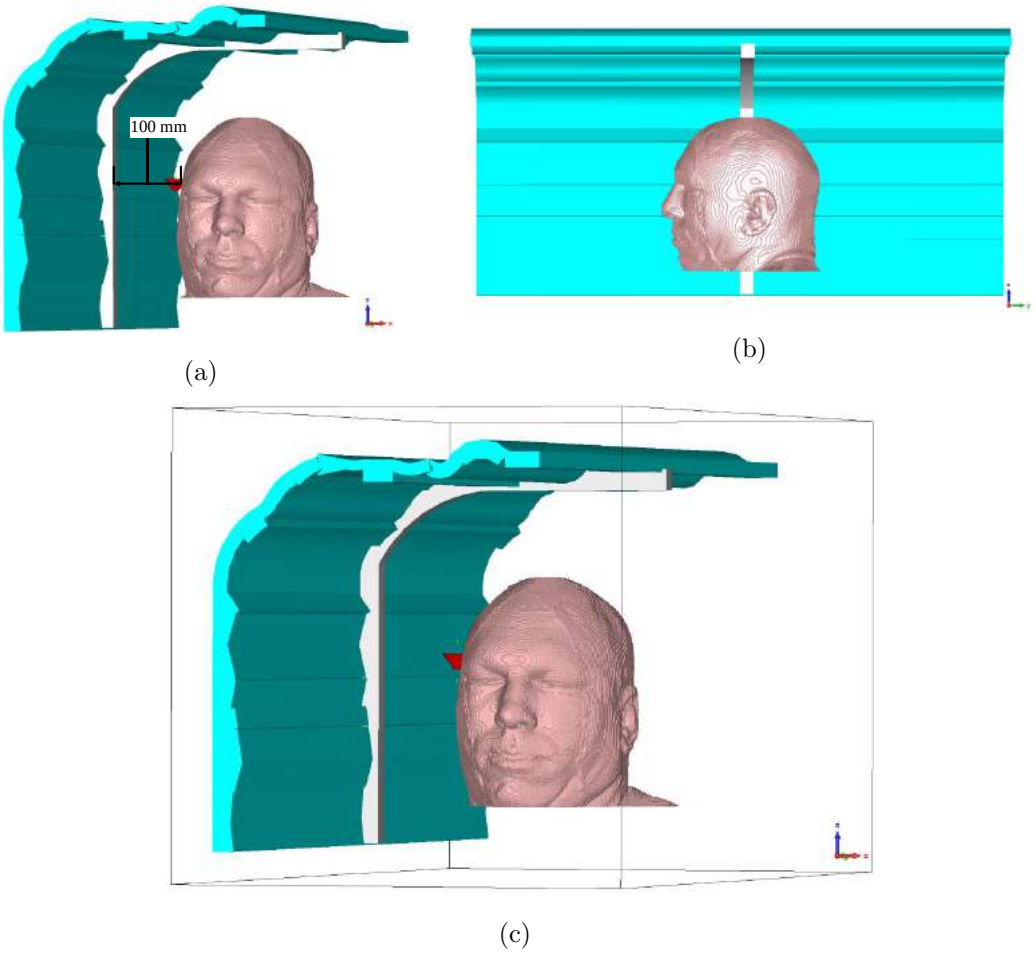



FIGURE 4.13: Complete simulation setup for the head in tunnel arch scenario (a) Distance between the Hugo model and the modelled arch of the mock mine tunnel (b) Position of the head of Hugo model with modelled tunnel arch scenario (c) Complete setup for simulation with its boundary box.

was repeated for the evaluation of SAR at 433 MHz and 868 MHz with both Hugo and Tom head for tunnel arch scenario.

### 4.5.4 Setup for Stope Scenario on Head without Helmet

This scenario corresponds to the most confined space environment of the underground mines. The stope area of the underground mine is a narrowly confined space with a number of metal support structures present in it. The total length and height of the modelled stope scenario was 800 mm and 550 mm, respectively. The following steps explain the procedure followed to simulate the stope scenario using Tom's head at a frequency of 2400 MHz:

1. The 3D CST MWS file of open space scenario with Tom head model was modified to evaluate the stope scenario on the head model.

2. The modelled CST MWS file of stope scenario for head was imported as a sub-project.

3. The human head was placed 200 mm away from the face of the stope and 200 mm from the support pillar, as shown in Fig. 4.14a. The distance between the sidewall of the stope and the human head model was kept as 100 mm, whereas the distance between the dipole antenna and the human head was kept as 10 mm.

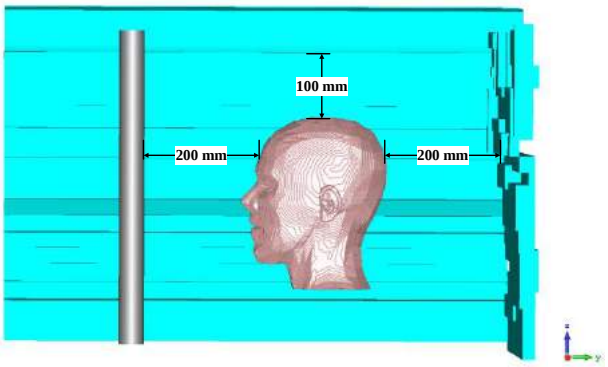
4. Both *far-field* and *power loss density/ SAR* monitors were defined at 2400 MHz. In post-processing the SAR was evaluated with 0.1 W of transmit power using same SAR averaging method.

5. The total number of mesh cells was 53 million after applying the mesh refinement on the volume and edges of the stope scenario. The simulation time for the stope scenario was 4 to 5 hours. The complete setup of the stope scenario is shown in Fig. 4.14b.

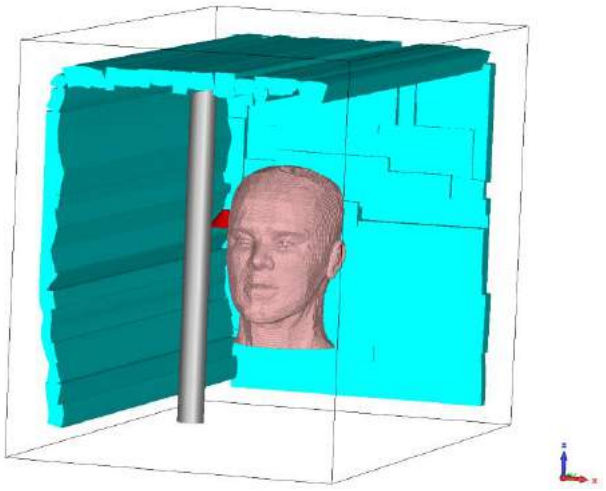
All the steps were repeated with Hugo head model at 2400 MHz for evaluation of SAR for stope scenario. Similarly, the complete procedure was repeated for the evaluation of SAR at 433 MHz and 868 MHz with both Hugo's and Tom's head for stope scenario.

## 4.6 Simulation Setup for Torso Scenario

In this section, the simulation setup on torso for open space and all modelled mock mine scenarios will be discussed. The standard procedure was followed for simulation setup for all scenarios on torso, as explained in IEEE/IEC 62704 standard. The one side of the torso facing to structure of the tunnel was investigated in this study. The testing on the other side of the torso was not provided due to limit of




(a)



(b)

FIGURE 4.14: Complete simulation setup for the head in stope scenario (a) Dimensions and Position of the head of Tom model from the face, roof and pillar of the stope (b) Complete setup for simulation with its boundary box.

time and it didn't provide the worst case analysis of SAR. The steps followed for all the simulation setups are explained below.

### 4.6.1 Setup for Open Space Scenario on Torso

In this scenario, the torso of both the Hugo and Tom voxel models were exposed to the electromagnetic source of frequency 433 MHz, 868 MHz and 2400 MHz in an open environment. The procedure described in IEEE standard [23] was followed for numerical simulations of SAR on the torso. The steps for simulation setup using Hugo model for open space scenario at 868 MHz frequency are given as follows:

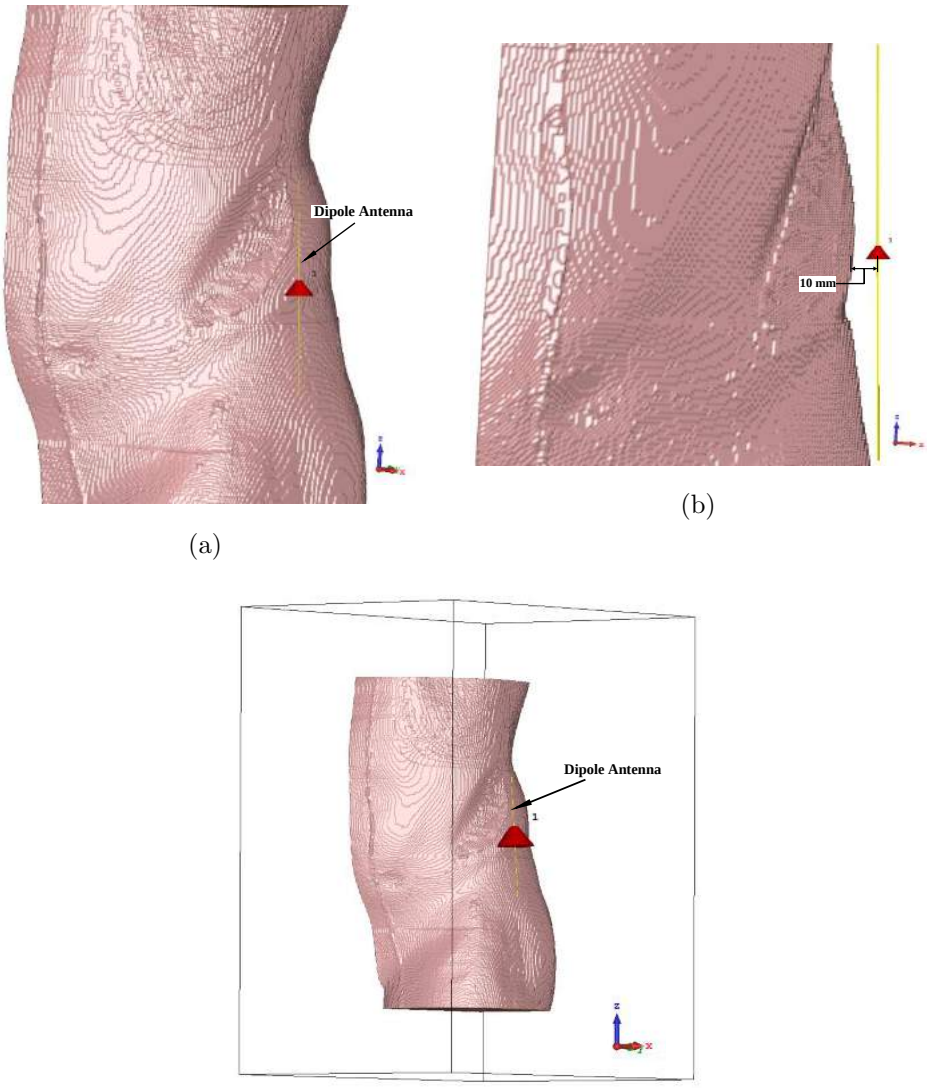
1. The human torso voxel model was imported from the CST voxel family with a resolution of $1 \times 1 \times 1mm^3$ and the CST MWS file was saved for provision of the same size of the torso used in other scenarios.

2. The electromagnetic source at 868 MHz was imported as a sub-project, and the dipole antenna was mounted on the torso. The position on the torso was critically determined. The front and back side of the torso have less reflections from the boundary of the tunnel due to more distance from the boundary. But, when the omnidirectional antenna is mounted on the front and back side of the torso, the radiations toward the torso gets absorbed in it and thus the signals cannot propagate in that direction. Therefore, it affects directional communication by absorbing more radiations in the body. The dipole antenna has more of an omnidirectional radiation pattern when it was mounted on the sides of the torso than on the front and back side of the torso. When the antenna is mounted on the side of the torso it will provide better communication. But, the side of torso is more closer to the boundary of tunnel than the front and back side of the torso. Therefore, the reflections from the boundary of the tunnel are maximum on the sides of the torso than the front and back side. Thus, this position provides the worst-case analysis of SAR, and more suitable for wearable devices to be worn in underground mines. The same position was used in this study to mount the dipole antenna on the torso for analyzing the exposure in different mock mine scenarios. The position of the dipole antenna on the torso is shown in Fig. 4.15a.

3. The torso and the dipole antenna were separated by a distance of 10 mm as shown in Fig. 4.15b.

4. The biological properties of the Hugo model were updated for 868 MHz using *macros* tool. The same steps were repeated for defining of monitors, post processing of SAR and mesh properties. The torso of Hugo model was simulated with 23 million mesh cells at 868 MHz. The time domain solver of CST MWS took 3-4 hours to complete the one simulation for open space

scenario for the torso at 868 MHz. The complete setup of open space scenario with boundary box is shown in Fig. 4.15c.




(a) (b)

(c)

FIGURE 4.15: Complete simulation setup for the torso in an open space scenario (a) Position of the dipole antenna on torso of the Hugo model (b) Distance between torso and the dipole antenna (c) Complete setup for open space scenario with a boundary box.

All the steps were repeated with the torso of Tom model at 868 MHz for evaluation of open space scenario. Similarly, the complete procedure was repeated for the evaluation of SAR at 433 MHz and 2400 MHz with the torso of both Hugo and Tom models.

### 4.6.2 Setup for Tunnel Scenario on Torso

In this scenario, the torso was exposed to EMR in the confined environment of the underground mine. The distance between the torso and tunnel was defined to be 100 mm in order to analyse worst-case SAR for tunnel scenario. The same procedure described in section 4.5.2 was followed for the simulation setup on the torso of Tom model with tunnel scenario at 2400 MHz. The post processing was performed for evaluation of SAR with 0.1 W of transmit power. The complete setup of tunnel scenario for simulation on the torso of Tom model is shown in Fig. 4.16.

All the steps were repeated with the torso of Hugo model at 2400 MHz for

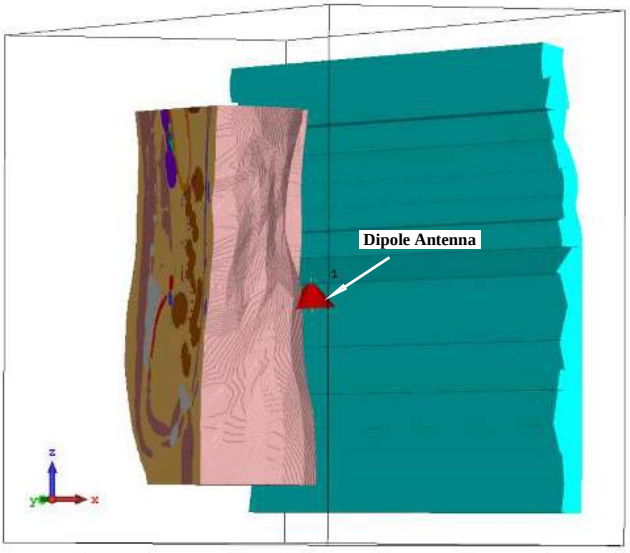



FIGURE 4.16: Complete simulation setup on the torso of Tom model for tunnel scenario.

evaluation of SAR with tunnel scenario. Similarly, the complete procedure was repeated for the evaluation of SAR at 433 MHz and 868 MHz with the torso of both Hugo and Tom models.

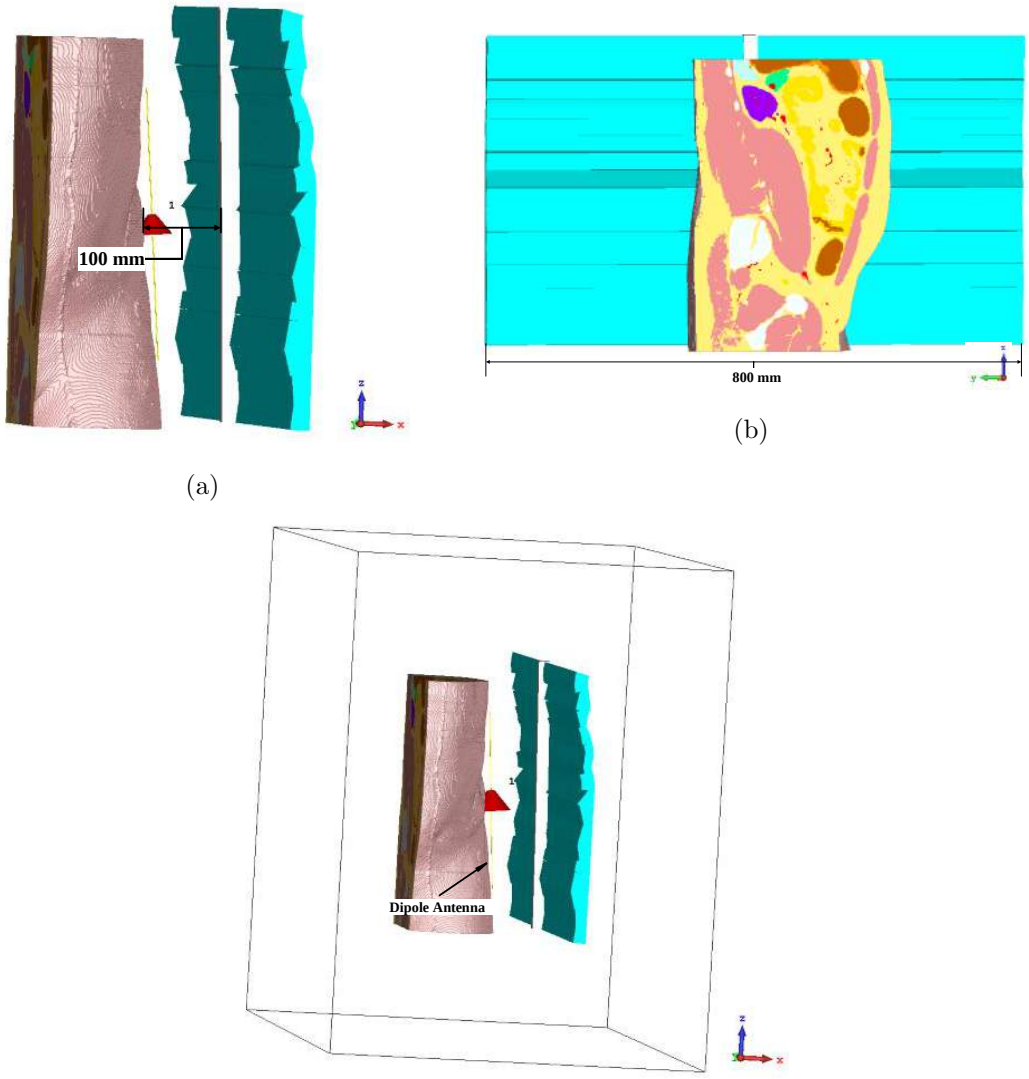
### 4.6.3 Setup for Tunnel Arch Scenario on Torso

In this scenario, the torso was exposed to EMR in metal arch scenario and using concrete boundary of the tunnel. The metal arch is used to support the tunnel structure in the underground mines. This scenario is vital as the straight length of the metal arch, and the electric field of the dipole antenna is parallel to each other due to the mounting position of the antenna on the torso. It may reflect additional number of the EMR reflections impacting upon the torso of the miner in underground mines. The distance between the torso and the tunnel arch was kept same i.e. 100 mm as shown in Fig. 4.17a. The distance between the torso and the dipole antenna was 10 mm, and the position of the torso with tunnel arch is shown in Fig. 4.17b. The procedure as described in section 4.5.3 was repeated for the simulation of tunnel arch scenario on torso. Similarly, the *far field* and *power density/ SAR* monitors were defined, and the biological properties of the tissues using *macros* tool were updated with same mesh properties. The complete setup for tunnel arch scenario on the torso of hugo model at a frequency of 433 MHz is shown in Fig. 4.17c. In post-processing, the volume of the tissues, peak spatial SAR, transmit power of 0.1 W and SAR averaging method (IEEE/IEC 62704) was specified for the evaluation of SAR. The tunnel arch scenario with the torso of Hugo model was simulated with approximately 32 million mesh cells, and it took more than 3 hours to complete one simulation and postprocessing calculations.

All the steps were repeated with the torso of Tom model at 433 MHz for the evaluation of SAR with the tunnel arch scenario. Similarly, the complete procedure was repeated for the evaluation of SAR at 868 MHz and 2400 MHz with the torso of both Hugo and Tom model for tunnel arch scenario.

## 4.7 Simulation Setup for Head with Helmet Scenario

A hard head safety helmet was modelled to investigate the impact of the helmet on the SAR value for different scenarios. The helmet on the head of the miner in underground mines can provide safety from the absorption of the EMR in the head.



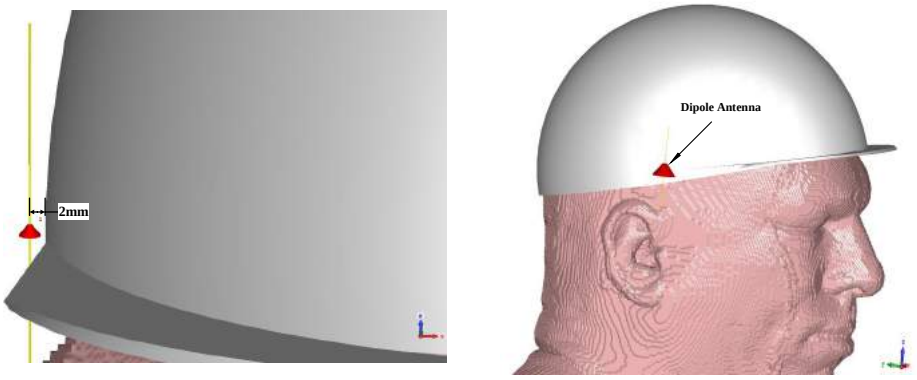

(a) (b) (c)

FIGURE 4.17: Complete simulation setup for torso in tunnel arch scenario (a) Distance between the torso of Hugo model and the arch of the modelled mock mine tunnel (b) Position of the torso with modelled tunnel arch scenario (c) Complete setup of tunnel arch scenario with its boundary box.

The modelled underground mine scenarios for the head, as outlined in section 4.3.1 were used in all simulations of the head with the helmet. A comparison between the open space and underground mine scenarios will provide the difference on the impact of EMR for both scenarios. The difference between the head without helmet and head with helmet will recommend the better location to mount the wearable devices on the helmet i.e. inside or outside of the helmet. The simulation setup for all scenarios on head with helmet are given as follows.

### 4.7.1 Setup for Open Space Scenario on Head with Helmet

In this scenario, the hard head helmet was placed on the head of both models to investigate the exposure to EMR in an open space environment. The electromagnetic source was placed outside the helmet at the same place as that selected for the simulations for the head without helmet. The distance between the dipole antenna and helmet was kept as 2 mm, as shown in Fig. 4.18a. The same steps as described in section 4.5.1 were repeated for evaluation of SAR with the helmet on the head. The complete setup for Hugo's head with helmet at 2400 MHz is shown in Fig. 4.18b. It was simulated with 18 million mesh cells after applying all the mesh refinements on the simulation setup. It took more than 2 hours to simulate one simulation for open space scenario. All the steps were repeated with




(a) (b)

FIGURE 4.18: Complete simulation setup for head with helmet in an open space scenario (a) Distance between the dipole antenna and modelled helmet (b) Mounting position of the dipole antenna on the head helmet.

the head of Tom model at 2400 MHz. The complete procedure was then repeated for simulation with the head of Hugo and Tom model at 433 MHz and 868 MHz.

### 4.7.2 Setup for Tunnel Scenario on Head with Helmet

The modelled tunnel scenario, as described in section 4.3.1 for the head without helmet scenario, was used in the simulation setup of the tunnel scenario with a helmet. The CST MWS file of open space for head with helmet was modified in this

simulation setup of tunnel scenarios. The distance between the head model and the boundary of the tunnel was kept as 100 mm. The same procedure as described in section 4.5.2 was repeated for the simulation setup. The mesh refinement was applied to reduces the number of mesh cells and increase the accuracy of the simulation. This setup was simulated with total mesh cells of 26 million, and took more than 3 hours to complete one simulation. The complete setup for Tom's head with a helmet at 868 MHz is shown in Fig. 4.19. All the steps were repeated

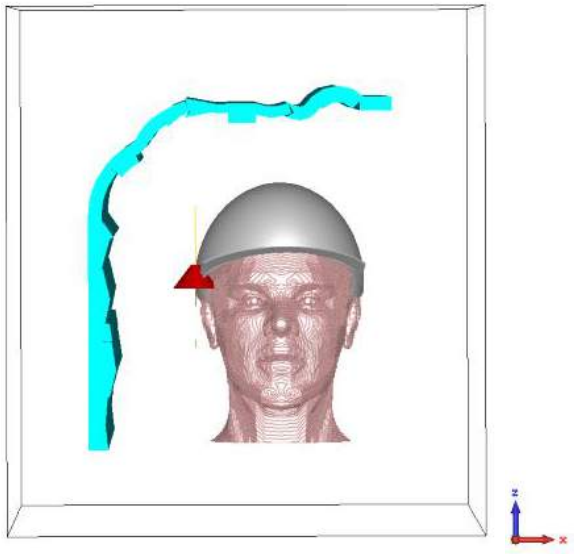


FIGURE 4.19: Complete simulation setup for head with helmet of Tom model in tunnel scenario.

with Hugo model at 2400 MHz. Finally, the complete procedure was repeated for simulation on Tom and Hugo head with a helmet at 433 MHz and 868 MHz for tunnel scenario.

### 4.7.3 Setup for Tunnel Arch Scenario on Head with Helmet

The modelled tunnel arch scenario, as described in section 4.3.1, was imported as a sub-project for the simulation setup on head with a helmet. The distance between the head model and the boundary of the tunnel was kept as 100 mm. The complete setup for Hugo's head with a helmet at 2400 MHz is shown Fig. 4.20.

After applying mesh refinement, the simulation was performed with approximately 55 million mesh cells which took 5 to 6 hours to complete one simulation. All the

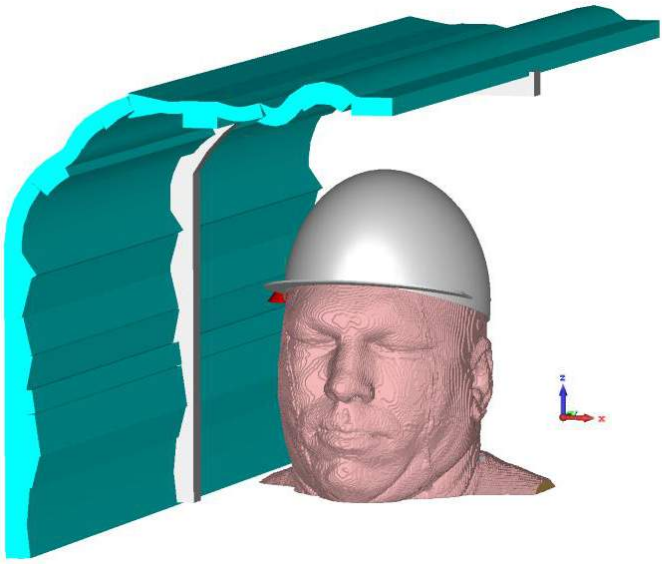


FIGURE 4.20: Complete simulation setup for head with helmet of Hugo model in tunnel arch scenario.

steps described in section 4.5.3 were repeated with Tom's head at 2400 MHz. Finally, the complete procedure was repeated for simulation on Tom and Hugo head with a helmet at 433 MHz and 868 MHz for tunnel scenario.

### 4.7.4 Setup for Stope Scenario on Head with Helmet

In the same manner, the stope scenario modelled for head was used in the simulation of head with a helmet scenario. The same steps performed in section 4.5.4 were followed for the simulation setup of stope scenario with a helmet. The same distances from the wall, face and pillar of the stope were employed for a fair comparison at different frequencies and scenarios. The complete setup for Tom's head with a helmet at 433 MHz is shown in Fig. 4.21. All the steps were repeated with Hugo's head at 433 MHz. The same procedure was repeated for simulation with the head of Tom and Hugo model at 868 MHz and 2400 MHz for stope scenario. The summary of all the simulation setups for head without helmet, torso and head

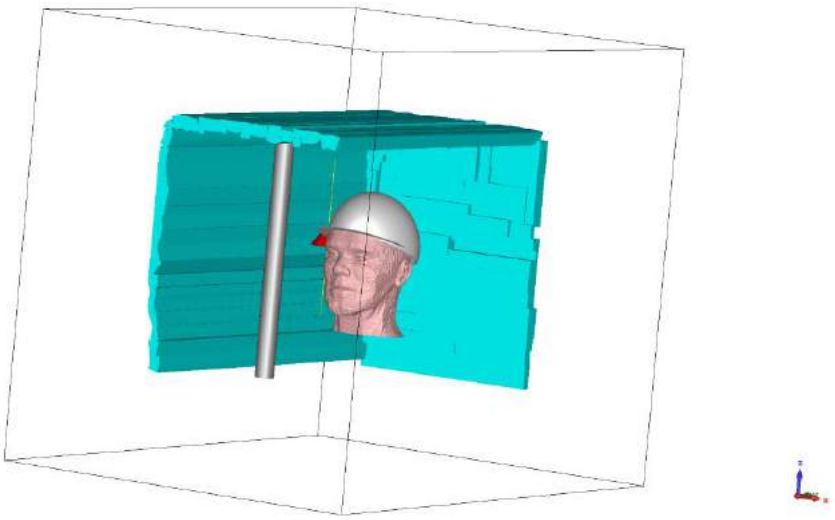


FIGURE 4.21: Complete simulation setup for head with helmet of Tom model in stope scenario with boundary box.

with helmet is shown in Table 4.4. It summarize the mesh size and approximate simulation time for all the setups at all frequencies.

## 4.8 Simulation Setup for Different Power Levels

In this section, different transmission power levels for wearable device in the underground mine scenarios were investigated. As suggested by some studies, the wearable devices can increase the power levels when the connection between two devices is lost, which may help to re-establish communication after a disaster for the rescue operation in underground mines [5]. In the post-processing of CST MWS, the SAR monitors with different power levels were defined to study the maximum power levels for wearable devices which would respect the SAR guidelines in such disaster scenarios in underground mines. All the simulations on head without helmet and torso were simulated for the analysis of maximum power level which can be allowed without contravening the SAR limits as per ICNIRP standards [67]. The transmit power threshold defined by Independent Communication Authority of South Africa for 433 MHz and 868 MHz is 0.1 W, whereas for 2400 MHz it is 0.01 W [69]. The transmit power levels used in this study for 433 MHz were 0.1 W, 0.5 W, 1 W, 1.2 W and 1.5 W, and for 868 MHz used

Table 4.4: Summary of all simulation setups for head without helmet, torso and head with helmet.

| | Scenarios | 433 MHz | | 868 MHz | | 2400 MHz | |
|---|---|---|---|---|---|---|---|
| | | Mesh Size (Millions) | Simulation Time (Hours) | Mesh Size (Millions) | Simulation Time (Hours) | Mesh Size (Millions) | Simulation Time (Hours) |
| Head without helmet | Free Space | 11 | 2-3 | 13.2 | 2-3 | 15 | 3-3.5 |
| | Tunnel | 40 | 5-5.5 | 45.5 | 5.5-6 | 55 | 6-6.5 |
| | Tunnel Arch | 44 | 5.5-6 | 49 | 5.5-6 | 52 | 6-6.5 |
| | Stope | 53 | 6-6.5 | 56 | 6.5-7 | 65 | 7.5-8 |
| Torso | Free Space | 23 | 4-5 | 34 | 5-6 | 42 | 5.5-6 |
| | Tunnel | 31 | 4.5-5 | 57 | 6.5-7 | 68 | 8-8.5 |
| | Tunnel Arch | 32 | 4.5-5 | 63 | 7-8 | 74 | 9-10 |
| Head with helmet | Free Space | 12 | 2-3 | 14 | 2-3 | 18 | 3-3.5 |
| | Tunnel | 26 | 3.5-4 | 38.5 | 4.5-5 | 48 | 6-6.5 |
| | Tunnel Arch | 33 | 4-5 | 40 | 5-5.5 | 55 | 6-6.5 |
| | Stope | 35 | 4-4.5 | 48 | 5-5.5 | 61 | 7-8 |

transmit power levels were 0.1 W, 0.5 W, 1 W and 1.2 W, and transmit power levels of 0.01 W, 0.05 W, 0.1 W, 0.15 W and 0.2W were used for 2400 MHz. Only the Hugo model was used in this investigation.

## 4.9 Simulation Setup for Variation of Distance

SAR is also affected by distance between the vicinity environment and the electromagnetic source. The distance between the electromagnetic source and the underground mine structure was varied in this simulation setup to investigate variation of distance. In all previous simulations, the distance between the human voxel model and boundaries of underground mine was kept as 100 mm which was varied to 150 mm and 200 mm. The variation of SAR was investigated at 868 MHz and 2400 MHz for head without helmet, torso and head with a helmet. Only Hugo model was used in this investigation.

# Chapter 5

# Simulation Results and Discussion

In this chapter, the simulation results have been presented and discussed in detail. The bar charts were used for the comparison of SAR values for different scenarios, frequencies and human voxel models. The SAR analysis at different frequencies led to recommendations concerning the best frequency to be used in terms of less absorption in the human body. The $SAR_{10g}$ values were analysed on head without helmet, torso and head with helmet for different scenarios and frequencies, which are discussed in section 5.1, section 5.2 and section 5.3, respectively. In section 5.4, the SAR values are discussed to find the maximum transmit power levels that can be used in underground mines to rescue the miner after a disaster. The variation of SAR values with different distances for different scenarios are analysed in section 5.5. Finally, in section 5.6, the results of this study are discussed and concluded.

## 5.1 SAR Analysis for Head without Helmet Scenario

The SAR values of human head for open space and three underground mine scenarios were compared at three different frequencies commonly used in underground mines for wireless communication. In this study, the SAR value for 10g of tissues was observed and denoted as $SAR_{10g}$. To validate the results, the SAR values for 1g of tissues at all frequencies were analysed for different scenarios. The $SAR_{1g}$ values on head without helmet for different scenarios and frequencies with both voxel models are given in Appendix C. The SAR values for 1g of tissues were found to have the same behavior to that of SAR values for 10g of tissues. It was

observed that the simulated $SAR_{10g}$ values in open and underground mine scenarios were under the limits prescribed by ICNIRP [67] and IEEE [25] at 433 MHz, 868 MHz and 2400 MHz. The $SAR_{10g}$ distribution in the head of Hugo and Tom model was analysed at 2400 MHz, 868 MHz and 433 MHz in open space scenario as shown in Fig. 5.1. The SAR distribution was different in Hugo and Tom model due to the difference in the amount of tissues and mass of the body. The SAR distributions for both voxel models were same in all underground mine scenarios for all concerned frequencies i.e. 433 MHz, 868 MHz and 2400 MHz. It indicates that the underground mine structure has no impact on the distribution of SAR on the body of the miner working in underground mines. The $SAR_{10g}$ values of Hugo and Tom head in open space scenario were found to be 1.5 W/Kg and 1.42 W/Kg, respectively, which are close to each other. The SAR values in the head of Tom model are slightly less than those in the head of Hugo model because the amount of fat, muscle and other tissues were different in both voxel models, and varies in human to human due to their different masses. When both the head models were exposed to EMR in the confined environment of the underground mines, the SAR values were found to be higher than those for the open space scenarios. From this, one can conclude that the reflections from the boundary of the underground mines are enhancing EMR exposed to the body and thus increasing the SAR values. For all underground mine scenarios, the corresponding SAR values were higher than those for the open space scenario at 2400 MHz, as shown in Fig. 5.2. The $SAR_{10g}$ values of Hugo and Tom models for tunnel arch scenario were found to be 1.6 W/Kg and 1.5 W/Kg, respectively, which were 10% and 8% higher from the other mock mine and open space scenarios, respectively. It exhibits that the metal arch reflects more electromagnetic signals, and results in additional EMR absorption by the body of the miner. Thus, it can be concluded that the presence of metal in underground mines increases the exposure of the miners to EMR. A similar behavior was also observed for 868 MHz, where the SAR values for both models were also found to be higher in all underground mine scenarios than those in the open space scenario. In this case, the $SAR_{10g}$ values were maximum for tunnel and tunnel arch scenarios in the head of Hugo and Tom models as shown

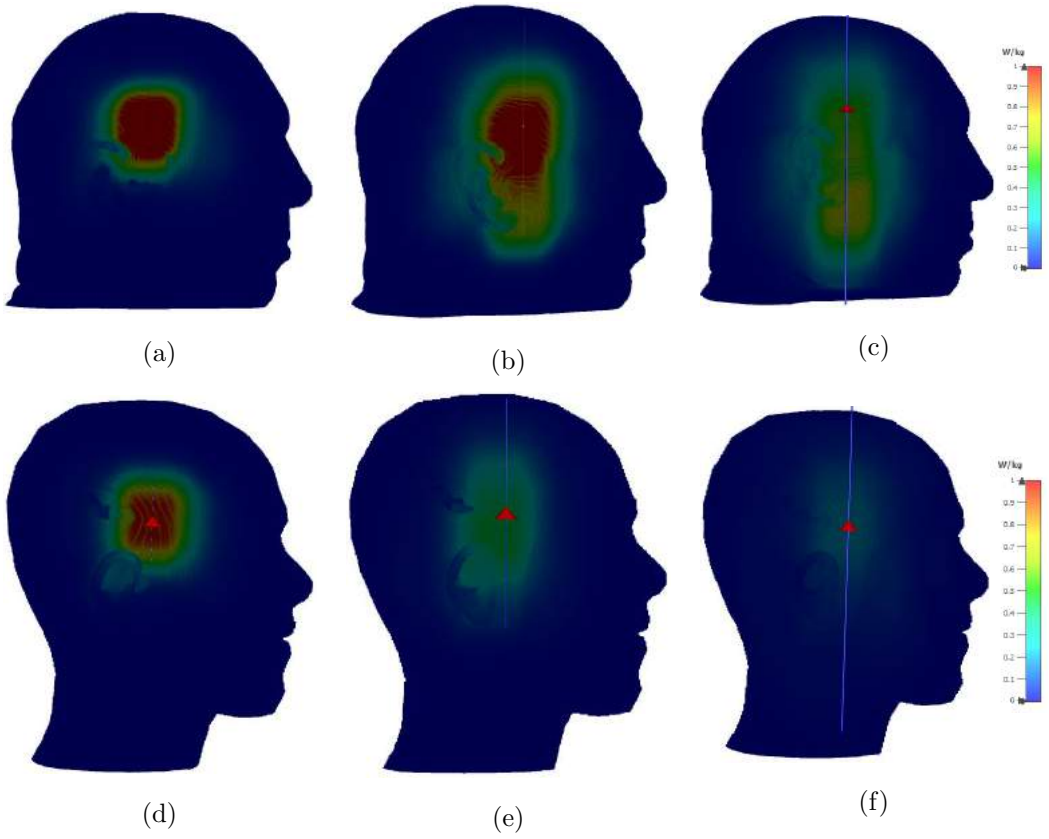



FIGURE 5.1: $SAR_{10g}$ distribution in the head of hugo model at (a) 2400 MHz, (b) 868 MHz and (c) 433 MHz, and in the head of Tom model at (d) 2400 MHz, (e) 868 MHz and (f) 433 MHz.

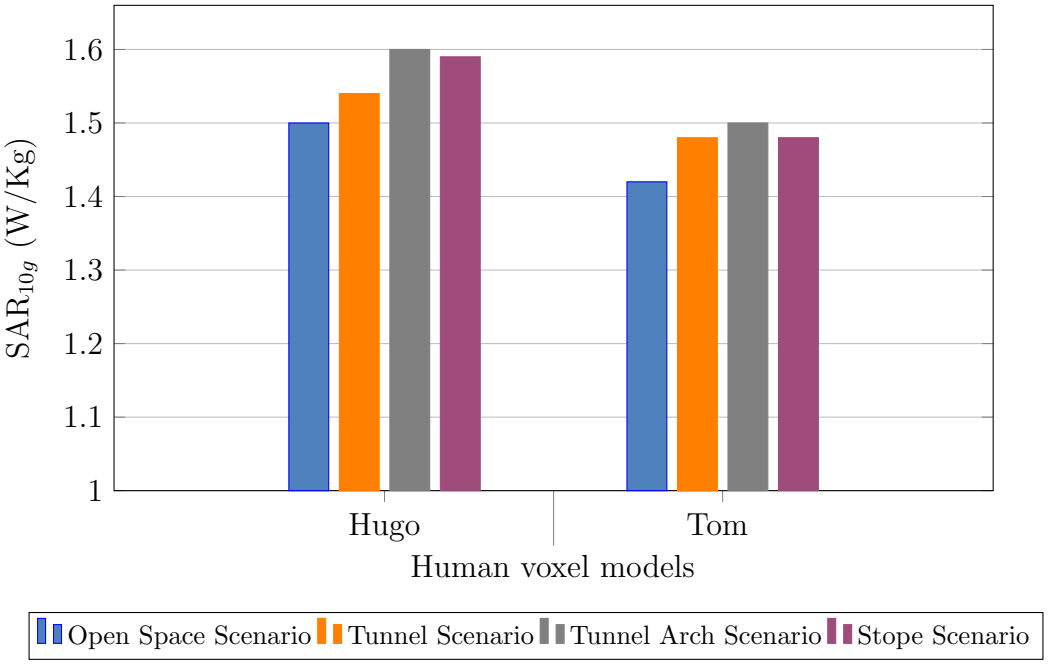



FIGURE 5.2: Comparison of $SAR_{10g}$ values in the head without helmet of both models for different scenarios at 2400 MHz.

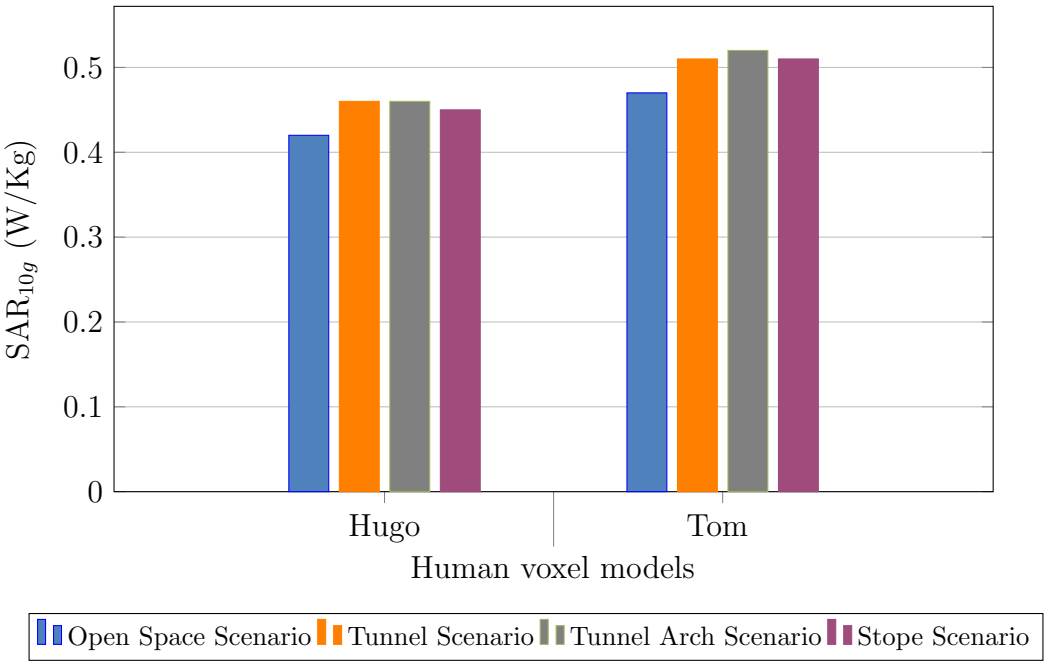



FIGURE 5.3: Comparison of $SAR_{10g}$ values in the head without helmet of both models for different scenarios at 868 MHz.

in Fig. 5.3. For tunnel arch scenario, the $SAR_{10g}$ values of Hugo and Tom were 4% and 5% higher than the open space scenario, respectively. The $SAR_{10g}$ values for Hugo and Tom models at 868 MHz were less than those at the 2400 MHz with the same transmit power defined for SAR evaluation i.e. 0.1 W. The difference was due to the different penetration behavior of the electromagnetic waves at different frequencies in the surrounding environment and human body. It can also be concluded that the electromagnetic signals at low frequency result in low SAR values because of fewer reflections from the boundary of the underground mines, but they have more absorption in the tissues deep inside the human brain.

Similarly, at 433 MHz, the $SAR_{10g}$ values for all underground mine scenarios were very close to those for the open space scenario, as shown in Fig. 5.4. This was due to the fewer reflections from the boundaries of the tunnel. It was observed that when the lower frequency was used, it has less reflections from the vicinity environment and hence, less absorption in the human body, however, the penetration was deep inside the tissues of the human body. The absorption in the human body at high frequency was more but has little penetration inside the body i.e. higher frequencies mostly interact with the skin of the human body and closer tissues of

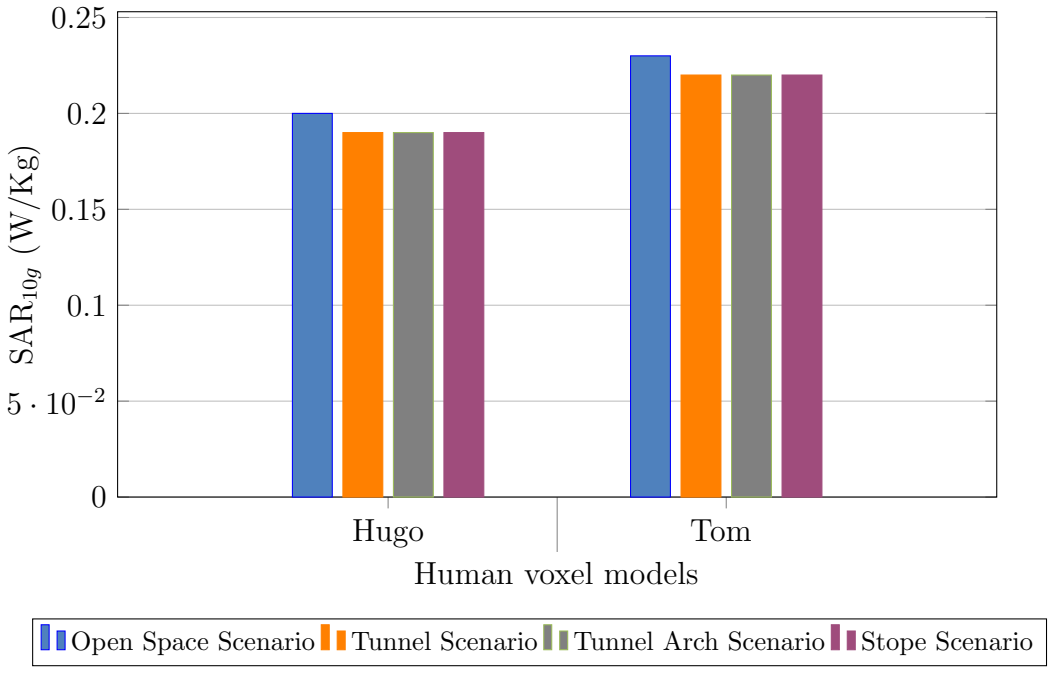
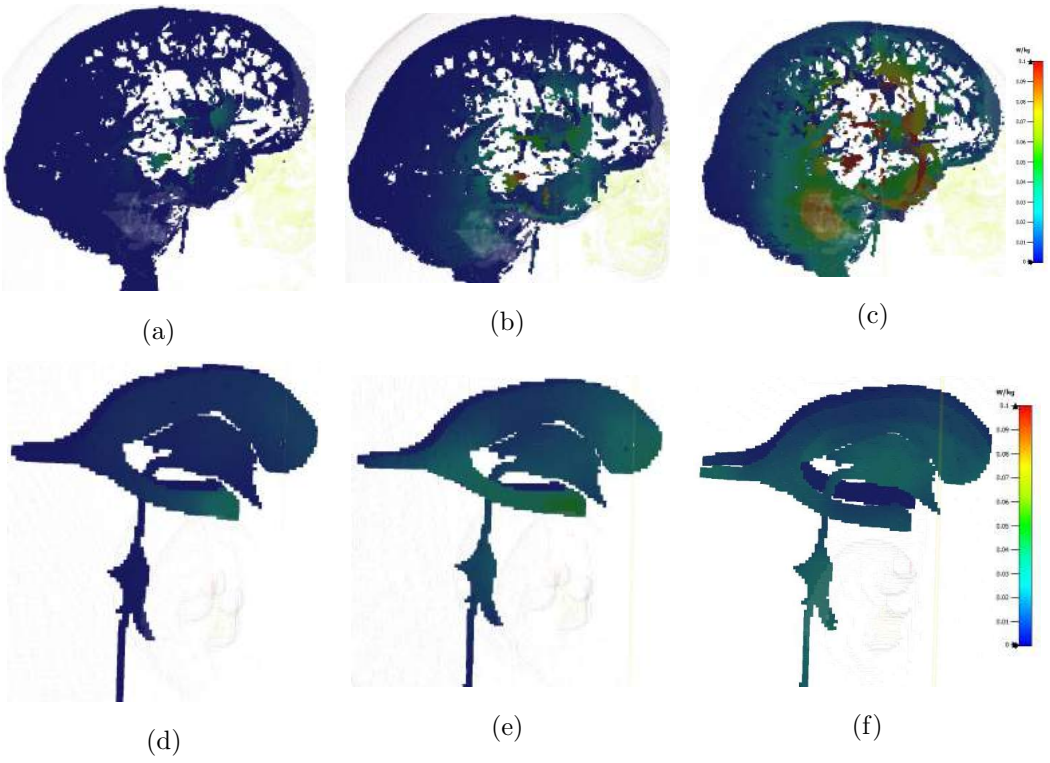



FIGURE 5.4: Comparison of $SAR_{10g}$ values in the head without helmet of both models for different scenarios at 433 MHz.

the skin. The SAR values at 433 MHz were lower than those at 2400 MHz and 868 MHz. Therefore, lower frequencies are better for usage in underground mines in terms of better propagation and lesser health impact on the miners.

Table 5.1 shows the $SAR_{10g}$ values in different types of tissues of head in Hugo model for all the frequencies under observation in this study. The head tissues under observation were skin, fat, muscle, brain grey matter, brain white matter and cerebrospinal fluid (CSF). It was observed that the $SAR_{10g}$ in the skin decreases as the transmit frequency of the source was lowered. This is due to EMR penetration deep inside the body at lower frequencies, whereas the impact from high frequencies remained concentrated near the skin. The $SAR_{10g}$ was higher for lower frequencies in the inner and more sensitive tissues of the human head such as CSF. The $SAR_{10g}$ distribution in CSF tissues for both models at 2400 MHz, 868 MHz and 433 MHz is shown in Fig. 5.5. It demonstrates that the SAR value is higher at 433 MHz than the higher frequencies. In general, it is observed that the SAR value is less for lower frequencies, but it has more impact in the tissues inside the human brain, although all the SAR values are within the safety limits prescribed by ICNIRP and IEEE.



(a) (b) (c)

(d) (e) (f)

FIGURE 5.5: $SAR_{10g}$ distribution in Cerebrospinal Fluid (CSF) for Hugo model at (a) 2400 MHz, (b) 868 MHz and (c) 433 MHz, and for Tom model at (d) 2400 MHz, (e) 868 MHz and (f) 433 MHz.

TABLE 5.1: Variation of $SAR_{10g}$ in different tissues of the head of Hugo model at different frequencies for open space scenario

| Frequencies | Different Tissues of Head | | | | | |
|---|---|---|---|---|---|---|
| | Skin | Fat | Muscle | Brain white matter | Brain grey matter | CSF |
| 2400 MHz | 0.47 | 0.02 | 0.1 | 0.02 | 0.07 | 0.02 |
| 868 MHz | 0.25 | 0.02 | 0.09 | 0.08 | 0.13 | 0.1 |
| 433 MHz | 0.18 | 0.02 | 0.09 | 0.07 | 0.1 | 0.15 |

## 5.2 SAR Analysis for Torso Scenario

The $SAR_{10g}$ values on the torso of both voxel models, i.e. Tom and Hugo, for open and underground mine scenarios are presented in this section. Firstly, the distribution of power loss density on the torso of Hugo and Tom model at 2400 MHz, 868 MHz and 433 MHz was analysed, and shown in Fig. 5.6. The power loss density determines the amount of power loss in the biological tissues. It exhibits

that the power loss density was reduced as the low frequency electromagnetic signal was used, and resulted in lower values of SAR at low frequencies. The SAR values corresponding to two underground mines scenarios i.e. tunnel and tunnel arch were compared with the open space scenario. The $SAR_{10g}$ values for all underground mine scenarios were higher than the open space scenario. It exhibits that the reflections from the boundary of the tunnels and metal arch increase the impact of EMR on the miner in confined environment of underground mine. All the $SAR_{10g}$ values at 433 MHz, 868 MHz and 2400 MHz for torso were under the safety limits prescribed by ICNIRP [67] and IEEE [25] for transmit power of 0.1 W. At 2400 MHz, the $SAR_{10g}$ values in the torso of Hugo and Tom for tunnel scenario were 5% higher than the open space scenario, as shown in Fig. 5.7. These values are higher than those for the other scenarios due to more reflections from the structure of the tunnel. The $SAR_{1g}$ values were also analysed on torso for different scenarios in order to validate the results as given in Appendix D. A similar behavior was observed for SAR with 10g and 1g of tissues on torso for all scenarios. The $SAR_{10g}$ value for torso of Tom was higher than that for torso of Hugo due to different amount of tissues and masses of the human body. The comparison of $SAR_{10g}$ values for torso in the open and underground mine scenarios at 2400 MHz is shown in Fig. 5.7.

The behavior observed for different scenarios at 848 MHz was similar to that at 2400 MHz. At 868 MHz, the $SAR_{10g}$ values for underground mine scenarios were higher than the open space scenarios. The $SAR_{10g}$ values in torso of Hugo and Tom models for tunnel arch scenario were 3% and 4% higher than the open space scenario, respectively, as shown in Fig. 5.8. Also, at 868 MHz, the $SAR_{10g}$ values for different scenarios are less than the SAR values for corresponding scenarios at 2400 MHz.

A similar behavior was observed for different scenarios at 433 MHz. The $SAR_{10g}$ values at 433 MHz for tunnel arch scenario was higher than those for the tunnel and open space scenarios. Also, the SAR values at 433 MHz for different scenarios are less than those for 868 MHz and 2400 MHz. The difference in SAR values between underground and open space scenarios gets reduced as a lower frequency

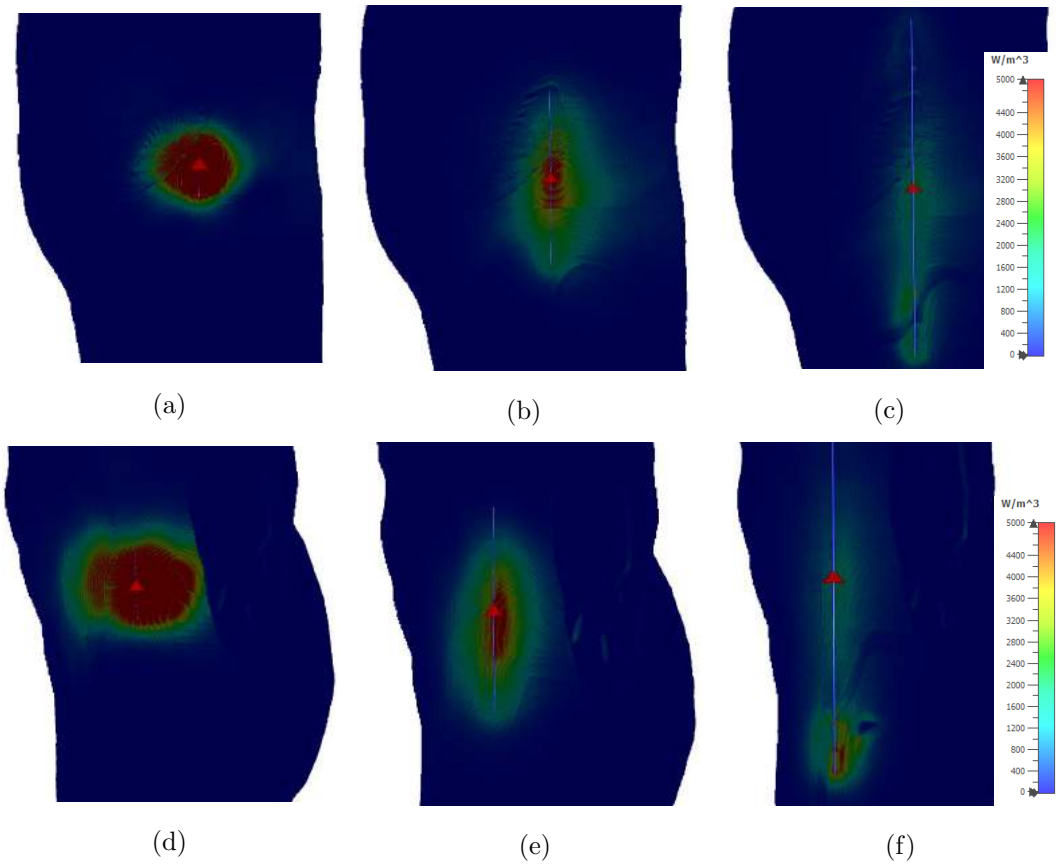



FIGURE 5.6: Power loss Density ($W/m^3$) in the torso of Hugo model at (a) 2400 MHz, (b) 868 MHz and (c) 433 MHz, and in the torso of Tom model at (d) 2400 MHz, (e) 868 MHz and (f) 433 MHz.

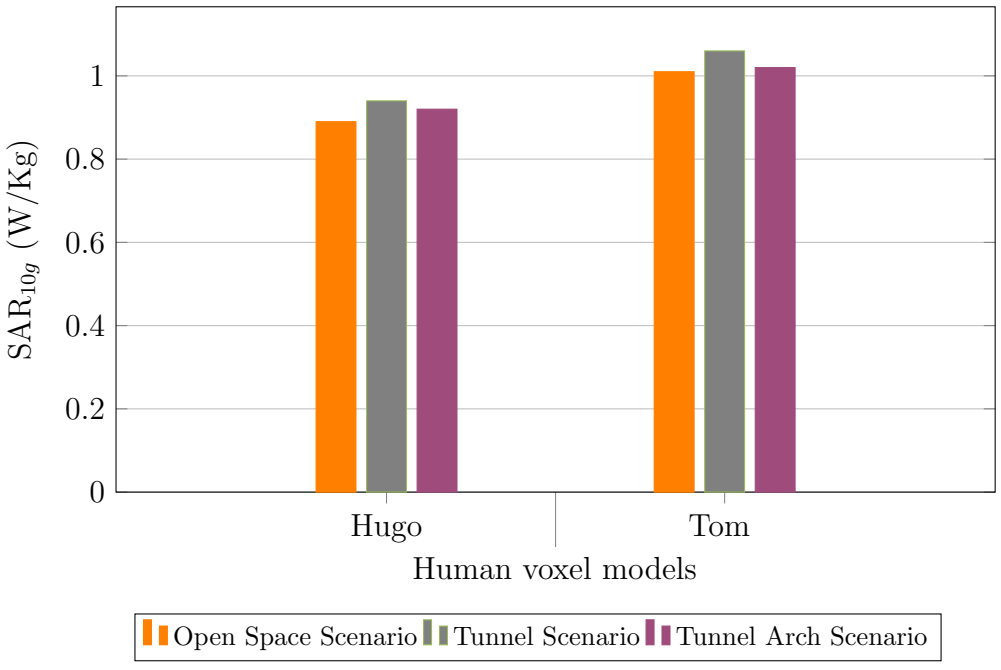



FIGURE 5.7: Comparison of $SAR_{10g}$ values in the torso of both models for different scenarios at 2400 MHz.

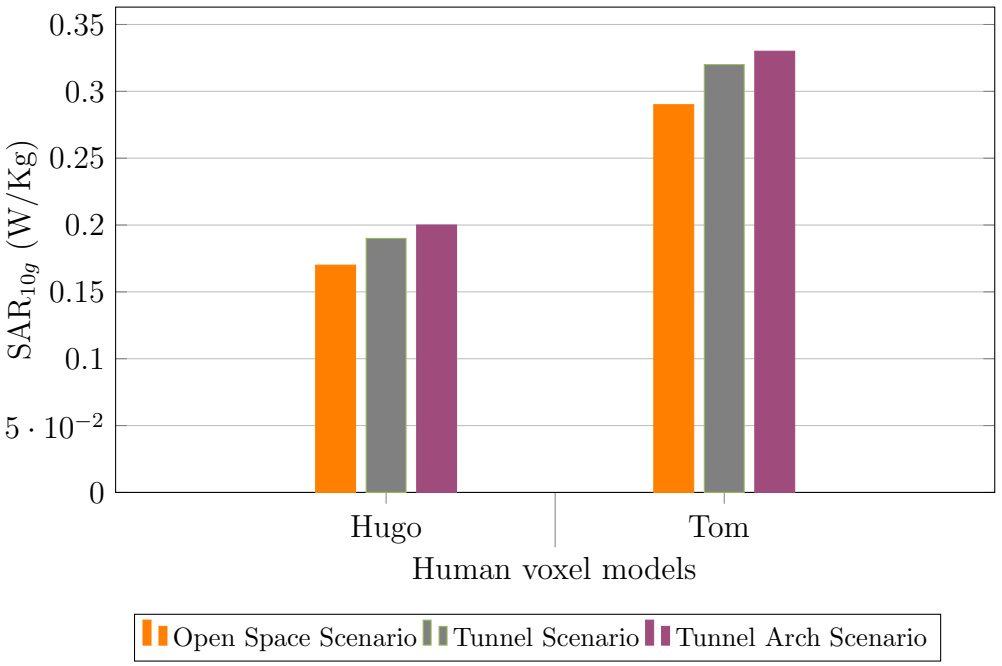



FIGURE 5.8: Comparison of $SAR_{10g}$ values in the torso of both models for different scenarios at 868 MHz.

was used because the lower frequency signals have lesser reflections from the surrounding environment. The penetration of EMR inside the body at low frequency is higher than that for high frequency. Consequently, at low frequency, the impact of EMR on the organs inside the human torso is more profound than that for the higher frequencies, which contributes to the elevation of the core temperature of the human body. The comparison of $SAR_{10g}$ values at 433 MHz for torso in the open and underground mine scenarios is shown in Fig. 5.9.

Table 5.2 shows the variation of SAR in different tissues of torso of Hugo model for all frequencies under consideration in this study. The $SAR_{10g}$ at 2400 MHz in the skin was higher than its value at 433 MHz, whereas, the SAR values for the organs inside of the torso such as kidney, small intestine and spleen, were higher at 433 MHz than the corresponding values at higher frequencies. It verifies that the absorption of EMR was deep inside the tissues of the torso at lower frequencies.

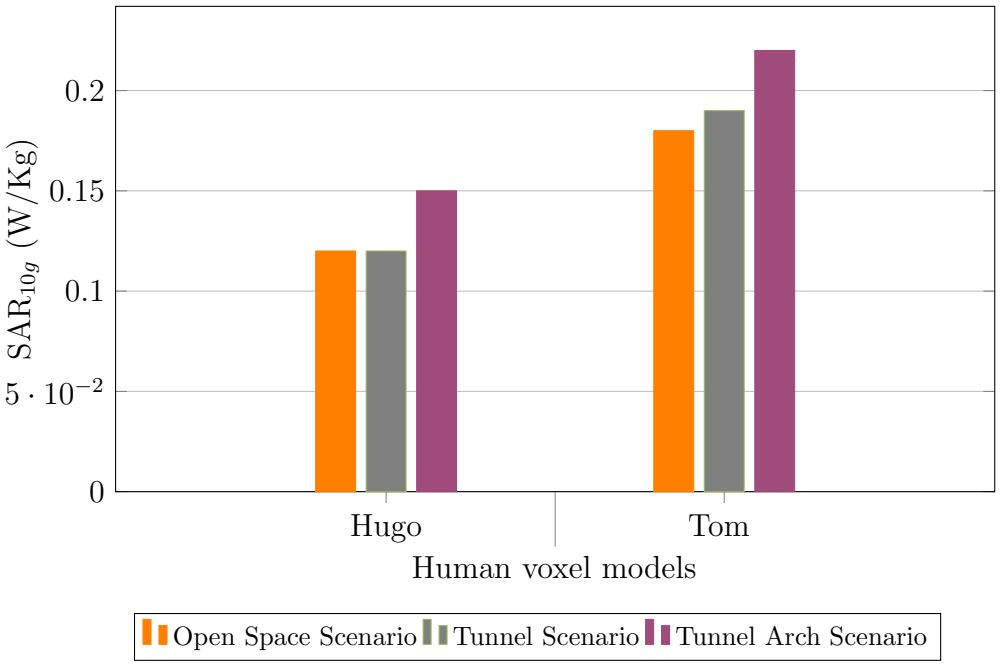



FIGURE 5.9: Comparison of $SAR_{10g}$ values in the torso of both models for different scenarios at 433 MHz.

TABLE 5.2: Variation of $SAR_{10g}$ in different tissues of the torso of Hugo model at different frequencies

| Frequencies | Different Tissues of Torso | | | | | |
|---|---|---|---|---|---|---|
| | Skin | Fat | Muscle | Small Intestine | Kidney | Spleen |
| 2400 MHz | 0.58 | 0.03 | 0.02 | $2.7 \times 10^{-4}$ | $7.8 \times 10^{-5}$ | $8.6 \times 10^{-5}$ |
| 868 MHz | 0.42 | 0.02 | 0.04 | $5.8 \times 10^{-3}$ | $2.1 \times 10^{-3}$ | $7.4 \times 10^{-3}$ |
| 433 MHz | 0.26 | 0.02 | 0.05 | 0.015 | $9.7 \times 10^{-3}$ | $3.4 \times 10^{-3}$ |

## 5.3 SAR Analysis for Head with Helmet Scenario

For the case of human head with a helmet, the SAR values at 2400 MHz for underground mine scenarios were closer to those for open space scenario. Each simulations was performed twice and repeated the same results. The helmet layer absorbs some of the EMR and provides shielding from the radiations. The comparison of SAR values at 2400 MHz for different scenarios and for both voxel models is shown in Fig. 5.10. The $SAR_{10g}$ values for Hugo and Tom model in stope scenario were 8% and 7% higher than the open space scenario, respectively. It was observed that the SAR values in both voxel models for different scenarios

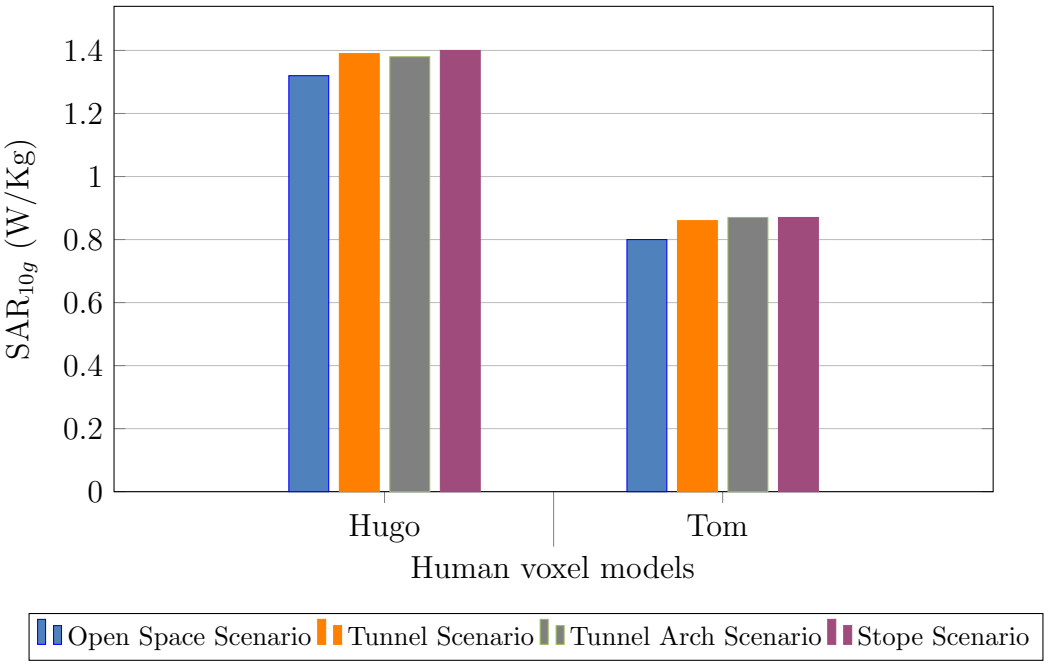



FIGURE 5.10: Comparison of $SAR_{10g}$ values in the head with helmet of both models for different scenarios at 2400 MHz.

were lower in case of head with helmet than those for head without helmet. This is due to the difference in the distance between the boundary of helmet and the dipole antenna. Moreover, when the dipole antenna was placed on the outside, it increases the distance between the head and the antenna which results in the low level of impact to the miner. The SAR values in the head of Tom model for all scenarios were less than those in the head of Hugo model. This is due to the fact that the standard size of the helmet was used in the analysis, which results in more space between the head and the helmet for Tom because of his smaller head than Hugo. Therefore, the smaller head has more safety from the exposure of EMR when the wearable device is mounted on the outside of the helmet.

The $SAR_{10g}$ values at 868 MHz for the head with a helmet were higher in all underground mine scenarios than those in the open space scenario. For tunnel arch scenario, the $SAR_{10g}$ values for Hugo and Tom model were 17% and 6% higher than the open space scenario, respectively, as shown in Fig. 5.11. It implies a similar conclusion that the presence of metal increases the reflections in a confined space of the underground mines, which causes a higher absorption of EMR in the head of the miner. The SAR values in the head of Tom model were lower than

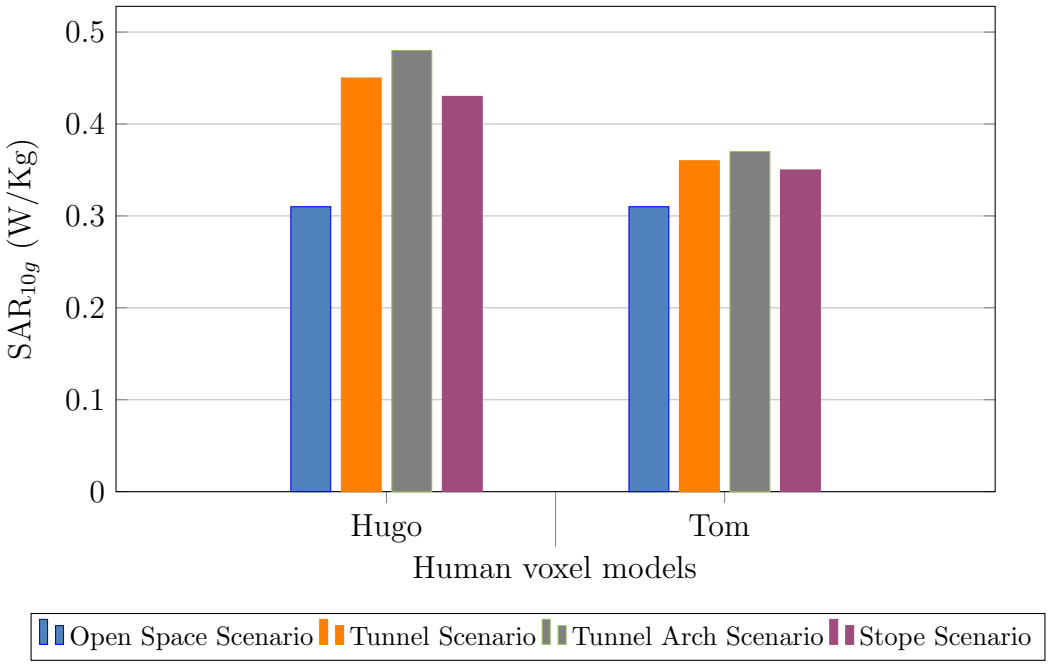



FIGURE 5.11: Comparison of $SAR_{10g}$ values in the head with helmet of both models for different scenarios at 868 MHz.

those in the head of Hugo model due to the difference in the distance between the antenna and the head model.

A similar behavior was observed at 433 MHz. The $SAR_{10g}$ values for the tunnel arch scenario were higher than those for the open space and other underground mine scenarios, as shown in Fig. 5.12. It can be observed from the figure that the SAR values at 433 MHz in both voxel models are comparable as the penetration inside the body at lower frequency is higher.

Therefore, the helmet is providing less safety than the amount of protection provided by the helmet for the case of the higher frequency. The SAR values are less for the head with a helmet which affirms that the presence of the helmet provides safety from the EMR. Thus, the outer surface of the helmet is the better location to mount the antenna on the head, which would provide more safety from the exposure to EMR in the underground mine scenarios. In order to enhance safety from EMR in underground mines, a shielding on the helmet can be used to provide more safety in terms of EMR exposure to the miner. The $SAR_{1g}$ values for all frequencies were also analysed on head with helmet for different scenarios to validate the results as given in Appendix E. A similar behavior for SAR values averaged

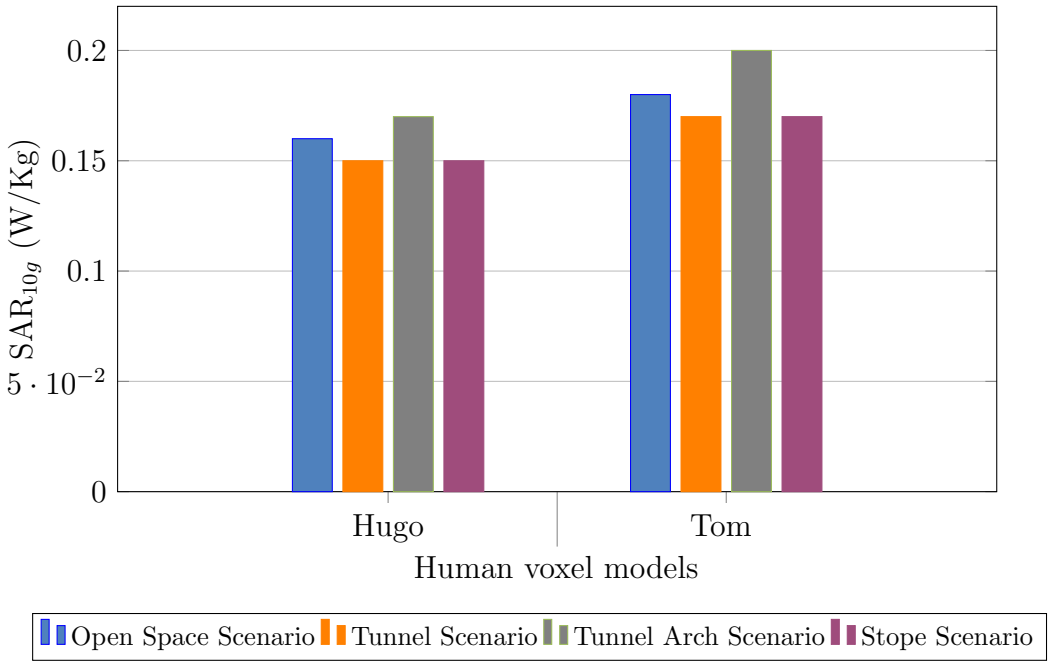



FIGURE 5.12: Comparison of $SAR_{10g}$ values in the head with helmet of both models for different scenarios at 433 MHz.

using 1g of tissues was concluded for all scenarios with both voxel models.

## 5.4 SAR Analysis for Different Power Levels

In case of a mine disaster, it is crucial to track the location of the miners trapped inside the collapsed mine. Generally, in this scenario, the communication between the miner and control room is lost due to which it takes a lot of time for the rescue teams to locate the trapped miners. Some recent studies [5] have suggested making use of wearable devices to track the miners in case of a mine disaster. These wearable devices could be made to increase the power level to restore communication, which may be blocked because of heaps of rock and debris. Therefore, it is vital to investigate the maximum power levels that can be used in underground mines in such scenarios. These maximum transmit power levels will be used for a brief interval of time in case of loss of communication with the miner after a disaster in underground mines. A small impact of EMR on the health of miner can be disregarded for that brief interval of time so as to save the life of the miner. Further research needs to be done in this direction to find out the interval and

the maximum level of the transmit power that could be used in such scenarios without causing severe damage to the miners, but that is out of the scope for this dissertation.

In this study, different power levels were investigated with Hugo voxel model for their SAR impact on head and torso. The reference levels for the transmit power provided by the regulatory body of South Africa i.e. ICASA (Independent Communications Authority of South Africa) at 433 MHz, 868 MHz and 2400 MHz were used in this study. The $SAR_{10g}$ values were evaluated at different power levels for head and torso, and the results are explained below.

**For Head:** The power levels used for head at 2400 MHz were 0.01 W, 0.05 W, 0.1 W, 0.12 W and 0.15 W. The variation of $SAR_{10g}$ on the head at 2400 MHz with different power levels for open space, tunnel arch and stope scenarios is shown in Fig. 5.13. As it can be seen from the figure, the SAR threshold of 2 W/Kg, as prescribed by IEEE and ICNIRP, gets violated at the transmit power level of 0.12 W for 2400 MHz. Therefore, the maximum transmit power that can be used in underground mines at 2400 MHz should be less than 0.12 W in case of a disaster when wearable device is mounted on the head of the miner. Also, the recommended maximum transmit power level should preferably be used for brief durations so as to cause minimal health damage during the rescue operation to track the location of the miner in collapsed mine scenario.

Similarly, for 868 MHz, the SAR values for the power levels of 0.1 W, 0.3 W and 0.5 W were investigated to find the maximum transmit power levels that can be used in underground mines. The variation of $SAR_{10g}$ at different power levels for open space, tunnel arch and stope scenarios is shown in Fig. 5.14. The maximum transmit power level, as per the regulatory authorities, is 0.1 W at 868 MHz, which is used for communication in underground mines in normal scenarios. However, in case of a disaster and loss of communication, a maximum transmit power of 0.3 W can be used for communication at 868 MHz without causing damage to the miners in terms of SAR when wearable device is mounted on the head of the miner working in underground mine.

Similarly, the $SAR_{10g}$ variation at power levels of 0.1 W, 0.5 W, 1 W and 1.2 W

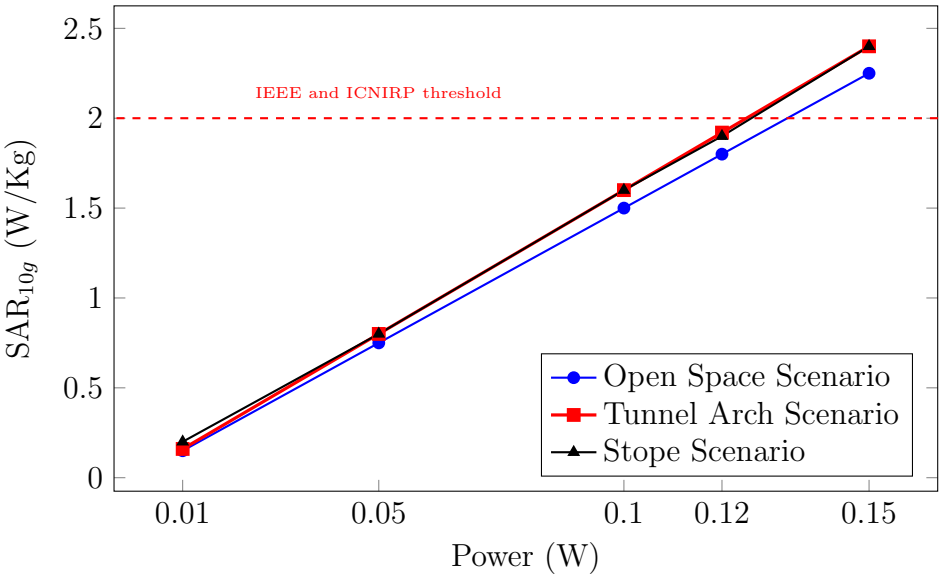



FIGURE 5.13: Variation of $SAR_{10g}$ in the head for different power levels and scenarios at 2400 MHz.

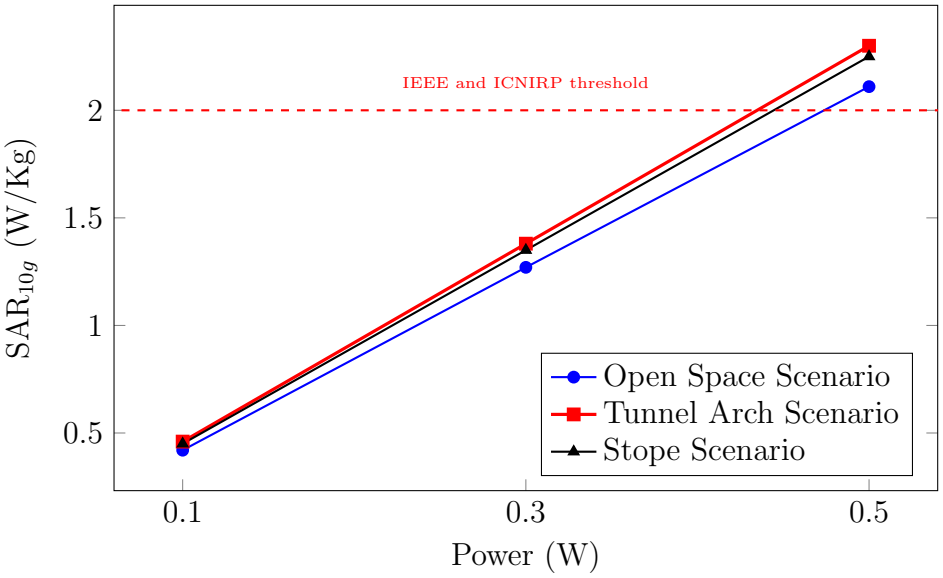



FIGURE 5.14: Variation of $SAR_{10g}$ in the head for different power levels and scenarios at 868 MHz.

were investigated for the transmit frequency of 433 MHz. The $SAR_{10g}$ values in the head of Hugo model for open space, tunnel and stope scenario is shown in Fig. 5.15. It can be seen from the figure that in case of head the prescribed $SAR_{10g}$ threshold gets violated at a power level of 1 W. Therefore, it is recommended that the maximum power level of 1 W should be used in underground mines at 433 MHz in case of a disaster when the device is mounted on the head of the miner.

**For Torso:** A similar approach has been used to investigate the maximum

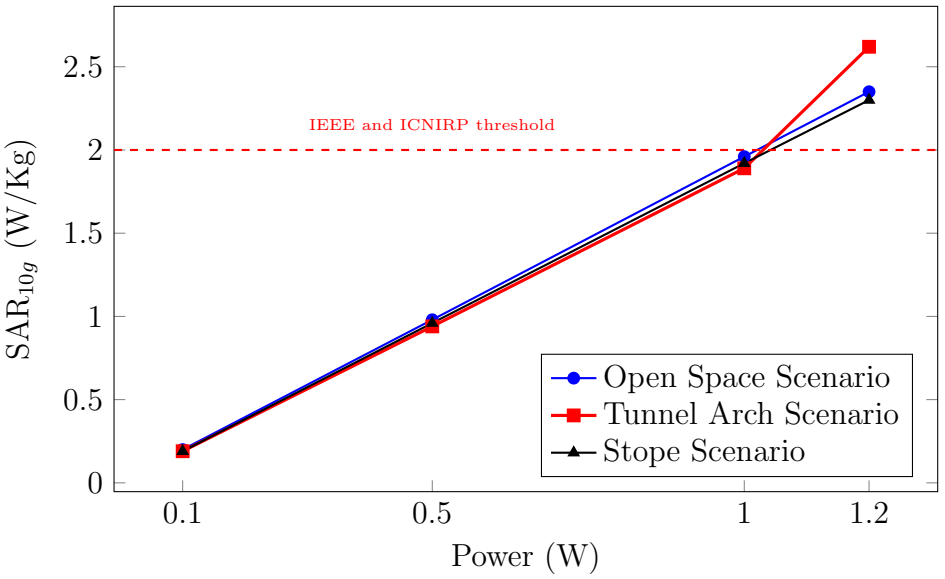



FIGURE 5.15: Variation of $SAR_{10g}$ in the head for different power levels and scenarios at 433 MHz.

transmit power levels that can be used without having adverse health impact on the torso of the miner in underground mines. At 2400 MHz, the same reference transmit power level of 0.01 W was used and increased till it violated the SAR threshold prescribed by ICNIRP [67] and IEEE [25]. The different power levels used in this investigation were 0.01 W, 0.05 W, 0.1 W, 0.15 W and 0.2 W. The results show that a maximum transmit power level of 0.2 W can be used without causing health risks, in terms of SAR, to the torso in underground mines, as shown in Fig. 5.16. In comparison with the results for the head, the SAR for the torso violated the SAR threshold at a higher power level which suggests that the torso is a better location to mount the wearable device on the human body.

Similarly, the $SAR_{10g}$ in the torso were also investigated for 868 MHz using similar parameters to the ones used for head at 868 MHz. The variation of SAR with

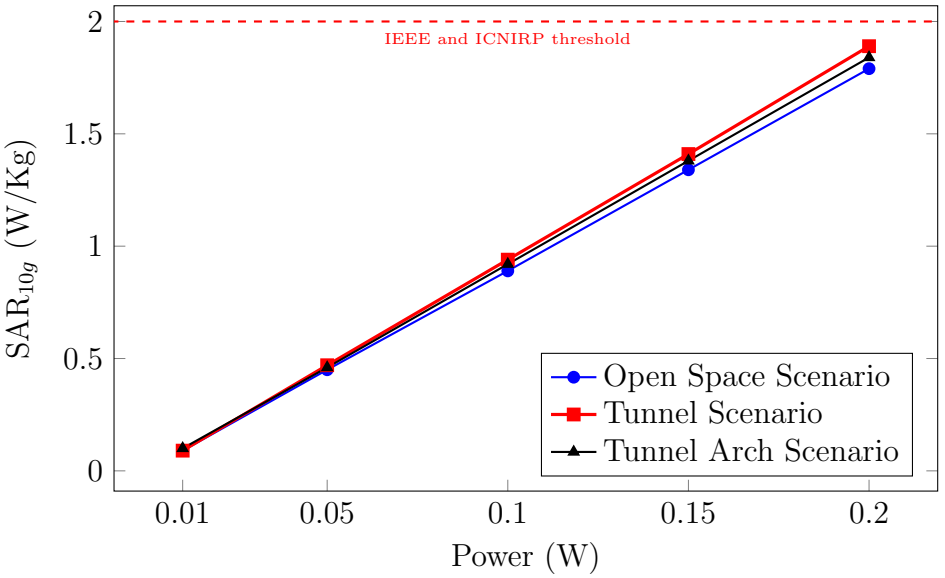



FIGURE 5.16: Variation of $SAR_{10g}$ in the torso for different power levels and scenarios at 2400 MHz.

different power levels at 868 MHz is shown in Fig. 5.17. It was recommended that a maximum transmit power level of 1 W can be used for the wearable device mounted on the torso in case of a disaster in underground mine. The maximum power level that violate the SAR limits is higher for the torso than those for the head which again recommends that the torso is a better location than the head to mount wearable devices in underground mines.

A similar values for transmit power level and scenarios were used for the case of head at 433 MHz. The results show that at the transmit power level of 1.2 W, the $SAR_{10g}$ threshold were violated, as shown in Fig. 5.18. Therefore, a maximum power level of 1.2 W can be used when the wearable device is mounted on the torso of the miner at 433 MHz for a short duration in case of no communication with the miner during a collapse in underground mines.

## 5.5 SAR Analysis for Variation of Distance

In a confined environment, the strength of the reflections from the surrounding environment mainly depend on the distance between the source and the reflectors. The effect of EMR depends on the distance between the surrounding environment

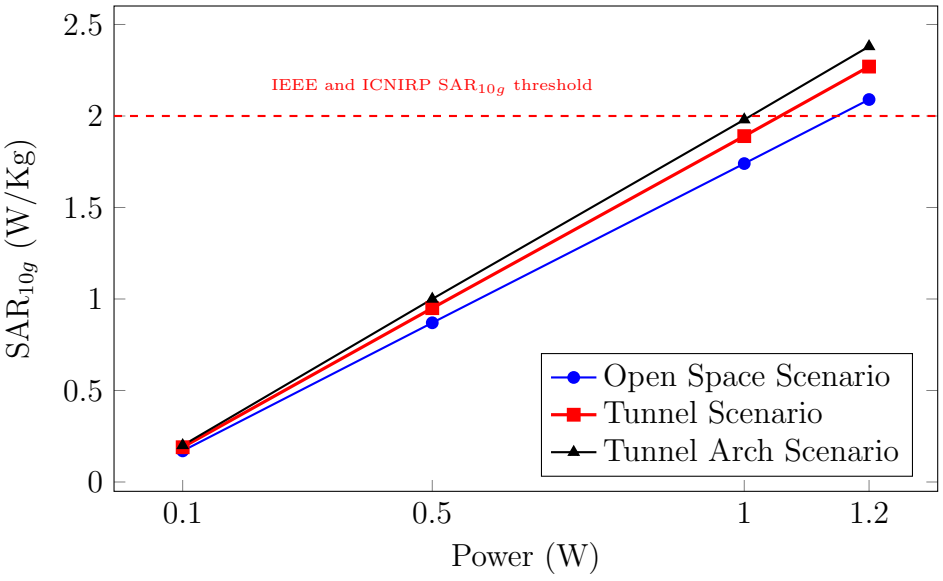



FIGURE 5.17: Variation of $SAR_{10g}$ in the torso for different power levels and scenarios at 868 MHz.

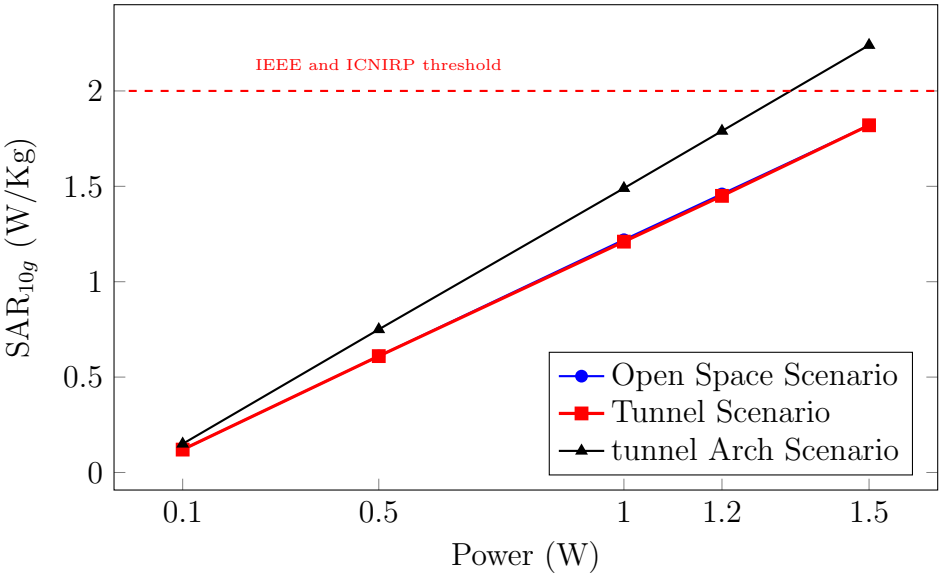



FIGURE 5.18: Variation of $SAR_{10g}$ in the torso for different power levels and scenarios at 433 MHz.

and the human body. It also depends on the distance between the antenna and human body but it was fixed to 10 mm in all simulations according to the IEEE standard [23]. In underground mines, the distance between the boundaries of the underground structure and the miner is inconsistence. Therefore, the SAR was analysed for a variation of distance between the surrounding environment and body of the miner. In all previous simulations for underground mine scenarios,

TABLE 5.3: Variation of $SAR_{10g}$ in head without helmet, torso and head with helmet for different underground mine scenarios and distances at 2400 MHz

| | | Distance (mm) | | |
|---|---|---|---|---|
| | Underground Mine Scenarios | 100 | 150 | 200 |
| Head without helmet | Tunnel | 1.6 | 1.52 | 1.45 |
| | Stope | 1.59 | 1.59 | 1.52 |
| Torso | Tunnel | 1.06 | 0.96 | 0.91 |
| | Tunnel Arch | 1.02 | 0.88 | 0.88 |
| Head with helmet | Tunnel | 1.38 | 1.33 | 1.27 |
| | Stope | 1.4 | 1.39 | 1.32 |

the distance between the boundaries of the underground mine and the voxel model was kept at 100 mm to evaluate worst-case SAR, and this distance was varied to 150 mm and 200 mm in this analysis. The $SAR_{10g}$ was analysed for the head without helmet, torso and head with helmet scenarios using Hugo model at 2400 MHz and 868 MHz. In this analysis, two different mock mine scenarios with higher SAR values were considered. The results showed, as expected, that the SAR values decreased as the distance between boundaries of the underground mine and human voxel models was increased. Table 5.3 shows the variation of SAR values for different distances at 2400 MHz. The $SAR_{10g}$ value at 868 MHz in the head without helmet for 100 mm was 0.46 W/Kg, and for 200 mm the $SAR_{10g}$ value was observed to be 0.40 W/Kg, as shown in Table 5.4. The smaller SAR values were because of reduced strength of the reflections from the boundaries of the underground mines. It was also observed that the SAR values for 200 mm were approximately equal to the open space scenario for most of the scenarios, which indicates that the EMR exposure to the miner in underground mines is higher than the open space scenario if the distance between the boundaries of the underground mine and the human body is less than 200 mm. A similar behaviour was also observed in torso and head with helmet for different mock mine scenarios at 2400 MHz.

A similar approach was used for the investigation of different distances at 868 MHz in the head without helmet, torso and head with helmet for different mock mine

scenarios. A similar behaviour was concluded that the impact of EMR on the miner is higher than the open space scenario when the distance between the boundaries of the underground mine and body of the miner is less than 200 mm. Table 5.4 shows the variation of SAR with distance at 868 MHz.

TABLE 5.4: Variation of $SAR_{10g}$ in head without hemet, torso and head with helmet for different underground mine scenarios and distances at 868 MHz

| | | Distance (mm) | | |
|---|---|---|---|---|
| | Underground Mine Scenarios | 100 | 150 | 200 |
| Head without helmet | Tunnel | 0.46 | 0.41 | 0.40 |
| | Stope | 0.45 | 0.42 | 0.42 |
| Torso | Tunnel | 0.2 | 0.17 | 0.16 |
| | Tunnel Arch | 0.2 | 0.17 | 0.16 |
| Head with helmet | Tunnel | 0.48 | 0.43 | 0.43 |
| | Stope | 0.43 | 0.41 | 0.41 |

## 5.6 Discussion

In this study, SAR was investigated for wearable devices in underground mines to analyse the impact of EMR on the health of the miners. In addition, SAR analysis was also used to determine the better location on the miner's body for mounting of the wearable device. The impact of different type of antennas, orientation and polarization of the antenna was not in the scope of this study. It was challenging to acquire the properties of the ores present in the underground mines. Therefore, the Wits mock mine tunnel and stope was modelled to investigate the EMR exposure to the miner in underground mine. Different underground mine scenarios for head and torso were modelled to evaluate the SAR on different parts of the human body. Some of the frequencies suitable for wearable wireless devices i.e. 433 MHz, 868 MHz and 2400 MHz were considered in this study.

It was observed that for all underground mine scenarios, the $SAR_{10g}$ values on head without helmet, torso and head with the helmet were higher at least 3%

than for the open space scenario which suggests that the miner has more exposure to EMR when present in the underground mine environment. The impact of EMR on the miner in terms of SAR was most significant in the stope scenario, which is the most confined space of the underground mine and it is challenging to track the location of the miner in such confined spaces. When the head and the torso were exposed to EMR, the $SAR_{10g}$ values for torso were less than those for the head with the same transmit power of 0.1 W used for communication. Therefore, it can be suggested that torso is a better place to mount the wearable devices on the body of the miners in underground mines. The $SAR_{10g}$ value was also investigated in the head with a helmet in order to compare corresponding values in the head without helmet. The SAR values at 2400 MHz and 868 MHz for the head with helmet scenario were 18% and 11% lower in comparison with the direct exposure of EMR to the head without helmet, respectively. It exhibits that the layer of the helmet between the antenna and biological tissues reduces the exposure to EMR and provide safety in underground mines. Consequently, it can be suggested that it is better to mount the wearable device on the outside of the helmet, if the device is to be mounted on the head. Moreover, additional shielding can be designed inside the helmet to further reduce the impact of EMR on the miner in underground mines. The SAR values for torso were lower than those for the head with a helmet which confirms that the torso is an even better location to mount these devices on the human body.

The best frequency with minimum SAR values was investigated for head without helmet, torso and head with helmet in all underground mine scenarios. The SAR values suggested that the low frequencies have low absorption in the human body and less reflections from the surrounding environment. The SAR values were minimum at 433 MHz for head without helmet, torso and head with a helmet for all underground mine scenarios, but lower frequencies have more penetration inside tissues of the human body. The low frequency has a lower SAR, but the deep penetration can also affect the sensitive tissues and organs of the human body, such as CSF in case of the human brain. It can also contribute to elevate the core temperature of the human body. The absorption at high frequencies is limited to

region near the skin, and these frequencies are reflected more by the surrounding environment. Therefore, there is a trade-off in the selection of the frequency used in underground mines. The low frequencies are good for the propagation of the electromagnetic waves in underground mines and for smaller SAR values but they tend to penetrate deep inside the body in comparison to higher frequencies whose impact is limited near to the skin. Further investigation is required for low frequencies to determine the elevation in the core temperature of the miner which was not in the scope of this study.

The maximum power levels were also investigated for use in case of no communication with the miner in collapsed mine scenarios. These power levels were recommended on the basis of the SAR guidelines provided by ICNIRP and IEEE. The power levels were investigated for head without helmet and torso at 433 MHz, 868 MHz and 2400 MHz in a one-by-one manner. It is recommended that in case of head without helmet the maximum transmit power levels of 1 W, 0.5 W and 0.12 W can be used at 433 MHz, 868 MHz and 2400 MHz, respectively for a short duration of time, without having a significant impact on the health of the miner to rescue the miner in a disaster scenario. Similarly, the SAR analysis has suggested that a maximum power level of 1.2 W can be used at 433 MHz and 868 MHz if the wearable device is mounted on the torso of the miner. For similar disaster scenarios, at 2400 MHz a maximum transmit power level of 0.2 W can be used if the device is mounted on the torso, without having a health impact on the miner in terms of SAR.

Lastly, the variation of SAR with the different distances of 150 mm and 200 mm was analysed. The variation of SAR was analysed on the head without helmet and torso for different scenarios at 868 MHz and 2400 MHz. It was observed that the $SAR_{10g}$ values decreased as the distance between the boundaries of the underground mine and the voxel model was increased. It was suggested that the impact of EMR on the miner in terms of SAR is higher than the open space environment if the distance between the boundaries of the underground mine and miner is less than 200 mm. Therefore, the miner has a higher impact of EMR in the confined environment of the underground mine, especially in the narrow stopes of

the underground mines.

# Chapter 6

# Conclusion and Future Work

## 6.1 Conclusion

In underground mines, different wearable devices are being used to communicate with the miner. Different frequencies and power levels are used for communication in these wearable devices. The use of wearable devices in the confined space of underground mines has increased the public concern to investigate the impact of EMR on the health of the miners in underground mines. To the best knowledge of the author, no study has been reported to analyse the effect of electromagnetic signals in underground mines for wearable devices. The objective of this study was to investigate the EMR impact on the head and torso of a miner working in an underground mine. The maximum power levels that can be used, in case of loss of communication with the miner after a disaster, have also been investigated for commonly used frequencies of 433 MHz, 868 MHz and 2400 MHz. In this study, two high-resolution voxel models have been used to estimate the impact of EMR at different frequencies. Different underground mine scenarios have been modelled similar to the Wits mock mine for head and torso as it is challenging to acquire the properties of the rocks and the ores present in the underground mines. SAR was investigated for a transmit power of 0.1 W and using the IEC/IEEE 62704-1 SAR averaging method [23].

The human head was evaluated with three different underground mine scenarios, and results are compared with the open space scenario at the frequencies of 433 MHz, 868 MHz and 2400 MHz. It is observed that the EMR absorption in

the human head is less at lower frequencies. However, the penetration of the electromagnetic waves is deeper, which can affect the sensitive organs inside the body and thus elevate the core temperature of the body. It is also concluded that the presence of the metal in underground mines enhances the impact of EMR.

The EMR impact on the torso is evaluated for different underground mine and open space scenarios at 433 MHz, 868 MHz and 2400 MHz. A comparison of SAR values for the two high-resolution voxel models has been used for validation of the analysis. It has been observed that the SAR values are lower in the torso than the head and less for lower frequencies. Therefore, it has been recommended that the torso is a better location on the miner's body for placement of the wearable devices in underground mines.

A hard head helmet was also modelled, and the SAR impact on the head in this case has been analysed. The SAR values on the head with the helmet were found to be lower than the SAR values for the case of head without helmet. Therefore, it is suggested to mount the wearable device on the outside of the helmet, if the device is to be mounted on the head. Moreover, the shielding can be provided to reduce the exposure of EMR on the head with a helmet. It was also recommended to use lower frequencies in underground mines as lower frequencies provide less exposure of EMR to the miner, and has less interaction with surrounding environment of the underground mines, and thus provide better communication.

The maximum transmit power levels for head and torso have been investigated for use in case of no communication with the miner. These power levels are recommended in order not to violate the SAR threshold prescribed by ICNIRP [67] and IEEE [25]. A maximum transmit power of 1 W, 0.5 W and 0.12 W is recommended at 433 MHz, 868 MHz and 2400 MHz, respectively, for a wearable device to be mounted on the head. Similarly, the recommended maximum transmit power level for torso at 433 MHz and 868 MHz is 1.2 W, and at 2400 MHz is 0.2 W.

Lastly, the variation of SAR with different distances was investigated on head without helmet and torso at 868 MHz and 2400 MHz for different underground mine scenarios. It was concluded that the impact of EMR on the miner was higher when the distance between the boundaries of the underground mine and

voxel model was less than 200 mm. Therefore, the miner has higher exposure of EMR than the open space environment when the distance between the wearable device and boundaries of the underground mine is less than 200 mm.

## 6.2 Future work

In this study, the variation of SAR for different types and orientations of the antenna has not been evaluated. This work can further be continued by studying the impact of EMR on the miner using different antennas and their orientation. In underground mines, these wearable devices will be used for a long duration of 5 to 6 hour shift/day. The impact of EMR concerning the time of exposure was not investigated in this dissertation, but can be worked upon as part of future continuation of this work. The impact of EMR on the human body results in elevating the core or local temperature of the body. Moreover, the underground mine environment has high temperatures, and continuous working of the miner can elevate the temperature of the body of the miner. It is thus recommended to study the impact of EMR in terms of elevation of temperature of the tissues especially in the high-temperature environment of underground mines.

# References


[1] R. Larik, G. Mallah, M. Talpur, A. Suhag, and F. Larik, "Effects of wireless devices on human body," *Journal of Computer Science and Systems Biology*, vol. 9, pp. 119–124, 2016.

[2] M. H. Repacholi, "Health risks from the use of mobile phones," *Toxicology Letters*, vol. 120, no. 1-3, pp. 323–331, 2001.

[3] Minerals Council South Africa, "Mining in SA - Gold," http://www.mineralscouncil.org.za/sa-mining/gold, [accessed June 20, 2020].

[4] M. Li and Y. Liu, "Underground coal mine monitoring with wireless sensor networks," *ACM Transactions on Sensor Networks*, vol. 5, no. 2, pp. 1–29, 2009.

[5] I. Zaman, A. Förster, A. Mahmood, and F. Cawood, "Finding trapped miners with wireless sensor networks," in *2018 5th International Conference on Information and Communication Technologies for Disaster Management*, 2018, pp. 1–8.

[6] M. Boutin, A. Benzakour, C. L. Despins, and S. Affes, "Radio wave characterization and modeling in underground mine tunnels," *IEEE Transactions on Antennas and Propagation*, vol. 56, no. 2, pp. 540–549, 2008.

[7] L. Hardell and C. Sage, "Biological effects from electromagnetic field exposure and public exposure standards," *Biomedicine and pharmacotherapy*, vol. 62, no. 2, pp. 104–109, 2008.

[8] J. Lin, R. Saunders, K. Schulmeister, P. Söderberg, b. Stuck, A. Swerdlow, M. Taki, B. Veyret, G. Ziegelberger, M. H. Repacholi, R. Matthes,

A. Ahlbom, K. Jokela, and C. Roy, "ICNIRP Guidelines for limiting exposure to time-varying electric and magnetic fields (1 Hz to 100 kHz)." *Health Physics*, vol. 99, pp. 818–836, 2010. [Online]. Available: https://hal.archives-ouvertes.fr/hal-01019994

[9] S. J. Genuis, "Fielding a current idea: exploring the public health impact of electromagnetic radiation," *Public Health*, vol. 122, no. 2, pp. 113–124, 2008.

[10] H. Lai and N. P. Singh, "Magnetic-field-induced DNA strand breaks in brain cells of the rat." *Environmental Health Perspectives*, vol. 112, no. 6, p. 687, 2004.

[11] S. Yarkan, S. Guzelgoz, H. Arslan, and R. R. Murphy, "Underground mine communications: a survey," *IEEE Communications Surveys Tutorials*, vol. 11, no. 3, pp. 125–142, 2009.

[12] M. R. Yenchek, G. T. Homce, N. W. Damiano, and J. R. Srednicki, "NIOSH-sponsored research in through-the-earth communications for mines: a status report," *IEEE Transactions on Industry Applications*, vol. 48, no. 5, pp. 1700–1707, 2012.

[13] T. Wadley, "Underground communication by rocks in gold mines on the witwaterrand," *South Africa wet. Nywerheid Navorsingsraad, Johannesburg, South Africa, Telekommunikasies Navorsing Laboratorium TRL*, 1946.

[14] A. E. Goddard, "Radio propagation measurements in coal mines at UHF and VHF," in *Proceedings of Through-the-Earth Electromagnetics Workshop*, 1973, pp. 15–17.

[15] J. J. Sammarco, R. Paddock, E. F. Fries, and V. K. Karra, "A technology review of smart sensors with wireless networks for applications in hazardous work environments," 2007.

[16] A. Chehri, P. Fortier, and P. Tardif, "Geolocation for UWB networks in underground mines," in *Proceeding of 2006 IEEE Annual Wireless and Microwave Technology Conference*, 2006, pp. 1–4.

[17] L. Cheng, C. Ong, C. Neo, V. Varadan, and V. Varadan, "Microwave electronics," 2004.

[18] J. Sun, W. Wang, and Q. Yue, "Review on microwave-matter interaction fundamentals and efficient microwave-associated heating strategies," *Materials*, vol. 9, no. 4, p. 231, 2016.

[19] Z. Peng, J.-Y. Hwang, C.-L. Park, B.-G. Kim, and G. Onyedika, "Numerical analysis of heat transfer characteristics in microwave heating of magnetic dielectrics," *Metallurgical and Materials Transactions A*, vol. 43, no. 3, pp. 1070–1078, 2012.

[20] C. A. Balanis, *Antenna theory: analysis and design*. John wiley & sons, 2016.

[21] Antenna-Theory.com, "S-Parameters," http://www.antenna-theory.com/definitions/sparameters.php, [accessed June 20, 2020].

[22] C. C. Johnson and A. W. Guy, "Nonionizing electromagnetic wave effects in biological materials and systems," *Proceedings of the IEEE*, vol. 60, no. 6, pp. 692–718, 1972.

[23] "IEC/IEEE international standard – determining the peak spatial-average specific absorption rate (SAR) in the human body from wireless communications devices, 30 MHz to 6 GHz - part 1: General requirements for using the finite-difference time-domain (FDTD) method for SAR calculations," *IEC/IEEE 62704-1:2017*, pp. 1–86, 2017.

[24] F. C. Commission *et al.*, "Office of engineering technology (oet) bulletin 65 (ed. 97-01, august 1997): Evaluating compliance with fcc guidelines for human exposure to radiofrequency electromagnetic fields," *Supplement C: Additional Information for Evaluating Compliance of Mobile and Portable Devices with FCC Limits for Human Exposure to Radiofrequency Emissions (Ed. 01-01*, 2001.

[25] "IEEE standard for safety levels with respect to human exposure to radio frequency electromagnetic fields, 3 kHz to 300 GHz," *IEEE Std C95.1-2005 (Revision of IEEE Std C95.1-1991)*, pp. 1–238, 2006.

[26] C. E. Fernández-Rodríguez, A. A. A. De Salles, and D. L. Davis, "Dosimetric simulations of brain absorption of mobile phone radiation–the relationship between psSAR and age," *IEEE Access*, vol. 3, pp. 2425–2430, 2015.

[27] M. N. Sadiku, *Numerical techniques in electromagnetics*. CRC press, 2000.

[28] R. Talhi, "Computational techniques and numerical analysis in EM wave propagation and scattering: An overview and trends," in *Proceeding EMTS 2007-International URSI Commission B-Electromagnetic Theory Symposium*, pp. 26–28.

[29] R. Courant, *Variational methods for the solution of problems of equilibrium and vibrations*. Sine loce: sine nomine, 1943.

[30] M. N. Sadiku, "A simple introduction to finite element analysis of electromagnetic problems," *IEEE Transactions on Education*, vol. 32, no. 2, pp. 85–93, 1989.

[31] K. Yee, "Numerical solution of initial boundary value problems involving Maxwell's equations in isotropic media," *IEEE Transactions on Antennas and Propagation*, vol. 14, no. 3, pp. 302–307, 1966.

[32] T. Weiland, "A discretization model for the solution of Maxwell's equations for six-component fields," *Archiv Elektronik und Uebertragungstechnik*, vol. 31, pp. 116–120, 1977.

[33] R. Schuhmann and T. Weiland, "A stable interpolation technique for FDTD on non-orthogonal grids," *International Journal of Numerical Modelling: Electronic Networks, Devices and Fields*, vol. 11, no. 6, pp. 299–306, 1998.

[34] A. Bossavit and I. Mayergoyz, *Computational Electromagnetism: Variational Formulations, Complementarity, Edge Elements*, ser. Electromagnetism.

Elsevier Science, 1998. [Online]. Available: https://books.google.co.za/books?id=RQ_9hc8U7MsC

[35] SIMULIA, "CST STUDIO SUITE ELECTROMAGNETIC FIELD SIMULATION SOFTWARE," http://www.cst.com, [accessed June 20, 2020].

[36] T. Weiland, "Time domain electromagnetic field computation with finite difference methods," *International Journal of Numerical Modelling: Electronic Networks, Devices and Fields*, vol. 9, no. 4, pp. 295–319, 1996.

[37] Q. K. Al-dulamey, A. Ismail, and Y. A. Al-Jawwady, "Biophysical effect of EMR with 5GHz on male reproductive system of mus musclus mice," *Current Journal of Applied Science and Technology*, pp. 1–11, 2019.

[38] R. R. Taye, M. K. Deka, A. Rahman, and M. Bathari, "Effect of electromagnetic radiation of cell phone tower on foraging behaviour of asiatic honey bee, apis cerana f.(hymenoptera: Apidae)," *Journal of Entomology and Zoology Studies*, vol. 5, pp. 1527–1529, 2017.

[39] I. Y. Belyaev, E. Markovà, L. Hillert, L. O. Malmgren, and B. R. Persson, "Microwaves from UMTS/GSM mobile phones induce long-lasting inhibition of 53bp1/$\gamma$-h2AX DNA repair foci in human lymphocytes," *Bioelectromagnetics: Journal of the Bioelectromagnetics Society, The Society for Physical Regulation in Biology and Medicine, The European Bioelectromagnetics Association*, vol. 30, no. 2, pp. 129–141, 2009.

[40] K. K. Kesari and J. Behari, "Microwave exposure affecting reproductive system in male rats," *Applied Biochemistry and Biotechnology*, vol. 162, no. 2, pp. 416–428, 2010.

[41] H. Nittby, G. Grafström, D. P. Tian, L. Malmgren, A. Brun, B. R. Persson, L. G. Salford, and J. Eberhardt, "Cognitive impairment in rats after long-term exposure to GSM-900 mobile phone radiation," *Bioelectromagnetics: Journal of the Bioelectromagnetics Society, The Society for Physical Regulation in Biology and Medicine, The European Bioelectromagnetics Association*, vol. 29, no. 3, pp. 219–232, 2008.

[42] B. R. Persson, L. G. Salford, and A. Brun, "Blood-brain barrier permeability in rats exposed to electromagnetic fields used in wireless communication," *Wireless Networks*, vol. 3, no. 6, pp. 455–461, 1997.

[43] A. Balmori, "Mobile phone mast effects on common frog (Rana temporaria) tadpoles: the city turned into a laboratory," *Electromagnetic Biology and Medicine*, vol. 29, no. 1–12, pp. 31–35, 2010.

[44] M. Capri, E. Scarcella, C. Fumelli, E. Bianchi, S. Salvioli, P. Mesirca, C. Agostini, A. Antolini, A. Schiavoni, G. Castellani, F. Bersani, and C. Franceschi, "In vitro exposure of human lymphocytes to 900 MHz CW and GSM modulated radiofrequency: studies of proliferation, apoptosis and mitochondrial membrane potential," *Radiation Research*, vol. 162, no. 2, pp. 211–218, 2004.

[45] Y. Okano and H. Shimoji, "Comparison measurement for specific absorption rate with physically different procedure," *IEEE Transactions on Instrumentation and Measurement*, vol. 61, no. 2, pp. 439–446, 2012.

[46] Y. Okano, R. Shimofusa, M. Anbai, and K. Someno, "Broadband measurement methodology for specific absorption rates above 300 MHz," *IEEE Transactions on Instrumentation and Measurement*, vol. 66, no. 10, pp. 2693–2702, 2017.

[47] S. Kodera, A. Hirata, D. Funahashi, S. Watanabe, K. Jokela, and R. J. Croft, "Temperature rise for brief radio-frequency exposure below 6 GHz," *IEEE Access*, vol. 6, pp. 65 737–65 746, 2018.

[48] G. Anzaldi, F. Silva, M. Fernandez, M. Quilez, and P. J. Riu, "Initial analysis of SAR from a cell phone inside a vehicle by numerical computation," *IEEE Transactions on Biomedical Engineering*, vol. 54, no. 5, pp. 921–930, 2007.

[49] G. Anzaldi, G. Anzaldi, P. J. Riu, F. Silva, and R. Santos, "Finite difference time domain low cost modeling for automotive environments," *Proceedign of 2004 International Symposium on Electromagnetic Compatibility*, vol. 3, pp. 775–780, 2004.

[50] K. M. S. Thotahewa, J. Redouté, and M. R. Yuce, "SAR, SA, and temperature variation in the human head caused by IR-UWB implants operating at 4 GHz," *IEEE Transactions on Microwave Theory and Techniques*, vol. 61, no. 5, pp. 2161–2169, 2013.

[51] A. Simba, S. Watanabe, T. Hikage, and T. Nojima, "Experimental and numerical investigation of the maximum specific absorption rate in a spherical phantom when operating a mobile phone near a metallic wall," *IET Science, Measurement and Technology*, vol. 5, no. 6, pp. 225–230, 2011.

[52] B. Tomovski, F. Gräbner, A. Hungsberg, C. Kallmeyer, and M. Linsel, "Effects of electromagnetic field over a human body, SAR simulation with and without nanotextile in the frequency range 0.9-1.8 GHz," *Journal of Electrical Engineering*, vol. 62, no. 6, pp. 349–354, 2011.

[53] N. Othman, N. A. Samsuri, M. K. A. Rahim, and N. A. Elias, "Specific absorption rate in the human leg and testicle due to metallic coin and zip," in *Procedding of IEEE International RF and Microwave Conference*, 2015, pp. 123–127.

[54] A. Lee and J. Yun, "A comparison of specific absorption rates in SAM phantom and child head models at 835 and 1900 MHz," *IEEE Transactions on Electromagnetic Compatibility*, vol. 53, no. 3, pp. 619–627, 2011.

[55] M. Moutaouekkil, C. Taybi, A. Ziyyat, and D. Picard, "The effect of metal braces on antenna parameters and the SAR distribution of the head exposed to popular cellular frequencies," in *Proceeding of 2017 Mediterranean Microwave Symposium*, 2017, pp. 1–4.

[56] M. Smondrk, M. Benova, and Z. Psenakova, "Specific absorption rate evaluation in human body model comprising of metallic implant," in *Proceeding of 19th International Conference Computational Problems of Electrical Engineering*, 2018, pp. 1–4.

[57] M. Tareq, D. A. Alam, M. Islam, and R. Ahmed, "Simple half-wave dipole antenna analysis for wireless applications by CST microwave studio," *International Journal of Computer Applications*, vol. 94, no. 7, pp. 21–23, 2014.

[58] National Library of Medicine, "The Visible Human Project," https://www.nlm.nih.gov/research/visible/visible_human.html, [accessed June 20, 2020].

[59] O. Bejenaru, C. Lazarescu, S. Vornicu, and V. David, "Specific absorption rate evaluation in case of exposure of the human body to radiofrequency electromagnetic field generated by mobile communications," in *Proceeding of 2018 International Conference and Exposition on Electrical And Power Engineering*, 2018, pp. 1004–1009.

[60] CST MPHYSICS STUDIO, "Biological Data," http://www.mweda.com/cst/cst2013/mergedprojects/CST_MPHYSICS_STUDIO/common_tools/Bio_Models.htm, [accessed June 20, 2020].

[61] K. S. Cole and R. H. Cole, "Dispersion and absorption in dielectrics I. Alternating current characteristics," *The Journal of Chemical Physics*, vol. 9, no. 4, pp. 341–351, 1941.

[62] Federal Communication Commission, "Body Tissue Dielectric Parameters," https://www.fcc.gov/general/body-tissue-dielectric-parameters, [accessed June 20, 2020].

[63] IfAC, "Dielectric Properties of Body Tissues in the frequency range 10 Hz - 100 GHz," http://niremf.ifac.cnr.it/tissprop/, [accessed June 20, 2020].

[64] F. Cawood, "Digital mine laboratory prepared for digital mining," https://www.ee.co.za/wp-content/uploads/2015/03/positionit-march15-p26-30.pdf, [accessed June 20, 2020].

[65] M. Creamer, "Wits 'digital mine' taking satellite communication underground," https://www.miningweekly.com/article/wits-digital-mine-bringing-satellite-communication-to-underground-mining-2014-03-12, [accessed June 20, 2020].

[66] I. Hussain, F. Cawood, and R. van Olst, "Effect of tunnel geometry and antenna parameters on through-the-air communication systems in underground mines: Survey and open research areas," *Physical Communication*, vol. 23, pp. 84–94, 2017.

[67] International Commission of Non-Ionizing Radaition Protection, "ICNIRP RF EMF GUIDELINES," https://www.icnirp.org/en/, [accessed June 20, 2020].

[68] CST MPHYSICS STUDIO, "Hexahedral Mesh," http://www.mweda.com/cst/cst2013/mergedprojects/CST_MPHYSICS_STUDIO/common_overview/common_overview_mesh.htm, [accessed June 20, 2020].

[69] THE INDEPENDENT COMMUNICATIONS AUTHORITY OF SOUTH AFRICA, "Notice of intention to amend Annexure B of the Radio Frequency Spectrum Regulation, 2015," https://www.icasa.org.za/uploads/files/Notice-of-intention-to-amend-Annexure-B-of-the-Radio-Frequency-Spectrum-Regulations.pdf, [accessed June 20, 2020].

[70] S. Leung, Y. Diao, K. Chan, Y. Siu, and Y. Wu, "Specific absorption rate evaluation for passengers using wireless communication devices inside vehicles with different handedness, passenger counts, and seating locations," *IEEE Transactions on Biomedical Engineering*, vol. 59, no. 10, pp. 2905–2912, 2012.

[71] C. Zhu, D. Wu, L. Ping, and W. Liang, "The effects of head parameters on the specific absorption rate in the human head," in *Proceedign of 2015 8th International Conference on Biomedical Engineering and Informatics*, 2015, pp. 423–427.

[72] R. Takei, T. Nagaoka, K. Saito, S. Watanabe, and M. Takahashi, "SAR variation due to exposure from a smartphone held at various positions near the torso," *IEEE Transactions on Electromagnetic Compatibility*, vol. 59, no. 2, pp. 747–753, 2017.

[73] M. Kozlov, N. Weiskopf, and H. E. Möller, "Evaluation of specific absorption rates with high resolution human head models at 890 MHz," in *Proceeding*

*of 2018 IEEE International Symposium on Antennas and Propagation USNC/URSI National Radio Science Meeting*, July 2018, pp. 903–904.

[74] A. Khan, S. Bashir, and F. Ullah, "Electromagnetic bandgap wearable dipole antenna with low specific absorption rate," in *Proceeding of 2018 International Conference on Computing, Mathematics and Engineering Technologies*, 2018, pp. 1–4.

[75] H. I. Hamd and H. I. Mohammed, "Comparison specific absorption rate (SAR) for human head between 2G and 4G mobile communication," in *Proceeding of 2018 International Conference on Engineering Technology and their Applications*, 2018, pp. 87–90.

[76] M. Cavagnaro and J. C. Lin, "Importance of exposure duration and metrics on correlation between RF energy absorption and temperature increase in a human model," *IEEE Transactions on Biomedical Engineering*, vol. 66, no. 8, pp. 2253–2258, 2019.

[77] W. He, B. Xu, M. Gustafsson, Z. Ying, and S. He, "RF compliance study of temperature elevation in human head model around 28 GHz for 5G user equipment application: simulation analysis," *IEEE Access*, vol. 6, pp. 830–838, 2018.

# Appendix A

## Studies using Medical Approach for Analysis of SAR

TABLE 1: Chronological record of studies using medical approach.

| **Reference/ year** | **Methodology** | **Frequency** | **Form of EMR** | **Exposure Duration** | **Observed/ Measured SAR** (W $Kg^{-1}$) | **Effect reported** |
|---|---|---|---|---|---|---|
| [42]/ 1997 | In-vivo (rat whole body) | 915 MHz | Continuous and pulsed wave | 2 - 960 min | - | both CW and pulsed have effect on BBB (blood brain barrier.) |
| [41]/ 2008 | In-vivo (rat whole body) | 900 MHz | GSM | 2 h/week, 55 weeks | 0.0006 | Reduced memory functions. |
| [39]/ 2009 | In-vitro | 915 MHz, 1947 MHz | GSM,UMTS | 24, 72 h | 0.037 | DNA repair mechanism in humans. |
| [44]/ 2010 | In-vitro | 900 MHz | CW | 14 days, 5, 10, 20 min per day | - | DNA damage in human glial cells. |
| [40]/ 2010 | In-vivo (rat whole body) | 2450 MHz | 50 Hz Modulation | 2 h/day, 35 days | 0.11 | DNA double strand breaks in brain cells. |
| [43]/ 2010 | In-vivo (tadpole of frog) | 88.5-1873.6 MHz | Cell phone BS emission | 2 months | - | Retarded development. |
| [1]/ 2016 | Survey (Doctors and radiologists) | - | wireless communication | - | - | brain tumor, male infertility and fetus. |
| [38]/ 2017 | In-vivo (Honey Bee) | - | Cell Phone Tower | 15 days | - | *Apis cerana* colonies were most affected by the EMR emitted by cell phone tower. |
| [37]/ 2019 | In-vivo (Mice) | 5 GHz | Different radiated power | 60 days | - | Microwave radiation has harmful effect of physiological and on reproductive system. |

# Appendix B

# Studies using Engineering Approach for Analysis of SAR

TABLE 2: Chronological record of studies using engineering approach.

| **Reference/ year** | **Frequency** | **Methodology** | **Antenna Type** | **Human Models** | **Important results** |
|---|---|---|---|---|---|
| [48]/ 2007 | 835 MHz | FDTD code | Half wavelength dipole | Custom model | Presence of metal body in vicinity changes the SAR distribution. |
| [54]/ 2011 | 835 & 1900 MHz | Simulations | Monopole, PIFA | SAM phantom, European and Korean child model | SAR varies with respect to the type of tissues in the body. |
| [51]/ 2011 | 900 MHz | FDTD simulation, MAP-SAR2 measurements | Dipole | Spherical phantom | Metallic wall increases the SAR value and depend on the distance and geometry of the wall. |
| [45]/2012 | 2-6 GHz | New method was proposed for Measurements of SAR | Dipole | Custom phantom | Proposed method is independent of frequency. |
| [70]/ 2012 | 900 MHz | Fidelity software | Dipole | Custom phantom | SAR values are much higher than the free space. |
| [50]/ 2013 | 4 GHz | CST simulation | - | Hugo Voxel model | SAR varies with input power, orientation of antenna and signal bandwidth. |
| [53]/ 2015 | 0.9, 1.8 GHz | CST simulation | Dipole, PIFA | Gustav Voxel model | Zip increases the SAR value whereas coin reduces the SAR value. |
| [26]/ 2015 | 900 MHz | SAMCADX simulation | Cell phone antenna | Different baby, male & female models | SAR values are higher in baby than the adult models. |
| [71]/ 2015 | 920 MHz | HFSS simulation | PIFA | Custom Phantom | SAR value increases with the increase in the size of the head. |
| [72]/ 2017 | 0.9 & 2 GHz | XFdtd simulation | CAD model of mobile phone | Japanese male & female model | SAR is higher in male model, SAR is higher at tilt angle. |
| [46]/ 2017 | above 300 MHz | Measurements | Dipole | Custom phantom | Proposed method shows deflection of 10% to 20%. |
| [73]/ 2018 | 890 MHz | HFSS simulation | Commercial mobile phone | High resolution CAD models | SAR values are higher in CSF. |
| [47]/ 2018 | below 6 GHz | Simulation | Dipole | TARO & custom model | No clear trend in temperature elevation with SAR. |
| [74]/ 2018 | 2.1 GHz | CST simulation | Dipole | Custom Phantom | Electromagnetic band gap reduces the SAR values. |
| [59]/ 2018 | 780, 900, 1800, 2100 & 2500 MHz | CST simulation, Measurement | Plane wave source | Hugo, custom phantom | SAR is smaller than unity. |
| [75]/ 2018 | 1.8 & 2.3 GHz | CST simulation | Rectangular patch | SAM phantom | SAR is higher at 2.3 GHz than at 1.8 GHz. |
| [76]/ 2019 | 700 to 2700 MHz | Simulations | – | Duke human model | SAR provides a better correlation with temperature compared to VAR for short exposures. |
| [77]/ 2019 | 28 GHz | CST simulation | Beam steering patch array, dipole & plane wave | High resolution custom phantom | Few square centimeters area is a good candidate for spatial average power density. |

# Appendix C

## Analysis of $SAR_{1g}$ for head without helmet

The $SAR_{1g}$ values are analysed on head without helmet for different scenarios at 2400 MHz, 868 MHz and 433 MHz in Fig. 1, Fig. 2 and Fig. 3, respectively. The SAR values are compared for both voxel models i.e. Hugo and Tom models.

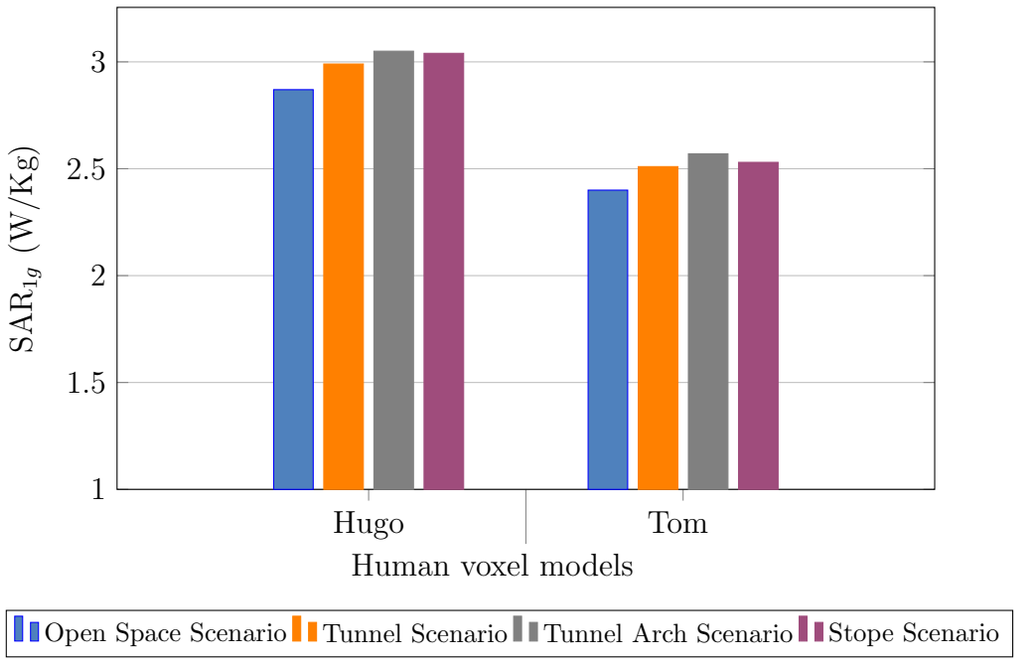



FIGURE 1: Comparison of $SAR_{1g}$ on head of both models without helmet for different scenarios at 2400 MHz.

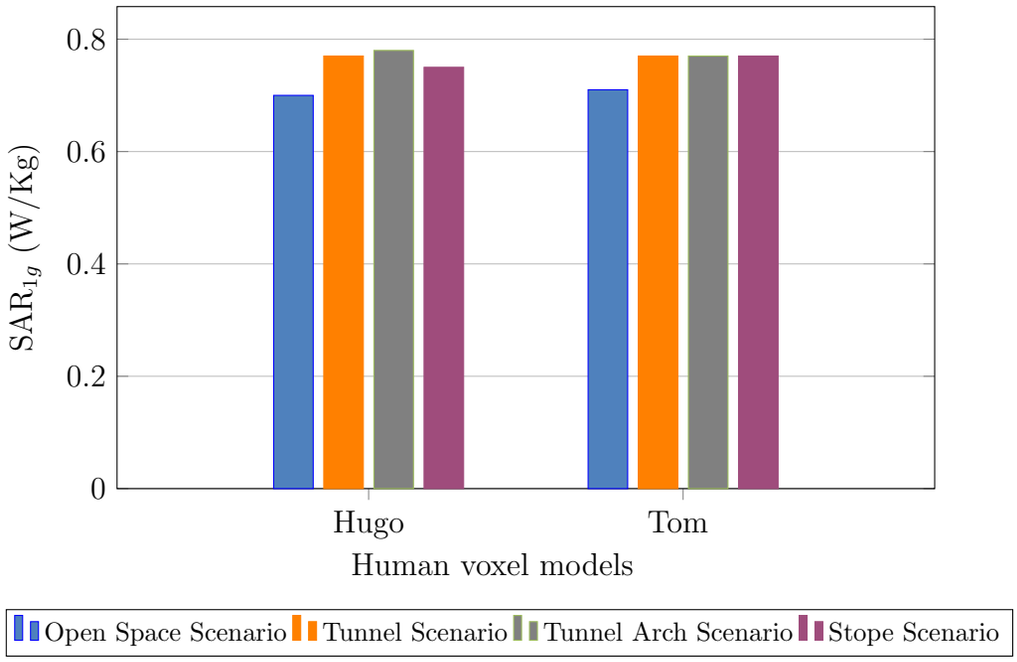



FIGURE 2: Comparison of $SAR_{1g}$ on head of both models without helmet for different scenarios at 868 MHz.

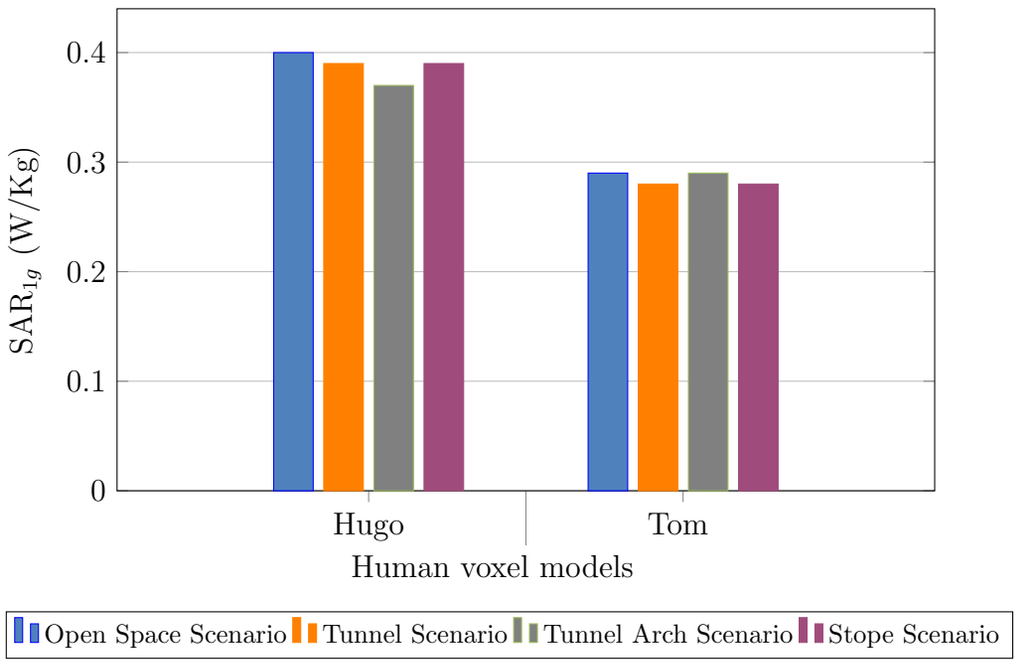



FIGURE 3: Comparison of $SAR_{1g}$ on head of both models without helmet for different scenarios at 433 MHz.

# Appendix D

## Analysis of $SAR_{1g}$ for torso

The $SAR_{1g}$ values are analysed on torso for different scenarios at 2400 MHz, 868 MHz and 433 MHz in Fig. 4, Fig. 5 and Fig. 6, respectively.

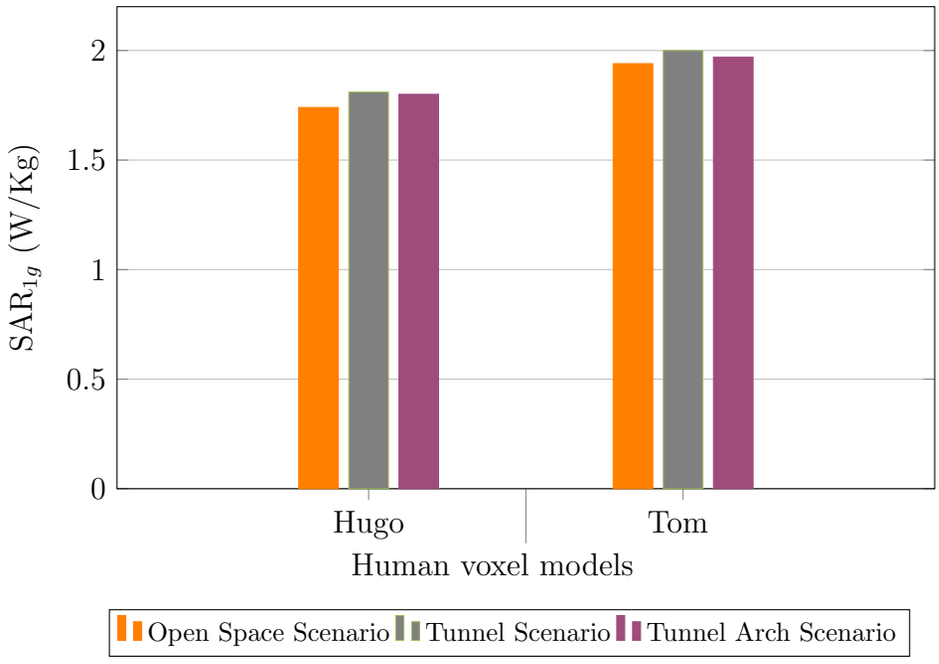



FIGURE 4: Comparison of $SAR_{1g}$ on torso of both models for different scenarios at 2400 MHz.

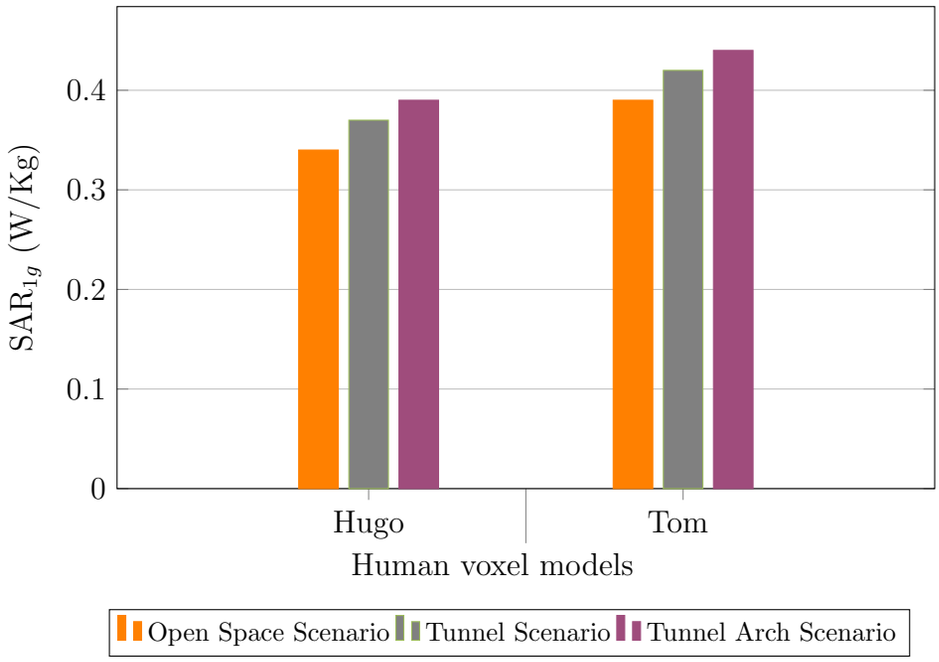



FIGURE 5: Comparison of $SAR_{1g}$ on torso of both models for different scenarios at 868 MHz.

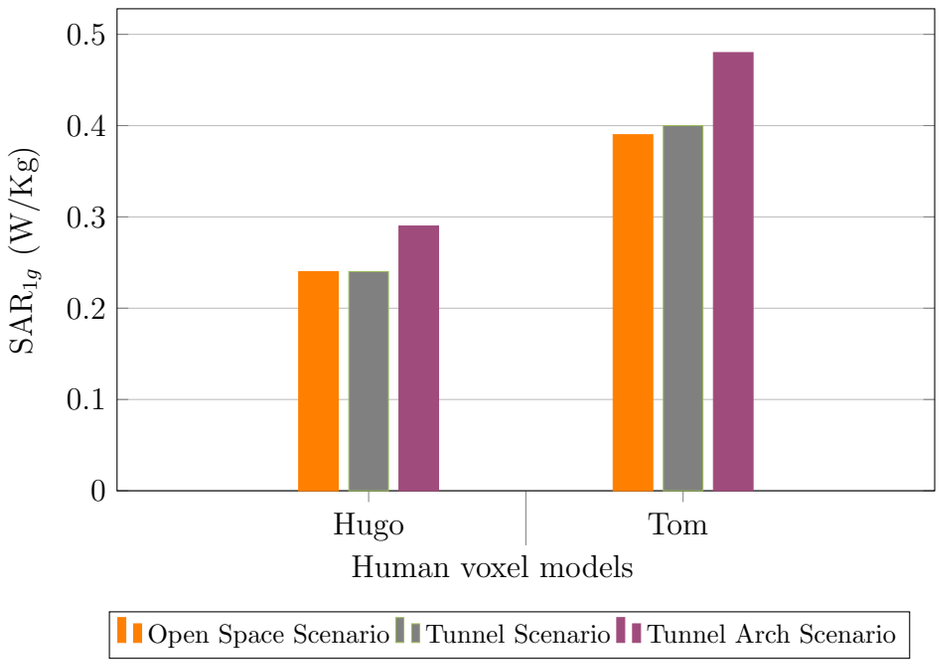



FIGURE 6: Comparison of $SAR_{1g}$ on torso of both models for different scenarios at 433 MHz.

# Appendix E

## Analysis of $SAR_{1g}$ for head with helmet

The $SAR_{1g}$ values are analysed on head with helmet for different scenarios at 2400 MHz, 868 MHz and 433 MHz in Fig. 7, Fig. 8 and Fig. 9, respectively.

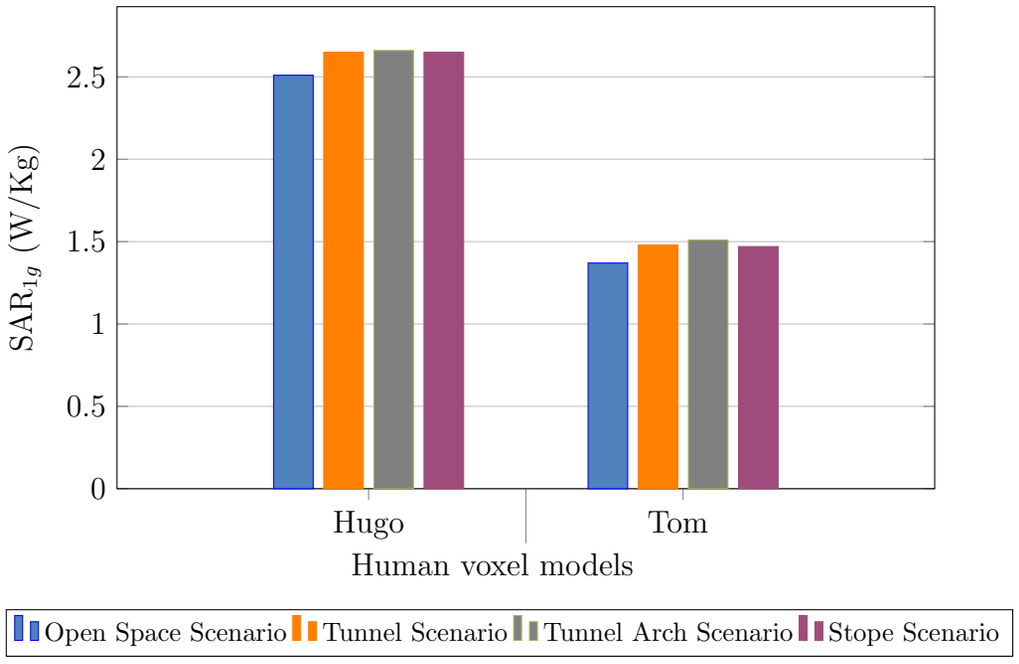



FIGURE 7: Comparison of $SAR_{1g}$ on head of both models with helmet for different scenarios at 2400 MHz.

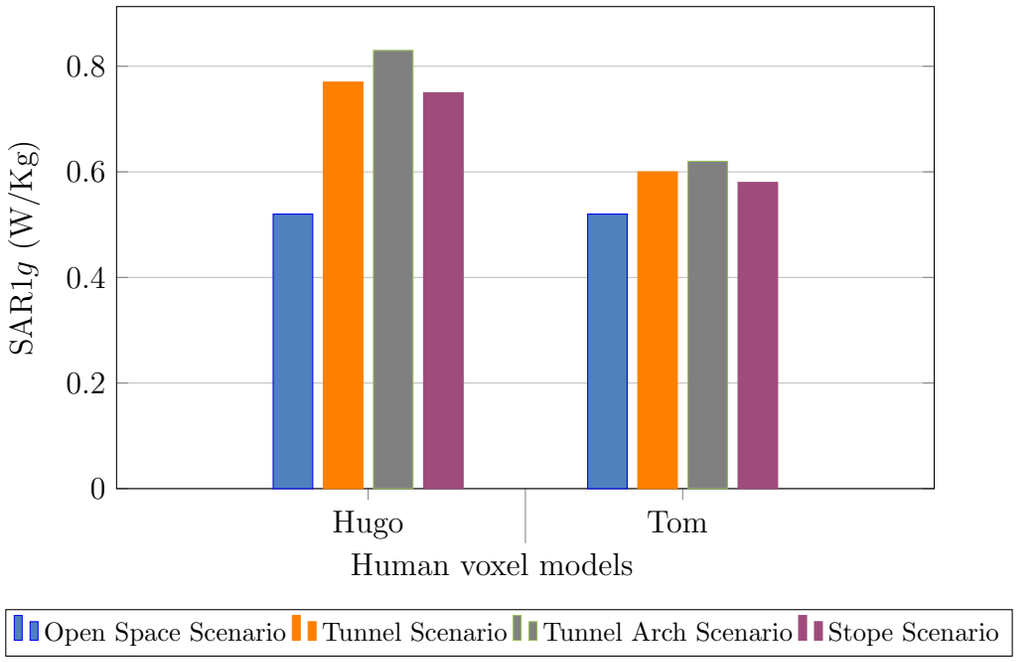



FIGURE 8: Comparison of $SAR_{1g}$ on head of both models with helmet for different scenarios at 868 MHz.

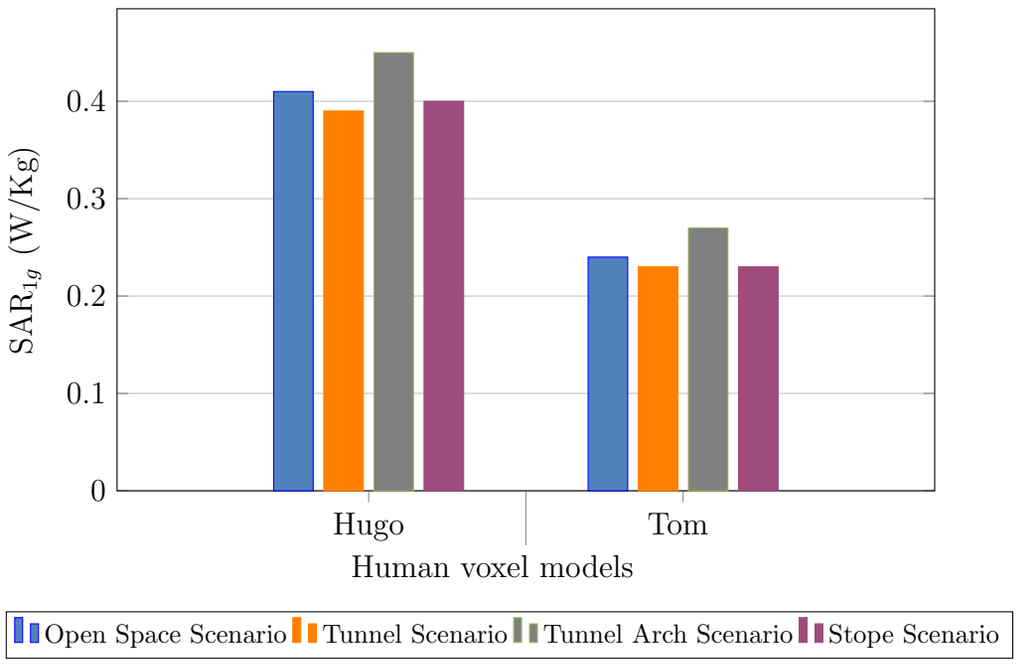



FIGURE 9: Comparison of $SAR_{1g}$ on head of both models with helmet for different scenarios at 433 MHz.